METHODOLOGY TO INVESTIGATE PROTEIN-PROTEIN INTERACTIONS OF JUN DURING NEURONAL DIFFERENTIATION OF PC12 CELLS

by

Heather Lee Leskinen

A Dissertation Submitted in

Partial Fulfillment of the

Requirements for the Degree of

Doctor of Philosophy

in Biological Sciences

at

The University of Wisconsin-Milwaukee

December 2023

ABSTRACT

METHODOLOGY TO INVESTIGATE PROTEIN-PROTEIN INTERACTIONS OF JUN DURING NEURONAL DIFFERENTIATION OF PC12 CELLS

by

Heather Lee Leskinen

The University of Wisconsin-Milwaukee, 2023
Under the Supervision of Professor Ava J Udvadia

In humans and other mammals, injury to the central nervous system (CNS) can cause a permanent loss of neuronal function, leading to cognitive defects, limb paralysis, and other neurological disabilities. In contrast, studies have shown that some non-mammalian vertebrates like zebrafish, have the remarkable ability to functionally regenerate axons after CNS injury by reactivating and sustaining the expression of regeneration-associated genes (RAGs). Some RAGs encode transcriptional regulators that dimerize to control downstream gene expression necessary for functional axonal recovery. Our lab has previously identified Jun as an important transcriptional regulator of regeneration after optic nerve injury in zebrafish. After axon injury in the peripheral nervous system, Jun is necessary for functional axonal regeneration and has been shown to heterodimerize to regulate gene expression. However, it is not known if these same binding partners interact with Jun during CNS regeneration. To investigate this, we have created a fusion protein of Jun tethered to one of the most recent generations of proximity labeling ligases, APEX2. Unlike traditional methods to investigate protein-protein interactions (PPIs), proximity labeling can also detect transient interactions, such as post-translational modifications performed by kinases, as well as stable binding seen in transcription complex formation. Using the nerve growth factor (NGF)-induced neuronal

differentiation of PC12 cells as a model, the PPIs of Jun were identified during the early stage of axon extension using proximity labeling, followed by mass spectrometry. Elucidating the PPIs of Jun will aid in developing new therapeutic approaches in human CNS regeneration.

TABLE OF CONTENTS

LIST OF FIGURES

LIST OF TABLES

LIST OF ABBREVIATIONS

ALS	amyotrophic lateral sclerosis
AP-1	activator protein 1
AR	androgen receptor
ARRE2	antigen receptor response element 2
BSA	bovine serum albumin
bZIP	basic-region leucine zipper
ChIP	Chromatin immunoprecipitation
cKO	conditionally knocked out
CNS	central nervous system
CRE	cAMP-responsive element
DAB	3,3'-diaminobenzidine
DAPI	4',6-diamidino-2-phenylindole
DPBS	Dulbecco's phosphate-buffered saline
DRG	dorsal root ganglion
EDTA	ethylenediaminetetraacetic acid
ef1α	elongation factor 1-alpha
eIF	eukaryotic translation initiation factor
EMSA	electrophoretic mobility shift assay
GAP43	growth-associated protein 43
GDNF	glial-derived neurotrophic factor
GR	glucocorticoid receptor
HRP	horse radish peroxidase
IL	interleukin
JNK	jun N-terminal kinase
LC-MS	liquid chromatography-mass spectrometry
MARE	Maf recognition element
MS	mass spectrometry
NFAT	nuclear factor of activated T-cells
NGF	nerve growth factor
NLS	nuclear localization signal
NuRD	nucleosome remodeling and histone deacetylation
PAGE	polyacrylamide gel electrophoresis
PCR	polymerase chain reaction
PIC	protease-inhibitor cocktail
PKC	protein kinase C
PMA	plasma membrane H^+-ATPase
PMSF	phenylmethylsulfonyl fluoride
PNS	peripheral nervous system
PPI	protein-protein interaction
PTM	post-translational mechanism
RGC	retinal ganglion cell
TBI	traumatic brain injury

TBP	TATA box-binding protein
TBST	tris-buffered saline-tween
TF	transcription factor
TNFα	tumor necrosis factor alpha
TPA	tissue plasminogen activator
TRE	TPA-responsive element
VEGF	Vascular endothelial growth factor

Chapter One Introduction

Axonal injury is a key feature of many nervous system diseases

The vertebrate nervous system contains both central and peripheral components. The central nervous system (CNS) consists of the brain, spinal cord, retinas, and optic nerve while the peripheral nervous system (PNS) consists of sensory and autonomic ganglia and segments of nerves protruding out of the spinal cord. Together, these systems control everything that our bodies do on a daily basis from simple movements to complex problem solving. Damage to these systems is a major problem as mammals have a low intrinsic ability to functionally regenerate neurons. Regenerative ability is correlated with temporally regulated changes in gene expression, including the expression of transcription factors. Recent studies hypothesize that changing interactions between transcription factors as well as post-translational modifications to transcription factors underlie the ability for regeneration. Understanding these interactions and how they mediate axon growth and regeneration may provide valuable information for the design of new therapeutics to treat traumatic and degenerative diseases of the nervous system.

Traumatic injury or diseases of the nervous system can vary in severity based on the site and extent of the injury. Injury to the soma, or cell body, of a neuron results in cell death and a loss of function. However, injury to the axon has different outcomes depending on the type of organism, extent of injury, and age (Gutmann et al., 1942, Black and Lasek, 1979, Pestronk et al., 1980, Blackshaw, 2022). After axonal injury in adult mammals, CNS neurons fail to re-grow to their targets, resulting in a permanent loss of function, but neurons of the PNS can functionally regenerate. Many non-mammalian vertebrates (e.g. zebrafish, lamprey, frog) can

fully regenerate components of both the central and peripheral nervous systems, but this phenomenon decreases with age (El Bejjani and Hammarlund, 2012, Blackshaw, 2022, Hibbard, 1963, Black and Lasek, 1979). Axon injury is a hallmark of direct trauma to the brain or spinal cord as well as many different neurodegenerative and neurodevelopmental diseases.

The nervous system can be damaged by a variety of sources. While several neurological conditions have been shown to have an underlying genetic component, there is also evidence that environmental factors contribute to the risk of developing certain diseases such as in the case of multiple sclerosis. Even aspects of our lives that we can control, such as our diet, can increase the likelihood of onset, like with diabetic neuropathies. Other times, axonal damage resulting in brain or spinal cord injury are unforeseen consequences of our surroundings, such as falls or vehicular crashes. The disease presentation, pathophysiology, and current treatments of multiple sclerosis, diabetic retinopathy, and traumatic brain injuries will be discussed as examples of CNS axonal damage.

Multiple Sclerosis

Multiple sclerosis is characterized by multiple sites of demyelination and inflammation within the CNS which appear to be a consequence of oligodendrocyte death. Multiple sclerosis is typically seen in young adults with symptoms including fatigue, ataxia, and muscle spasms amongst others (Compston and Coles, 2002). Prognosis is quite good with a life expectancy about 25 years after disease onset, however, multiple sclerosis presentation is variable with 25% of patients reporting no impact on daily activities due to symptoms while 15% become severely disabled shortly after symptoms develop (Ascherio, 2013). While genetics appear to play a role in developing multiple sclerosis, there are environmental factors that seem to

influence it such as childhood obesity, smoking, vitamin D deficiency, and contracting the Eppstein-Barr virus (Ascherio, 2013).

One hypothesis for disease development ascribes molecular mimicry as a main component of the immune response that causes the characteristic lesions and plaques seen in multiple sclerosis. Following this, some therapeutic approaches aim to deplete B-cells by targeting particular class II molecules such as the monoclonal antibody ocrelizumab (Montalban et al., 2017). This treatment was shown to slow disease progression as measured by lesion volume, loss of brain volume, and performance in timed physical tests. These immunosuppressant therapies are ongoing treatments while immune reconstitution therapies can be delivered in short time courses. The latter aims to produce a longer-term immune response, such as the synthetic deoxyadenosine, cladribine, which destroys B-cells through adenosine deaminase depletion (Giovannoni et al., 2018). These drugs do not cure multiple sclerosis, but such therapies have the potential to significantly delay disease progression such that patients could be asymptomatic.

Diabetic Retinopathy

Of the approximately 37 million Americans with diabetes, about 20% of those individuals do not even know that they are diabetic (CDC). Patients with Type I, II, or gestational diabetes are at risk for other co-morbidities with more than half eventually developing diabetic retinopathy (NIH – National Eye Institute). Over time, vision becomes distorted and acuity decreases, but the ultimate symptom of this disease is blindness. The exact pathogenesis is uncertain, but several contributing factors have been identified. Hyperglycemia dysregulates metabolic pathways which eventually increase the permeability of or block the blood vessels

within the eye (Ono et al., 1998). Retinal ganglion cells are the neurons within the retina whose axons makeup the optic nerve. A loss of dendritic arborization in or death of these cells are some of the earliest signs of diabetic retinopathy, yet the molecular mechanisms underlying this are unclear (Amato et al., 2022).

As the effects of hyperglycemia are widespread over the body, there are many therapies against diverse targets ranging from immune, to neurotrophic, to metabolic. Vascular endothelial growth factor (VEGF) levels are increased in the vitreous of patients with diabetic retinopathy and several anti-oncogenic drugs aim to deplete VEGF and subsequently decrease vision loss (Aiello et al., 1994, Wells et al., 2015). In cases that do not respond well to anti-VEGF treatments, it is presumed that multiple cytokines are at play and thus anti-inflammatories are used. Biodegradable corticosteroid (dexamethasone and fluocinolone acetonide) implants are placed in the eye for sustained-release which have been shown to increase visual acuity, but some patients develop adverse effects such as cataracts and increased ocular pressure (Boyer et al., 2014, Campochiaro et al., 2011). However, there remains no cure for diabetic retinopathy. The best treatment is prevention by maintaining appropriate blood sugar levels as well as blood pressure.

Traumatic Brain Injury (TBI)

Worldwide, an estimated 69 million people suffer from traumatic brain injury (TBI) each year (Dewan et al., 2018). Each day in 2021, nearly 200 Americans died as a result of TBI-related injuries (CDC – National Center for Injury Prevention and Control). Patients who suffer from TBIs tend to have a range of neuronal deficits that will affect their physical and emotional well-being. TBIs are commonly the result of motor vehicle crashes, falls, and physical assault. Injuries

can be either focal (resultant of a localized and direct impact) or diffuse (occurring over a large area of the brain) with effects such as swelling, bleeding, and metabolic changes. These can result in secondary damages in which the brain swells due to pressure build from intracranial bleeding or a breakdown of the blood-brain barrier (NIH-National Institute of Neurological Disorders and Stroke).

TBIs present differently in each patient which profoundly impacts their clinical treatment. The variables underlying pathophysiology are unique to each individual which does not fit the current grouping paradigm of the intensive care unit used today. As there is no cure or pharmacological approach to healing TBIs yet, most advances have been towards better characterization of each patient to individualize treatment as best as possible with the available tools. A new approach will identify sub-groups of patients who may benefit from individual treatment. A multi-omics study of data from severely injured humans determined that delivery of pre-hospital (in transit) thawed plasma to high-risk trauma patients showed that patients who received plasma showed improved mortality at 30 days in comparison to those who received standard of care (Sperry et al., 2018). These early results suggest that read-outs of patient biomarkers, metabolic derangement, co-morbidities, medication, and other confounding factors upon hospitalization could create grouping for better clinical outcomes. However, at present, typical treatments are rest and over-the-counter pain relievers with prevention being the best treatment, such as by wearing personal protective equipment during activities in which a TBI is likely to occur.

Intrinsic and extrinsic factors contribute to neuronal regeneration

Axonal injury to the mammalian nervous system involves multiple systems (i.e., immune system) and cell types whose precise interactions occur over a time course. These interactions often induce changes in gene expression resultant of proteins binding with one another. The fate of a neuron is greatly influenced by specific protein-protein interactions depending on the cellular context, the specific protein binding partner, their relative concentrations, etc. Therefore, understanding which proteins interact at specific times to elicit functional axonal regeneration will aid in developing therapies and treatments.

The process of axon regeneration is an interplay between many cellular pathways and extracellular signals. The time for successful regeneration varies depending on type of organism, extent of injury, and age (Gutmann et al., 1942, Black and Lasek, 1979, Pestronk et al., 1980). PNS axonal regeneration is slow in humans and animals with rates of 1 and 3 mm/day, respectively (Gutmann et al., 1942, Sunderland, 1947). The farther an axon must travel, the longer regeneration takes and the less likely the nerve is to successfully reinnervate its target.

Furthermore, the extent of the damage to the axon can affect its ability to regenerate. Injuries that do not sever the endoneurial sheaths (connective tissue that surrounds the myelin) are more likely to functionally regenerate (Young, 1942). When the endoneurial sheaths are completely severed, such as in a nerve transection, it is less likely that the regenerating axons will enter the correct endoneurial tube at the distal end of the nerve stump (Haftek and Thomas, 1968, Brushart and Mesulam, 1980, Thomas et al., 1987). While mammalian PNS regeneration is far more robust than that of the CNS, a functional outcome is still difficult to

achieve due to incomplete re-growth or aberrant re-innervation leading to chronic pain (David and Aguayo, 1981). This highlights the importance of understanding the molecular mechanisms that underly functional axonal regeneration to develop better treatments to ultimately improve patient outcomes and quality of life. To illustrate the complexity of functional axonal regeneration, we will discuss the intrinsic and extrinsic factors of axonal injury to the mammalian nervous system.

Peripheral nervous system (PNS) regeneration

The response to injury in the PNS is well-documented, but the molecular mechanisms that underly these processes are still not completely understood (Waller, 1850, Ramón y Cajal, 1928). After peripheral axotomy, the cell body begins to swell, the nucleolus and nucleus reposition, and Nissl bodies on the rough endoplasmic reticulum start to disintegrate (Nissl, 1892, Lieberman, 1971). The neuron reverts from a "maintenance" to a "growth/regenerative" state. What is known about the molecular response to axonal injury in the mammalian PNS will be discussed below.

Upon rupture of the axon, an influx of calcium ions initiates a rapid cellular response to re-seal the membrane and begin the process in which the axon and myelin are disintegrated, largely by non-neuronal cells referred to as Wallerian degeneration. Upon axonal injury in the PNS, the distal tip of the proximal stump and the entire distal stump begin to degenerate. This process begins with axonal fragmentation and is followed by an increase in permeability of the blood-nerve-barrier which allows for macrophages to enter the site of injury to phagocytize the myelin debris (Waller, 1850). The calcium ion influx at the site of injury is key to initiating the regenerative response (Schlaepfer and Bunge, 1973, Ziv and Spira, 1995). The ion-sensitive

protease calpain degrades neurofilament proteins and its pharmacological inhibition prevents axonal degradation (Zimmerman and Schlaepfer, 1982, George et al., 1995). The ubiquitin proteasome system dismantles the microtubules and is independent of the calcium influx associated with opening the axonal membrane (Zhai et al., 2003). The distal axon and myelin sheath disintegrate, and the debris is cleared by Schwann cells and macrophages (Miledi and Slater, 1970, Stoll et al., 1989). Most of the distal axon degeneration is carried out by glial cells, but they also have other roles in axon regrowth.

A concerted effort between multiple cell types is required for functional regeneration in the PNS, mainly Schwann cells and macrophages. There are Schwann cells that secrete neurotrophic factors such as nerve growth factor (NGF) and glial-derived neurotrophic factor (GDNF) to support axon re-growth. NGF secreted from Schwann cells binds to NGF receptors of the growth cone to attract and guide growing neurites (Taniuchi et al., 1988). The NGF and its receptor are internalized and undergo retrograde transport to the soma to exert their neurotrophic effects (Johnson et al., 1987). GDNF is up-regulated in Schwann cells while its receptor, GFRα, is up-regulated in nerves after PNS injury (Naveilhan et al., 1997, Fontana et al., 2012). The GDNF-GFRα complex recruits the RET receptor tyrosine kinase which auto-phosphorylates to initiate signaling cascades such as Ras/MAPK and PI3K/Akt (Coulpier et al., 2002). In mouse embryonic sensory neurons from the nodose ganglion, blocking RET phosphorylation induced by GDNF reduced neuronal survival (Coulpier et al., 2002). Mediated by toll-like receptors, the debris from degenerated axons stimulates Schwann cells to express monocyte chemotactic protein-1 (MCP-1 or CCL2) which recruits macrophages to the site of injury (Boivin et al., 2007). This recruitment is further stimulated by Schwann cell secretion of

tumor necrosis factor alpha (TNFα), IL-1α, and IL-1β (Shamash et al., 2002). Upon arrival, macrophages secrete these same factors (Shamash et al., 2002). While glial cells contribute to generating an appropriate immune response to degrade axonal fragments, the regenerating neuron itself is responding to damage.

In mammals, this process of Wallerian degeneration occurs over 7-14 days during which the distal tip of the proximal axon is also undergoing regeneration (George and Griffin, 1994). The damaged plasma membrane re-seals and a growth cone forms which responds to external cues to correctly orientate the axon for re-growth (Spira et al., 1993, Sperry, 1963). These cues are either attractive or repulsive which aid in guiding the axon to its end target for re-innervation. Some of these cues are located on the cell membranes (e.g. adhesion molecules such as ephrins and semaphorins) or secreted by cells (e.g. netrins, Sema3A, NGF, Slit) to create a chemogradient (Giger et al., 2010). The distal nerve stump and end targets secrete factors that contribute to neurite extension such as NGF, ciliary neurotrophic factor, and GDNF (Heumann et al., 1987, Sahenk et al., 1994, Hoke et al., 2000). Many of the extracellular cues function to affect cytoskeletal dynamics through signaling cascades and retrograde transport (Tetzlaff et al., 1988, Fu and Gordon, 1997). While many extra-cellular cues and glial cells are important in eliciting a regenerative response in PNS neurons, the neural cell itself must undergo intrinsic changes to facilitate regrowth, as well.

Upon axonal injury, the PNS neuron undergoes many rapid changes that transition the cell from a “maintenance” state to a “growth state”. Immediate calcium ion-induced signals play a role in formation of growth cones, local protein synthesis, induction of further signaling molecules, and relocation and activation of chromatin modifiers (Friede and Bischhausen,

1980). As a consequence of increased intracellular calcium levels, protein kinase Cμ (PKCμ, also known as PKD) is phosphorylated which activates its translocation to the nucleus within one hour of dorsal root ganglion (DRG) axotomy in rats (Cho et al., 2013). In response to PKCμ activation, histone deacetylase 5 (HDAC5) is exported from the nucleus and histone acetylation is increased (Cho et al., 2013). These modifications to the nucleosomes induce changes to the DNA ultrastructure. This appears to precede the transcription of immediate early genes suggesting that restructuring the chromatin landscape primes the regulatory regions of genes necessary for axon regeneration. This is supported by a transcriptome microarray study of successfully regenerating rat DRGs after sciatic nerve lesion that showed that significant changes in gene expression were not observed until 8-12 hours after surgery in comparison to sham-operated controls (Michaelevski et al., 2010). The most pronounced and widespread changes were not observed until 18-28 hours post injury. Thus, later retrograde responses of injury are more highly correlated with influencing gene expression.

After axonal injury, the neurons of the PNS re-express a transcriptional program that can revert them to a growth-competent state. Many of these re-expressed genes encode transcription factors (TFs) that are believed to regulate and maintain the long-term response to injury by controlling the expression of further sets of genes. Notably, axon regrowth is supported by increased expression of growth-associated proteins such as immediate early genes (e.g. JunB and cJun), growth-associated protein 43 (GAP43), cytoskeletal proteins (e.g. tubulin and actin), and neuropeptides (e.g. calcitonin gene-related peptide (CGRP)) (Haas et al., 1993, Skene and Willard, 1981, Tetzlaff et al., 1988, Haas et al., 1990). Differential regulation of regeneration-associated genes occurs in many models of axon injury, and increased expression

of immediate early genes is common among them (Herdegen et al., 1991, Michaelevski et al., 2010, Chronis et al., 2017, Dhara et al., 2019).

Immediate early genes are those whose expression is up-regulated in response to extracellular stimuli and their transcription has been shown to increase in response to injury. After facial nerve axotomy in rats, transcription of immediate early genes is rapidly induced and maintained above baseline levels for at least 11 days (Haas et al., 1993). Many immediate early genes encode transcription factors (TFs) which modulate gene expression. The TF cJun has long been implicated in regeneration, is up-regulated in response to both PNS and CNS axonal injury, and is necessary for axonal regeneration in the PNS (Leah et al., 1991, Herdegen et al., 1991, Ruff et al., 2012). Axons that successfully regenerate down-regulate cJun once they re-innervate their targets (Herdegen et al., 1991, Leah et al., 1991, Jenkins et al., 1993). After facial nerve axotomy in mice, the TFs Ascl1, Stat5b, and Maf are all up-regulated, but this trend is reversed after Jun knock out, suggesting their dependence on Jun expression (Mason et al., 2022). Interestingly, Jun knock out did not affect expression of most TFs until the later phases of regeneration at 4 and 14 days after injury with no significant changes seen at 1 day (Mason et al., 2022). In turn, the products of these Jun-regulated genes carry out long-term cellular responses to injury.

Another group of early-induced proteins, GAPs are upregulated in regenerating axons and are highly associated with successful functional neuronal regeneration in response to axonal injury. GAP43 is a cytosolic protein that localizes to the internal surface of axon terminals and is implicated in cytoskeletal organization of growth cones and synaptic function in developing and regenerating axons (Aigner and Caroni, 1995, Laux et al., 2000, Haruta et al.,

1997). Cytokines and neurotrophins released after axon injury induce JAK/STAT3 and PI3K/Akt pathways that are linked to GAP43 upregulation and increased neurite outgrowth *in vitro* (Yang et al., 2015, Yang et al., 2012). GAP43 mRNA expression is strongly up-regulated in regenerating dorsal root ganglion (DRG) axons following sciatic nerve injury but not after injury to the regeneration-incapable DRG central axons following dorsal rhizotomy (Mason et al., 2002). In a rat model of stroke, GAP43 up-regulation was associated with axon sprouting in the barrel cortex (Carmichael et al., 2005). These data demonstrate the link between increased GAP43 and cytoskeletal dynamics in axon extension.

Actin and tubulin are two of the main proteins that make up the cytoskeletal structure of a cell. After axonal injury, a neuron needs to re-grow towards its target cells which requires elongation of the axon. In regenerating rat nerves, the rate at which a regenerating axon grows is positively correlated with the rate of actin and tubulin axonal transport (Wujek and Lasek, 1983). While tubulin and actin synthesis increases, neurofilament levels decrease in response to PNS axonal injury (Tetzlaff et al., 1988). Neurofilament is associated with maintaining axonal diameter and its downregulation during regeneration has been suggested to accelerate transport by increasing fluidity in the axonal cytoplasm (Hoffman et al., 1984, Gordon et al., 1991). These changes in cytoskeletal protein organization are key structural changes required for successful PNS neuronal regeneration.

While axotomy is normally associated with down-regulation of classical neurotransmitters, some neuropeptides increase expression. Calcitonin gene-related peptide (CGRP) mRNA is upregulated in axotomized motoneurons which could increase blood flow to proximal nerve stumps by stimulating vasodilatation to recruit proinflammatory cells, such as

macrophages, mast cells, and lymphocytes (Haas et al., 1990, Edvinsson et al., 1988). While its exact mechanistic action is not known, intravenous injection of CGRP increased blood flow and reduced the volume of the brain injury in a rat model of focal cerebral ischemia (Holland et al., 1994). In response to PNS axonal injury, increasing the permeability of the blood-nerve-barrier is an important step in regeneration, (George and Griffin, 1994) Thus, CGRP upregulation in response to axotomy may be playing a role in this process.

The delay in transcriptional changes may be partially due to the later arrival of retrograde signaling from the injury site delivered by dynein-mediated axonal transport. Kinases are a key component of many cellular pathways and have long been implicated in retrograde signaling of injury. Jun amino-terminal kinase (JNK) signaling has been linked to multiple physiological responses to extracellular stress (Ip and Davis, 1998). After PNS injury, JNK scaffolding protein (JNK-interacting protein, JIP3) and activated JNK are retrogradely translocated via the dynein motor (Cavalli et al., 2005). Phosphorylated JNK precedes the phosphorylation of the transcription factor cJun whose expression is maintained throughout regeneration (Herdegen et al., 1991, Kenney and Kocsis, 1998). Levels of cJun are increased after both PNS and CNS axon damage, but cJun is also implicated in neuronal cell death (Estus et al., 1994, Herdegen et al., 1998, Maggirwar et al., 2000).

Barriers to central nervous system (CNS) regeneration

While the PNS can mount a regenerative response to axonal injury, the CNS is not able to overcome either extrinsic or intrinsic barriers. Within the mammalian CNS, the debris from disintegrated distal axon stump and myelin are not efficiently cleared after degeneration, creating a regeneration-prohibitive environment (Schwab, 1990, George and Griffin, 1994).

Within the PNS, this is largely completed by Schwann cells and macrophages, but their equivalents in the CNS, oligodendrocytes and microglia, clear debris far less efficiently (Ludwin, 1990). In mammalian CNS neurons cultured on either oligodendrocytes or myelin, growth cones collapse and axon extension is decreased (Caroni and Schwab, 1988, Schwab and Caroni, 1988). Furthermore, growth inhibitory molecules, like netrin-1, have been shown to inhibit axon regrowth and are known to be within CNS myelin and secreted from oligodendrocytes (Low et al., 2008). These factors are obstacles to axon extension in the CNS, but so are factors intrinsic to the glial cells themselves.

In animals capable of CNS axon regeneration, Wallerian degeneration is rapid and regeneration is functional (Turner and Glaze, 1977). After spinal cord injury in mammals, oligodendrocytes undergo apoptosis at areas distal to the site of injury, an event that occurs after axonal degeneration (Li et al., 1999). During development, maintaining contact with the axon promotes survival of oligodendrocytes, so it may be the loss of this interaction that contributes to cell death after injury in mature cells (Barres et al., 1993). A loss of trophic support and activation of Fas (a member of the TNF cytokine receptor superfamily) also appear to contribute to oligodendrocyte apoptosis (D'Souza et al., 1996). Conversely, 60-70% of oligodendrocytes survive throughout Wallerian degeneration after enucleation, but appear to enter a resting state (Ludwin, 1990). This suggests that there may be different pathways elicited by different types of injury. Outside of their poor myelin clearance, oligodendrocytes near sites of spinal cord injury up-regulate the semaphorin, Sema4D (also known as CD100, an inhibitory growth cue), which has been shown to decrease neurite extension of postnatal cerebellar and sensory neurites *in vitro* (Moreau-Fauvarque et al., 2003). While oligodendrocytes are already

present at the site of injury, microglia chemotaxis is induced by increased ATP levels from the compromised cell membranes (Davalos et al., 2005).

In response to CNS axon injury, microglia migrate to the lesion, activate, and undergo hypertrophy (Barron, 1995). Microglia-derived macrophages remain at the site of injury for months to years and most do not switch from a pro-inflammatory (M1) to a pro-repair (M2) state (Popovich et al., 1996, Kigerl et al., 2009). In addition to their role in the immune response, microglia phagocytize debris from degraded myelin along with other recruited macrophages. Furthermore, the blood-brain barrier is open only at the site of injury within the CNS, unlike in the PNS in which the blood-nerve barrier permeability is increased over the length of the degenerating axon (George and Griffin, 1994). This may limit the available space through which necessary microglia and immune cells can enter the lesion to assist in protective mechanisms. While microglia initially exert protective effects, they do not adapt a pro-repair role to encourage axon outgrowth.

A key characteristic of damage to the CNS axon is the formation of the glial scar at the site of injury. Within days of axonal damage, a glial "scar" is formed around the lesion by injury-recruited non-neuronal cells largely made up of reactive astrocytes, microglia, and meningeal fibroblasts. In a maintenance state, astrocytes are important for regulating neurotransmitters, producing extracellular matrix molecules, and maintaining the blood-brain barrier (Mennerick and Zorumski, 1994, Bernstein et al., 1985, Risau and Wolburg, 1990). After injury, they are the main cells responsible for preventing further damage to the delicate brain tissue by isolating and containing immune and fibroblast-like cells within the core of the scar (Fitch et al., 1999, Soderblom et al., 2013). While astrocytes protect surrounding tissue, they and other

components of the scar prevent the neuron from entering a state of regeneration. At the epicenter of the scar, meningeal cells secrete Sema3s (class 3 semaphorins) which act as repulsive signals (Pasterkamp et al., 1998). Proteoglycans (e.g., keratan sulfate, chondroitin sulfate, etc.) are up-regulated by reactive glia and commonly found at CNS injury sites (Andrews et al., 2012). These and other extracellular matrix molecules have well-established roles in the inhibition of neurite outgrowth both *in vitro* and *in vivo* (Snow et al., 1990, Bradbury et al., 2002). While many elements of the CNS extracellular matrix inhibit axon re-growth, their absence in the PNS presents an environment more conducive to axon regeneration.

The formation of a growth cone is an essential component of successful axonal regeneration in the PNS. Notably, microtubules maintain stability and bundling which supports the growth cone (Erturk et al., 2007). Within the mammalian CNS, however, a retraction bulb, or frustrated growth cone, is often formed at the proximal nerve stump of an axonal injury in which microtubules are depolymerized and disorganized (Li and Raisman, 1995, Erturk et al., 2007). Microtubules not only maintain the structure of the growth cone, but also aid in transport of cellular materials. The retraction bulb of a CNS neuron grows in size after axotomy due to accumulation of vesicles, suggesting that disorganized cargo transport also contributes to the failure of axonal extension (Erturk et al., 2007). Even if a growth cone successfully forms, components of the extracellular matrix and molecules secreted from reactive glia prevent regenerative growth (Caroni and Schwab, 1988, Schwab and Caroni, 1988, Bradbury et al., 2002). Thus, the growth-inhibitory extrinsic environment of the CNS influences the ability of the neuron to effectively respond to injury.

In addition to the extrinsic factors that inhibit successful CNS regeneration, there are also cell-intrinsic mechanisms that prevent axon re-growth after injury. Efficient retrograde transport is observed in regenerating PNS axons, but this is not so in the CNS. Integrins are transmembrane receptors that bind to the molecules of the extracellular matrix and transmit environmental information to the actin cytoskeleton. In the developing rat cortex, integrins were seen in the axons within the corpus callosum and readily travel towards the synapse in the corticospinal tract (Andrews et al., 2016). However, adult rat CNS neurons were unable to transport integrins a significant distance after injury. Retrograde transport is an important mechanism through which the regenerating axons can transduce transcriptional signals to the nucleus, so its impairment in injured CNS neurons could impact gene expression necessary for regrowth.

Within the PNS, neurons re-initiate and maintain a genetic program of re-growth, a phenomenon not achieved in the CNS. While up-regulation of the transcription factor cJun is observed after axonal injury in both the PNS and CNS, only the former can functionally regenerate (Leah et al., 1991, Herdegen et al., 1991, Ruff et al., 2012). cJun is an obligate dimer and its binding partner affects which genes are expressed (Angel and Karin, 1991). Therefore, it could be that cJun heterodimer partners necessary for regeneration are expressed in injured PNS neurons, but not in the CNS. Transcription factors are not the only proteins that are important for a successful regenerative response.

The proteins PTEN and SOCS3 prevent the CNS neuron from properly responding to injury by inhibiting the PI3K/Akt and JAK/STAT signaling pathways, respectively. Deletion of either protein increases axonal regrowth in the regenerating murine optic nerve and axon

extension is further enhanced with co-deletion (Smith et al., 2009, Park et al., 2008, Sun et al., 2011). In conditional knock out PTEN murine hippocampal neurons, severely reduced synaptic transmission at excitatory synapses was measured by pair-pulse ratio (Fraser et al., 2008). This was likely due to the structural abnormalities in postsynaptic densities visualized by electron microscopy as no defects were observed in presynaptic neurotransmitter release. In the developing cells of the optic nerve, PTEN/mTOR signaling decreases with age and 90% of adult cells show no activity until injured (Park et al., 2008). While PTEN is active during development, it must play a different role in response to axonal injury. Embryonic neurons that are implanted into the adult CNS are able to grow quite efficiently even within the inhibitory environment (Lu et al., 2012). This suggests that adult CNS neurons maintain the ability to regenerate but are not able to re-express genes necessary for regrowth.

Molecular manipulations to enhance axon regeneration

To identify proteins important for enhancing axon outgrowth in response to injury, the over-expression of one or multiple proteins in concert has been extensively studied. Aside from PTEN/SOCS3, transcription factors (TFs) are also common targets for manipulation. TFs are proteins that bind to DNA to regulate gene expression. Therefore, determining which TFs are necessary to promote axon regrowth is an attractive strategy to also identify putative downstream effectors. The TFs Jun and Atf3 are up-regulated in response to injury in DRGs (Tsujino et al., 2000). Jun and Atf3 have each been shown to increase neurite outgrowth *in vitro* in PC12 cells and sensory DRG neurons, with an additive effect when combined (Pearson et al., 2003, Chandran et al., 2016, Danzi et al., 2018). This outgrowth could not be repeated in early postnatal murine cortical neurons (Venkatesh et al., 2016, Danzi et al., 2018). However,

significant outgrowth was induced when forcing Jun and Atf3 to dimerize by expressing the proteins in a tethered form as a single polypeptide (Danzi et al., 2018). This suggests that the Jun-Atf3 dimer may not form endogenously when expressed as monomers, but that their dimer may outcompete endogenous complexes to bind DNA and affect transcription. This highlights that individual protein over-expression is likely not a feasible therapeutic strategy as transcription requires the cooperative activities of many proteins and multimeric complexes in addition to having the appropriate DNA regulatory regions exposed.

The PNS injury response is unlikely to be perturbed by manipulating one or two components due to the highly redundant nature and interconnectivity of signaling networks. In rat DRGs after sciatic nerve injury, several proteins have been identified as significant regulators of injury response as "hubs" whose manipulation could have substantial effects on signaling networks (Michaelevski et al., 2010). *In vitro* inhibition of PKCα/β isoforms, c-Abl (Abelson proto-oncogene), or p38 (a MAPK) decreased total neurite outgrowth between 24-48 hours after injury with the latter two kinases increasing branching frequency. Network analyses of the kinases predicted each to influence ≥ 25 TFs (Michaelevski et al., 2010). Therefore, determining how those kinases are regulated could provide more information regarding the molecular mechanisms of successful PNS regeneration.

Glial cells contribute to the overall likelihood that a neuron will successfully regenerate. Unlike in neurons after sciatic nerve injury, functional axonal regeneration is severely hindered *in vivo* when cJun is conditionally knocked out (cKO) in Schwann cells (Arthur-Farraj et al., 2012). After sciatic nerve damage in cJun cKO Schwann cells, there was increased death of Schwann cells and the sensory DRG neurons were twice as likely to die after injury (Arthur-

Farraj et al., 2012). Not only did the mutant motoneuron DRGs reach targets cells 55% as often as wild type, the cJun cKO axons that did manage to grow did not extend as far as wild type nerves. Schwann cells displayed aberrant morphology and regeneration tracks. Schwann cells form cellular columns that act as substrate to guide regrowing axons, so abnormal morphology likely contributed to the decreased reinnervation. Interestingly, reduced axon regrowth is apparently exclusive to injury as cJun had no effect on Schwann cell development or maintenance state function (Arthur-Farraj et al., 2012). This suggests that manipulation of both the neurons and glial cells will be necessary for adapting successful axon regeneration to the CNS.

Transcription factors (TFs) modulate gene expression

Transcription factors (TFs) are a class of proteins that directly interact with DNA to regulate gene expression. TFs bind to the regulatory regions of DNA (e.g., promoters and enhancers) and the combined activity of multiple TFs determines the temporal transcription of many genes to form gene regulatory networks. TFs regulate gene expression in a variety of fashions. For example, the activity can be cooperative in which one TF will depend on the DNA-protein interaction of another. Other times, the binding of a single TF to a regulatory element may enhance the transcription of a gene in an additive manner though interactions with another protein. Furthermore, the effect of a TF may not be through direct protein-protein interactions (PPIs), but by changing the conformation of DNA to facilitate the binding of another TF. Often, it is a combination of these modes of interactions which regulate the expression of gene. This is seen in interactions by “enhanceosomes” in which the interactions of many TFs act synergistically to arrange modules of protein-DNA complexes. Through these

mechanisms, the transcriptional output of a gene can be modulated to further fine-tune expression.

Transcription factors can be grouped into families that share similarities in the structure of their various domains which is often conserved across species (Fischer et al., 1988, Kakidani and Ptashne, 1988, Ma et al., 1988). Most TFs have three main domains: DNA binding, dimerization, and transactivation. The highest amount of homogeneity is seen in the DNA-binding and dimerization domains of a TF with greater degrees of variability in the transactivation domain. Many TFs are obligate dimers in that they must bind to another TF to exert their function. TFs may bind to an identical TF (homodimerization) or a different TF (heterodimerization) to form a dimer. Individual TFs or their dimers bind to DNA in a sequence-specific manner, in which they recognize short, cognate binding sites (Mangelsdorf and Evans, 1995, Fujii et al., 2000). The transactivation domain often undergoes post-translational modifications to alter the transcriptional activity of the protein. The interplay between all three domains of a transcription factor(s) determines the overall effect on gene expression via DNA sequence specificity, DNA binding affinity, and transcriptional activity.

The bZIP family, AP-1 complex, and cJun

One of the largest families of TFs in eukaryotes is the basic region-leucine zipper (bZIP) family (Landschulz et al., 1988). These proteins are obligate dimers and the physical interaction of their leucine zipper dimerization domains enables their ability to bind to their consensus DNA sequence. The leucine zipper domain contains leucine residues every seven amino acids (heptad sequences) which structures the domain into a coiled coil. The interaction between the leucine-containing α-helices of two bZIP TFs forms the bipartite interface of the dimer. The

amino terminal of the coil contains the basic residues that compose the DNA-binding domain while the other half coil nearer the carboxy terminal makes up the leucine zipper dimerization domain (Ellenberger et al., 1992). The two N-terminals of the dimer recognize “half-sites” and directly interact within the major groove of DNA in a sequence-specific manner. The human bZIP TFs contain 5-9 heptads within the zipper domain and the amino acid composition varies within the coiled coil. The hydrophobicity of residues at specific positions of the helix will affect the stability of the interaction between two bZIP TFs as well as the sequence-specificity of the DNA binding domain (Acharya et al., 2002). This is exemplified by the differing DNA binding preferences between specific heterodimers of Jun family members with either Fos or Atf family members (Hai and Curran, 1991, Danzi et al., 2018). Furthermore, other proteins, like the pX hepatitis B virus protein, can interact with bZIP monomers to stabilize the bZIP-DNA interaction and therefore affect otherwise endogenous dimerization formation (Schneider and Schepartz, 2001). The human genome contains 53 known bZIP proteins, so there are potentially 1,405 dimer compositions (Vinson et al., 2006). Therefore, the transcriptional regulation can be drastically altered by the presence of specific dimers.

The activator protein 1 (AP-1) is a bZIP dimeric protein of variable composition involved in many different cellular responses as a consequence of extracellular signals. Its over-expression is highly correlated with cancer in which, typically, upstream signaling events lead to up-regulation of one or more of the AP-1 components (Karin, 1995, Talotta et al., 2010). The conventional AP-1 dimer consists of Jun (cJun, JunB, and JunD) and Fos (cFos, FosB, Fra-1, and Fra-2) proteins, but sometimes includes other members from the Atf (Atf2 through 7, Batf, Batf2, Batf3, JDP2) and Maf (cMaf, Mafa, -b, -f, -g, -k, and Nrl) families (Hai and Curran, 1991,

Chinenov and Kerppola, 2001). Even with the diverse possibilities for heterodimer composition, AP-1 typically binds to three different palindromic sequences: cAMP-responsive element (CRE), TPA-responsive element (TRE), and Maf recognition element (MARE) I or II motifs. However, the various combinations of TFs within the AP-1 complex influences their DNA-specificity. For example, the Fos:Jun, Jun:Jun, and Atf-containing dimers prefer CRE motifs, while Maf-containing dimers bind either MARE I or MARE II motifs that are extensions of TRE and CRE motifs, respectively (Angel and Karin, 1991). The dimer composition is greatly influenced by the concentrations of the bZIP monomers with specific combinations stabilizing upon DNA binding (Patel et al., 1994, Kovary and Bravo, 1991). As a cell responds to extracellular signals, the expression of necessary genes can be modulated by the relative amounts of bZIP proteins, such as Jun.

The bZIP TF and immediate early gene cJun is a major component of the AP-1 complex and involved in numerous cell responses including growth factor stimulation and cell-stress (Angel et al., 1987). cJun is considered proto-oncogenes as it is over-expressed or up-regulated in many cancers such as glioblastoma, Hodgkin lymphoma, and breast cancer (Blau et al., 2012, Mathas et al., 2002, Smith et al., 1999). The role of Jun in regeneration is unclear as it is involved in both cell death and successful regeneration after axonal injury (Leah et al., 1991, Watkins et al., 2013). cJun has protective effects as it is necessary for PNS axonal regeneration, but it also up-regulated during apoptotic events such as during NGF-deprivation of neuronal PC12 cells (Leah et al., 1991, Mesner et al., 1995). However, there is evidence that cJun is phosphorylated by different kinases during these different events, but also may be interacting with different binding partners based on their varying levels of protein expression (Mesner et

al., 1995, Leppä et al., 1998, Le-Niculescu et al., 1999, Leppa et al., 2001). The activity and transcriptional role of Jun is dependent upon many factors including its obligate dimerization partner, post-translational modifications, as well as cell-type and context.

The role of cJun in gene regulation

As previously discussed, the exact dimer composition will determine the effect of the AP-1 complex. cJun is known to bind many other bZIP proteins and these dimers have various effects. This is, in part, due to differences in the DNA binding sequence specificity and affinity (Hai and Curran, 1991). Dimers of cJun and cFos show preference for TRE sequences whereas cJun and Atf2 efficiently bind CRE elements (Bakiri et al., 2002). This ability of cJun to homo- or hetero-dimerize enables combinatorial transcriptional control. For instance, dimer transactivation activity correlates with luciferase reporter assays of various promoters of genes with known binding motifs. cJun-Atf2 displayed poor activation of the TRE-containing *MMP1* promoter, but strongly activated the CRE-containing *Jun* promoter (Bakiri et al., 2002). Reasonably, the opposite was true for cJun-cFos dimers. The dimers of cJun with either Fra-1 or Fra-2, however, showed intermediate activation from either promoter sequence. This exemplifies how different binding partners of cJun can differentially regulate gene expression from the same DNA binding sequence *in vitro*.

In vivo, the DNA binding specificities of various dimers influence the choice in promoters, and therefore gene expression. cJun differentially stimulates axon extension depending on its binding partner. The cJun-Atf3 dimer drastically enhanced neurite length while cJun-Atf4 significantly hindered outgrowth in cultured early postnatal rat cortical neurons (Danzi et al., 2018). Similarly, the same cJun dimer can lead to different outcomes in different

cellular contexts. Whereas the cJun-Atf4 dimer decreased neurite length in cultured early postnatal rat cortical neurons (CNS), neurite length was increased by Jun-Atf4 expression in cultured sensory DRG neurons (PNS) (Danzi et al., 2018). Depending on the cell type and conditions, the dimerization partner of cJun can drastically affect cellular fate.

There are many factors that influence the choice of cJun's binding partner such as DNA sequence, electrostatic interactions, and thermodynamics. bZIP monomers are at a dynamic equilibrium with dimers in which there is active exchange between the unfolded and folded states in a concentration-dependent manner (Patel et al., 1994). The dimer is stabilized once bound to DNA. The affinity of cJun for another bZIP is dependent upon the exact distribution of hydrophilic and hydrophobic amino acids within both leucine zipper regions in which fewer repulsive interactions predicts a more likely event of dimerization (Vinson et al., 2002). DNA specificity requires a conformational change (coil to helix) within the DNA binding domain to correctly position the DNA-binding residues for sequence-specific interactions with nucleotides (Spolar and Record, 1994). The DNA sequence specificity of a dimer is dependent upon the net free energy loss which is an interplay between the loss of entropy from structural ordering and whether or not it is outweighed by the entropy gain from internalization of nonpolar residues upon complexing of bZIPs (Bracken et al., 1999, Hollenbeck et al., 2002). Therefore, DNA binding affinity and specificity are dependent upon the precise amino acid sequence of the DNA binding and bZIP domains which will vary from between individual bZIPs.

While dimerization and DNA sequence-specificity will influence which promoters are bound, the transcriptional activity of cJun is largely regulated by post-translational modifications. Phosphorylation by kinases is a key regulatory step in signaling to control many

cellular responses and processes. The transactivation domain of cJun contains four residues whose phosphorylation correlates most highly with transcriptional modulation: serines 63/73 and threonines 91/93 (Pulverer et al., 1991, Papavassiliou et al., 1995). Within the transactivation domain, the δ-domain of cJun acts as a binding or docking site for the kinase JNK which serves to both increase the accuracy and efficiency of phosphorylation (Hibi et al., 1993, Karin, 1995, Kallunki et al., 1996, Kallunki et al., 1994). Phosphorylation is enhanced by "specificity-conferring residues" that flank the phospho-acceptor serine or threonine, thus enabling differentiation between Jun family members (Kallunki et al., 1996). Furthermore, different isoforms of JNK have differential binding affinities for cJun (Gupta et al., 1996). As for specificity regarding cJun-containing dimers, certain kinases phosphorylate homodimers or heterodimers more efficiently depending on whether or not the dimer is bound to DNA (Abate et al., 1993). By discriminating against specific heterodimer compositions, phosphorylation events may contribute to the specificity of neighboring protein-protein interactions, recruitment of other proteins, or assembling higher order complexes.

Signaling through the JNK kinase is an important pathway that regulates cJun transactivation. In resting cells that are not actively proliferating, inactive JNKs are bound to the δ-domain of cJun which prevents phosphorylation of cJun's N-terminal transactivation domain (Dai et al., 1995). In response to cellular stressors like UV damage, JNKs are first activated, phosphorylate cJun at serine 63/73, and finally dissociate from cJun (Dai et al., 1995). Other proteins are known to bind to cJun's transactivation domain, as well, such as MBD3, a subunit of the nucleosome remodeling and histone deacetylation (NuRD) repressor complex. When the transactivation domain is unphosphorylated, MBD3 recruits NuRD to promoters bound by cJun

to repress transcription (Aguilera et al., 2011). After JNK activation, repression is relieved by JNK phosphorylating cJun which can then interact with other TFs, such as TCF4, to promote transcription (Aguilera et al., 2011). The docking site within the transactivation domain of cJun can modulate transcription by binding different factors.

The carboxy-terminal of cJun can also regulate its transcriptional abilities. Similar to the transactivation domains, this capability is typically resultant of post-translational modifications to specific amino acids. Within residues 226-249 of cJun's C-terminus near the DNA binding domain, serines and threonines can be phosphorylated by kinases such as glycogen synthase kinase 3 (GSK-3) and nuclear casein kinase II (CKII) to affect DNA-binding activity and transactivation potential (Baker et al., 1992). The dimer composition affects the extent of modification as cJun-cFos dimer phosphorylation is ten-fold less than that of cJun homodimers (Abate et al., 1993). cJun can also directly interact with proteins other than bZIPs and kinases. AP-1 and glucocorticoid receptor (GR) can either activate or repress transcription of AP-1-dependent genes stimulated by steroids (Diamond et al., 1990, Miner and Yamamoto, 1992, Teurich and Angel, 1995). As these promoters lack GR binding motifs and GR can differentiate between dimer composition and cJun phosphorylation state, the DNA binding domain of cJun mediates the interaction with GR. Post-translational modifications at cJun's C-terminal mediate its interaction with other proteins to modulate transcription.

Aside from phosphorylation, cJun can undergo other types of post-translational modifications. For example, the transcriptional co-regulator p300 has histone acetyltransferase activity and has also been shown to acetylate non-histone substrates (Bannister and Kouzarides, 1996, Ogryzko et al., 1996). In gliomas, both cJun and p300 have been shown to

directly interact with astrocyte elevated gene 1 (AEG-1), induce cJun and chromatin acetylation, and increase transcription of cJun downstream target genes (Liu et al., 2017). The up-regulation of these genes significantly promoted tumor cell proliferation and survival both *in vitro* and *in vivo* (Liu et al., 2017). While normally functioning to activate transcription, p300 has been shown to interact with both cJun and E1A (the adenovirus oncoprotein) to repress transcription at the collagenase promoter (Vries et al., 2001). The acetylation of cJun's lysine 271 by p300 is essential to repress this transcription and is acetylated both *in vitro* and *in vivo* (Vries et al., 2001). Ubiquitination is another post-translational modification that influences the fate of cJun. Under normal cellular conditions, cJun is rapidly turned over, with evidence suggesting that its stability is regulated by its state of ubiquitination (Jariel-Encontre et al., 1997, Treier et al., 1994). Multi-ubiquitin chains attached to proteins mark them for degradation by the proteasome complex while deubiquitinating enzymes remove these chains to increase the protein's half-life. The ubiquitin-specific protease 6 (USP6) protein prevents cJun degradation by removing ubiquitin and its expression in cancer cells increases the stability of cJun and its down-stream signaling pathways (Li et al., 2018). Therefore, post-translational modifications regulate cJun transcriptional activity and stability by mediating its interactions with other proteins.

The exact mechanisms by which cJun activity is regulated to direct axon regrowth remains unclear, but there are many cases outside of regeneration in which cJun interacts with other proteins to carry out its transcriptional effects. These interactions can be between proteins directly or indirectly bound to the same DNA regulatory element. When bound to promoters, cJun can initiate transcription by directly interacting with subunits of the general

transcription machinery or by recruiting other factors to do so. Residues within the bZIP region of cJun directly interact with the N-terminus of the human TBP-associated factor-1 (hTAF1), causing a de-repression of TFIID-driven transcription (Lively et al., 2004). cJun can also activate transcription through interactions with other proteins such as the TATA box-binding protein (TBP) (Ransone et al., 1993). Importantly, TFs bound to DNA can interact with other TFs that are not actively bound to a regulatory element. Within the promoter of the gene encoding the cytokine interleukin 2 (IL-2), there are many TF binding sites including one nuclear factor of activated T-cells (NFAT) binding motif and four antigen receptor response element 2 (ARRE2) composite sites (Rooney et al., 1995). While three of the ARRE2 motifs can be bound by NFAT and AP-1, the NFAT motif coordinates the synergistic activation of IL-2 by these TFs in which the C-terminal activation domain of NFATc2 binds to the bZIP domain of free cJun homodimers (Walters et al., 2013). These examples show that cJun can regulate gene expression through different protein-protein interactions.

In addition to directly interacting with other proteins to regulate transcription, it has been posited that cJun can induce conformational changes in DNA to affect binding of other proteins. This binding, in turn, may open or close binding sites for other TFs. DNA acts like a flexible chain at a long length of many hundreds to thousands of nucleotide pairs, but is much stiffer when viewed as a short fragment of <300 base pairs (Wang and Giaever, 1988). The Fos and Jun proteins induce bends in DNA in opposite directions such that there is a 200° difference in the relative orientation of DNA between cFos-cJun and cJun-cJun dimers (Kerppola and Curran, 1991). By reducing the thermodynamic barrier posed by the unfavorable free energy of looping the short DNA fragment within a gene promoter, cJun dimers may facilitate the

interactions of nearby proteins with DNA or one another. This suggests that cJun dimers may play a larger role in the assembly of multi-protein transcriptional complexes by altering the local topology of DNA.

The accessibility of TF binding sites is dependent upon both the high-level chromatin organization and local positioning of nucleosomes (Pique-Regi et al., 2011). Most TFs require chromatin to be open and accessible to bind to their recognition motifs (Li et al., 2011). The chromatin landscape varies between cell types in which different regulatory elements are exposed, conferring differential gene expression (Natarajan et al., 2012). Amongst open, nucleosome-depleted regions of the genome that overlap between different cell types, promoters near transcription start sites are prominent, especially for genes with tissue-independent expression, e.g., housekeeping genes (Handstad et al., 2012, Song et al., 2011). Chromatin accessible only in a specific cell type tends to be in enhancers away from transcription start sites that are sensitive to DNaseI and Formaldehyde Assisted Isolation of Regulatory Elements sequencing (FAIRE-seq) (Song et al., 2011). Furthermore, cell type-specific gene expression is regulated by TF occupation of DNaseI-hypersensitive enhancers with acetylated H3K27 markers, histone post-translational modifications associated with DNA in an open conformation (Heintzman et al., 2009, Song et al., 2011). The location of open chromatin within the genome influences both active genes and cell-type specificity.

The AP-1 complex has been implicated in both maintaining a state of open chromatin as well as inducing chromatin accessibility. In breast cancer cells, cytokine IL-6 transcription is elevated with a concomitant increase in cJun protein levels and occupation of the IL-6 promoter along with other AP-1 and NF-κB factors (Ndlovu et al., 2009). Both IL-6 transcript and cJun

protein levels were higher in more malignant cancer cells than less invasive cell types supporting the role of cJun and IL-6 expression in advanced progression cancer. Interestingly, chromatin accessibility and transcription of IL-6 were most highly impacted by knocking down multiple TFs, suggesting an important interplay between several TFs for determining chromatin environment and gene expression. In murine mammary epithelial cells, cJun-cFos dimers facilitate the repositioning of nucleosomes to expose glucocorticoid receptor (GR) binding sites, recruiting GR at ~50% of its binding sites in the genome (Biddie et al., 2011). Analysis of 72 cell types in 112 human samples revealed that Jun-Fos binding motifs were the most highly enriched binding motif within both cell type-specific and nonspecific DNaseI-hypersensitive sites (Sheffield et al., 2013). Due to this ubiquitous AP-1 binding motif prevalence, this could indicate that cJun acts as a pioneer factor to promote open chromatin or that it may require other factors to do so. While these data support Jun's role in influencing chromatin accessibility in different cell types, there is evidence that this effect could be temporally regulated.

Differential expression of TFs and changes in chromatin state are observed during development, differentiation, and regeneration. During mammalian development, regeneration capability is down-regulated in the CNS. In comparison to postnatal rat retinal ganglion cells (RGCs, low intrinsic growth capacity), the regeneration-associated TFs Smad1, Myc, Jun, Klf2, and Klf9 had higher levels of transcription in embryonic RGCs (high intrinsic growth capacity) (Pita-Thomas et al., 2021). Furthermore, the promoters of those TFs were also more open in embryonic cells. TF binding motif analysis revealed that CREB, MYC, HIF1, and c-JUN were more prevalent in embryonic RGCs than postnatal suggesting that the genes they regulate may vary depending on the cell context. In induced-pluripotent stem cells and neural progenitors, cell

programming is influenced by stage-specific TFs and enhancer availability (Chronis et al., 2017, Mattar et al., 2021). Similarly in regenerating neurons, the peak expression of groups of TFs and chromatin accessibility change throughout the time course of regeneration. Analysis of crushed DRG cells in adult rats revealed that Jun, Fosl1, Atf3, Klf6, Myc, and Fos transcript levels were highest during the stage in which genes associated with axonal regeneration, the immune response, and neuropathic pain were up-regulated (Zhao et al., 2023). Within the regeneration-capable CNS of zebrafish, changes in TF transcript levels and chromatin state were observed as regenerating RGCs re-grew from the site of injury to their targets within the optic tectum (Dhara et al., 2019). While most transcriptionally accessible regions of chromatin did not change throughout the time course of regeneration, differentially open chromatin was mainly observed during early or late regeneration. Interestingly, each stage of regeneration was characterized by a distinct set of TFs that displayed peak transcription levels. This suggests that the varying levels of TFs expressed at different times is what controls differential gene expression. It is likely that cascades of TFs act to progressively alter the chromatin landscape, but how these changes in molecular signals and DNA conformation interact to control temporal cellular identity transitions remains unclear.

Protein-protein interactions (PPIs) are dynamic and influence cell fate

All aspects of cellular functions are dependent upon the interactions of proteins with one another. Important cellular processes such as DNA replication, transcription, and protein translation rely on the formation of protein complexes which involve direct protein-protein interactions (PPIs). More transient PPIs, such as post-translational modifications, are also necessary for events such as enzyme activation and cellular signaling propagation. Regardless of

the type of PPI, all are dependent upon a multitude of factors including relative protein abundance, affinity, and cellular environment. Diseases such as Huntington's, amyotrophic lateral sclerosis (ALS), Parkinson's disease, and many more are characterized by irregular structure, function, or cellular localization of a protein, thereby leading to detrimental health outcomes (Labbadia and Morimoto, 2013, Brown et al., 2022, Van der Perren et al., 2020). Proper protein function underlies both normal cellular function and, ultimately, quality of life.

The PPIs of cJun can change depending on its post-translational modifications and/or presence of other proteins, potentially resulting in drastically different outcomes. For example, the acetylation of cJun and its interaction with E1A may switch its transcriptional effect. The acetylation of lysine 271 of cJun within its DNA binding domain is necessary for E1A-mediated repression of the collagenase promoter both *in vitro* and *in vivo* (Vries et al., 2001). In the same cellular context, p300/CBP binds to the topologically-associating domain (TAD) of cJun and may switch its acetylation activity from histones to cJun in the presence of E1A as indicated by mutation and acetylation assays (Vries et al., 2001, Duyndam et al., 1999). Like their effect on cJun, both p300 and E1A activate ATF2 by acetylating its N-terminal domain, stimulating *cjun* expression (Duyndam et al., 1999). Post-translational modifications to cJun and ATF2 can either activate or repress transcription.

Dimerization of cJun can affect cellular localization and degradation of other TFs. These outcomes may vary depending on cell context. ATF2 contains a nuclear export signal within its bZIP domain but remains localized to the nucleus upon heterodimer formation with cJun (Liu et al., 2006). Ubiquitination and degradation of ATF2 is dependent upon heterodimerization with cJun and phosphorylation by JNK in 293T human embryo kidney cells (Fuchs and Ronai, 1999).

Conversely, dimerization of ATF2 and cJun is essential for activation of the *cjun* promoter in murine F9 cells (Liu et al., 2006). The TRE binding motif within the *cjun* promoter is constitutively bound by cJun-ATF2 dimers, but the gene is not actively transcribed until the heterodimer is phosphorylated by JNK (Rozek and Pfeifer, 1993, Devary et al., 1992). Depending on the cellular context, cJun heterodimerization can either potentiate its own expression or promote proteasome-dependent degradation.

Transcription is affected by the binding partner and the post-translational modifications of cJun. Phosphorylation of a cluster of amino acids near the DNA binding domain of cJun will inhibit DNA binding as a homodimer, but not as a cFos heterodimer (Boyle et al., 1991). Conversely, phosphorylation of serines 63 and 73 within cJun's transactivation domain enhance its transcriptional abilities as either a homo- or heterodimer with cFos (Pulverer et al., 1991, Smeal et al., 1991, Deng and Karin, 1994). Phosphorylation of the homologous cJun serine 73 site in cFos (threonine 232) also stimulates cFos activity (Sutherland et al., 1992). While serine 73 of cJun is phosphorylated by JNK1/2, however, threonine 232 is modified by a different MAPK, FRK (Deng and Karin, 1994). Dimer composition, DNA binding, and phosphorylation state influence the transcription efficiency of cJun.

As evidenced by these examples, the stable (e.g., dimerization) and transient (e.g., post-translational modification) PPIs of cJun and other TFs dictate their DNA binding preferences, stability, and transcriptional abilities, and thus cellular outcomes and fate. Some of the common techniques used to resolve these interactions will be reviewed.

Current methods to detect PPIs

Methodology to identify PPIs can widely be grouped into discovery and validation methods. These approaches are best used together in which PPIs are first predicted and then validated. Methods that detect specific proteins via their stable interactions are validation methods, such as co-immunoprecipitation and affinity or tandem affinity purification. They identify strong binding between two or more proteins in a larger complex. PPI discovery methods reveal potential interactions with other proteins, ranging from direct to indirect as well as one to hundreds of possible interactors. Such methods to identify potential PPIs are DNA binding site analysis, *in silico* computation, and proximity labeling.

In co-immunoprecipitation methods, a protein of interest is immunopurified from a protein lysate which is then subsequently probed via Western blot using an antibody for a predicted interacting protein. These assays are easy to perform and detect endogenous interactions as proteins remain in their native form. However, immuno-based methods require the use of antibodies which require time-consuming validation and are biased towards highly-used model systems. Furthermore, many antibodies are developed using peptides and the epitope may not be detected in a protein's native form due to protein folding and post-translational modifications. This limitation can somewhat be overcome by analysis with mass spectrometry (MS). Co-immunoprecipitation will detect just the interaction between two proteins, but MS is able to identify other proteins that may be complexing with those. For instance, out of 63 identified proteins, co-immunoprecipitation-MS revealed novel interactors of a highly invasive p53 variant in a human non-small cell lung carcinoma cell line (Coffill et al., 2012). Immuno-based methods are more reliable as higher affinity antibodies are developed

but are limited to common model species and un-validated antibodies require extensive time and resources to qualify.

Affinity or tandem affinity purification involves genetically tagging a protein of interest to determine direct binding partners of a heterodimer or larger protein complex using one or more affinity purification steps, respectively. After isolating the protein from either method, the material can be characterized in multiple fashions, including Western blot or MS. In tandem affinity purification, two genetic tags are tethered via a Tobacco Etch Virus (TEV) site for two elution steps, thus increasing the purity of the collected protein and decreasing non-selective binding (Puig et al., 2001). Tandem affinity purification-MS was used to map the yeast interactome of 1,440 distinct gene products, mapping 549 proteins with 78% of those presenting protein partners (Gavin et al., 2002). Gentler washes are used in tandem affinity purification as compared to co-immunoprecipitation, leaving the protein complex in a native state for additional downstream functional assays. Affinity purification assays tend to over-express the protein of interest which may bias results toward non-physiological interactions or chaperone/heat-shock proteins due to misfolded bait proteins (Swaffield et al., 1995). Furthermore, affinity purified proteins may have higher background due to non-specific bead binding and are biased towards high-abundance proteins with stable or high-affinity PPIs (Von Mering et al., 2002). Affinity purification methods can validate endogenous PPIs but are limited to stable protein complex formation.

While immunoprecipitation methods focus on the interactions of one or two proteins, protein microarrays are high throughput and easy to interpret. Typically, either antibodies or full-length/fragments proteins are immobilized on a glass surface which is then probed with a

protein lysate or purified protein of interest. Interactions can be determined by fluorescence, affinity, or other methods. Protein microarrays are commonly used to screen patient samples for immune deficiencies, disease detection, and personalized medicine (Rosenberg and Utz, 2015, Jayaraman et al., 2020, Neagu et al., 2019). Microarrays are useful for screening up to thousands of PPIs but are limited in that they do not reflect physiological conditions and rely on pre-selected targets. While protein microarrays are capable of confirming PPIs in high-throughput, the interactions may require further validation *in vivo*.

There are also discovery assays that are solely based on prediction from previously obtained data or computer models. These are typically derived from chromosome proximity data (ChIP-seq) or structure- or sequence-based approaches (*in silico*). Chromatin immunoprecipitation sequencing (ChIP-seq) data is unbiased towards specific DNA-sequences, can be cell- or context-specific, and delivers massive datasets for a genome-wide view of chromatin binding dynamics. These interactions are only inferred based on DNA binding site proximity and thus require validation. Not all TFs directly interact when bound to adjacent TF binding motifs and many TFs have varying affinity for specific DNA sequences depending on their binding partner. High throughput ChIP-seq analysis of two human colorectal cell lines revealed that many actively bound TF binding sites were at low-affinity DNA sequences suggesting that cooperative TF interactions influence DNA specificity and binding (Yan et al., 2013). This highlights the importance of testing for direct physical interactions as binding site analysis does not always reflect the physiological interactions of TFs.

Computational methods are capable of developing approaches to understand and predict a whole range of putative PPIs. There are several different in silico approaches including

sequence- or structure-based, phylogenetic conservation, and gene ontology. Based on structural similarity, the interaction of two proteins can be predicted using known crystal structures or by creating algorithms inferred from a sequence of a protein with unknown structure (Hosur et al., 2011, Zhang et al., 2012a). Using the theory that proteins may show similarity in interactions through co-evolution, PPIs can be approximated between proteins between different organisms using the distance within a phylogenetic tree (Craig and Liao, 2007). Many computational analyses are open-source and are fast at delivering potential PPIs, albeit at a lower confidence score without functional validation.

Proximity labeling identifies putative PPIs

Transcription is tightly regulated and therefore requires the interactions of many proteins within the promoter/enhancer as well as post-translational modifications to those proteins. These are important interactions necessary for transcription and such transient or further distance interactions are missed by traditional methods for investigating PPIs. Therefore, a proximity labeling-MS approach is ideal to predict how the PPIs of TFs change over a time course. The original biotin proximity labeling ligase has evolved through three generations of enzymes to address different drawbacks of each. The advantages, disadvantages, and caveats of each enzyme will be discussed.

Proximity labeling detects endogenous protein interactions as they are occurring in the cell. As the interacting proteins are labeled *in vivo*, low affinity or transient interactions will not be removed with stringent washes unlike affinity purification or immunoprecipitation methods. In this technique, an engineered enzyme is genetically linked to a protein of interest and will covalently tag neighboring proteins with activated biotin within a small radius (Fig. 1, left).

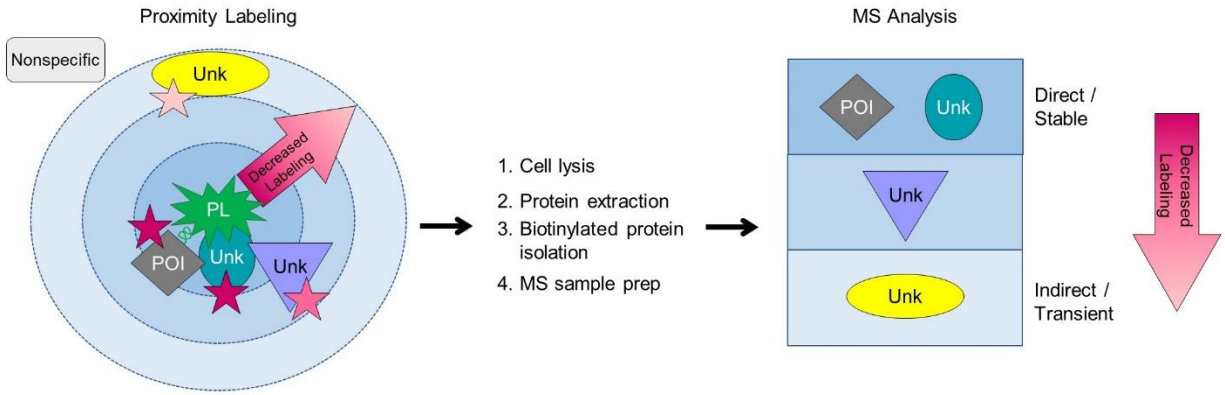

Figure 1: **Schematic and workflow of proximity labeling technique**. *Left*: The engineered proximity labeling enzyme (PL, green explosion) is genetically tagged to the protein of interest (POI, grey diamond). The enzyme will covalently tag neighboring proteins with biotin within proximity to its catalytic site (radius of outer blue circle). The extent of tagging of a particular protein will depend upon both the stability of its interaction with the protein of interest and its distance from the enzyme active site (decreasing blue intensity of "bull's eye" emphasized by pink ombre arrow). The proteins that are farther away from the enzyme are less likely to be labeled (fewer tags represented with lighter pink stars). The proteins with the most tags (denoted with the darkest pink star) will be within close proximity of the protein of interest and have stable interactions. *Middle*: After proximity labeling is performed, cells are lysed, and the total protein is extracted. The labeled proteins are isolated and prepared for analysis by mass spectrometry (MS). *Right*: Following analysis of MS data, the identified proteins are ranked to determine direct versus indirect protein-protein interactions. Based on their proximity to the protein of interest, it is predicted that direct interactors will include the protein of interest itself along with any stably binding proteins, such as dimerization partners. Indirect interactions include both proteins near the protein of interest, such as those farther away within a multi-protein complex, and also transient interactions, such as those by modifying enzymes.

The extent that a neighboring protein will be labeled is dependent upon two main factors: the stability of its interaction with the protein of interest and its distance from the enzyme catalytic site. The extent of labeling is represented by an arrow with a decreasing pink intensity (Fig. 1). The probability of a protein being labeled is dependent upon the distance from the enzyme catalytic site and the amount of time they reside within the labeling radius. Therefore, the least-labeled proteins will be farther away from the protein of interest and/or will have fleeting interactions. These may be proteins located within the labeling radius or proteins that may physically interact with the protein of interest transiently, such as post-translational modifying enzymes. The most highly labeled proteins will be within close proximity of the protein of interest and will have stable interactions. This will include proteins that directly bind to the protein of interest, such as other proteins within a larger complex, and also the protein of interest itself.

To determine which proteins are putative interactors with protein of interest, proximity labeling is performed to label nearby proteins. The labeled proteins are specifically isolated using streptavidin magnetic beads and analyzed via MS. After quantitative MS, a contour map is made, and the proteins are ranked based on the extent of labeling (Fig. 1, right). The proteins most highly represented in the data should be direct interactors. As the extent of labeling decreases, the interactions are less stable, or the proteins are farther away from the protein of interest. Nonspecific proteins should not be present in the data as they are removed when the labeled proteins are isolated.

Most proximity labeling techniques to examine TF interactomes have used the engineered biotin ligase, BioID. This inaugural generation of biotin-based proximity labeling

enzymes uses an engineered enzyme derived from the *E. coli* BirA biotin ligase (Roux et al., 2012). In this method, BioID combines biotin with ATP to form biotinoyl-5'-AMP which reacts with primary amines in proteins near the modified BirA enzyme catalytic site (Choi-Rhee et al., 2004). For detectable biotinylation to occur, cells must be supplemented with biotin and labeled over a 24-hour period to generate sufficient levels protein to be detected by fluorescence microscopy, Western blot, or MS. BioID has been used to identify putative interactions of the nuclear pore complex and nuclear lamina, but has also been used with TFs (Kim et al., 2014, Mehus et al., 2016).

To investigate the temporal factors involved in the transition of retinal progenitor cells to neurons and glia, the PPIs of the Casz1 zinc finger TF were examined using BioID proximity labeling (Mattar et al., 2021). In perinatal murine primary retinal cell cultures, Casz1-BioID detected several core subunits of the nucleosome remodeling and deacetylase (NuRD) complex which were validated using immunoprecipitation methods. Both pharmacological inhibition and CRISPR interference of Hdac1/2 of NuRD biased cultured retinal progenitor cells towards the fate of Müller glia over rod cells versus controls, mimicking the results seen in *Casz1*$^{Flox/Flox}$ explants. The linker histones Hist1h1b/d (H1.3 and H1.5), and histone 2B were also revealed with BioID, implicating a role for Casz1 in heterochromatin compaction. These proximity labeling results support the role of Casz1 in determining cell fate in retinal progenitors.

BioID was used to identify 140 putative TWIST1 (basic helix-loop-helix TF) interactors including 4 of 56 known interacting proteins (TCF3, TCF4, TCF12, and GLI3) in the cranial NCC cell line O9-1 (Fan et al., 2021). Among these were proteins that participate in chromatin organization, cranial skeletal development, and ribosome biogenesis. Also identified were

chromatin regulators that interact with TWIST1 exclusively in NCCs versus 3T3 fibroblasts: chromodomain helicases (CHD7, CHD8), a histone methyltransferase (WHSC1), and a member of the SWI/SNF complex (SMARCE1). The physical interaction of TWIST1 amino terminal with CHD7/8 was verified using co-immunoprecipitation, but SMARCE1 did not display any significant interaction. Furthermore, CRISPR knockout experiments of TWIST1 and CHD8 showed a genetic interaction between the two proteins, resulting in significantly exaggerated morphological defects in embryonic mice over single-gene mutants. Proximity labeling-MS elucidated the interactions of the TF TWIST1 with previously unknown epigenetic modifiers.

The TF Sox2 has been implicated in the development of squamous cell carcinoma but is difficult to target for cancer treatment as it lacks a small molecule binding domain (Bass et al., 2009). To circumvent this problem, BioID was used to identify putative interactors of Sox2 in 293 T-REx cells (Kim et al., 2017). Of 82 high-confidence interactors including Jun, 44% had not been previously identified including chromatin modifiers and remodeling complexes. The localization of the histone acetylase EP300 within 30 nm of Sox2 was validated using proximity ligation assays in both basal and squamous cell carcinoma cells and was further validated using shRNA knock-down. EP300 contains several PPI regions and an autoregulatory acetyltransferase RING finger domain which makes it an attractive target for chemical modulation. proximity labeling can identify potential therapeutic targets of proteins that are otherwise refractory to common inhibitors and drugs.

BioID has revealed the interactomes of other TFs such as Hox and OsFD1, but the long labeling periods are unsuitable for studying the rapid kinetics involved in dynamic cellular processes (Carnesecchi et al., 2020, Lin et al., 2017). Two biotin ligases were evolved from a

BirA mutant using yeast display coupled to fluorescence activated cell sorting (FACS) to select for higher greater enzymatic activity (Branon et al., 2018). Two enzymes were generated with different molecular masses: TurboID (35 kDa) and miniTurbo (28 kDa). Both ligases have a similar substrate specificity as BioID, but significantly higher catalytic activity: TurboID and miniTurbo are 9-31 fold and 7-26-fold more active than BioID, respectively. The extent of biotinylation increases with longer labeling period, detectable in just 10 min by Western blotting. Furthermore, TurboID is functional at lower temperatures than BioID and non-lethal in both *c. elegans* and *drosophila* which grow at 20°C and 25°C, respectively. The higher catalytic activity combined with the ability to function at a broader range of temperatures enhance the efficiency of PPI detection of TurboID enzymes over BioID. As such, TurboID is instrumental to determine the PPIs of over a much shorter time span than 24 hours.

Table 1: Proximity labeling enzymes.

Enzyme	Mass	Labeling Period	Substrate
BioID	35 kDa	18-24 h	Biotin
TurboID	35 kDa	≥ 10 min	Biotin
miniTurbo	28 kDa	≥ 10 min	Biotin
APEX2	28 kDa	1 min	Biotin phenol, H_2O_2

The TF forkhead box transcription factor 1 (FOXO1) has been implicated in the development of many diseases and its PPIs were investigated to determine its mechanism of action induced by cytotoxicity. A cell line was created to stably over-express FOXO1-TurboID in U251 astrocytes (Su et al., 2023). In cells over-expressing FOXO1, 176 proteins were identified while cells treated with lipopolysaccharide contained 227 interacting proteins. Due to their roles in gene expression regulation, transcriptional activation, and DNA repair, the physical interaction between heterogeneous nuclear ribonucleoprotein K (hnRNP) and RNA-binding

motif protein 14 (RBM14) with FOXO1 were verified using immunoprecipitation and immunofluorescence techniques. Further gene ontology and pathway analyses of the putative PPIs suggest that FOXO1 may play a role in several biological processes ranging from ribosome maintenance to cholesterol metabolism.

Using TurboID-MS, the potential PPIs of a TF in a rare *Arabidopsis* sub-type were identified. Due to their natural low abundance, investigating the PPIs of TFs is made even more difficult in rare cell types, such as stomatal guard cells. Using affinity purification-MS methods, the only interactor of the basic helix-loop-helix TF, FAMA, detected was its obligate dimerization partner, INDUCER OF CBF EXPRESSION 1 (ICE1), even when using large amounts of sample material and cross-linking agents (Mair et al., 2019). To determine the feasibility of proximity labeling, the FAMA-TurboID was expressed in guard cells of seedlings and labeled for 3 hours (Mair et al., 2019). Of the 44 high-confidence proteins that were identified, ten were detected in previous studies within the guard cell proteome. A novel interactor, the histone reader, SHL (SHORT LIFE), was present which is known to bind histones at active promoters and has been associated with seed dormancy and flower repression, suggesting that FAMA plays a role in determining cell fate.

While the labeling period of the TurboID enzymes is significantly shorter than that of BioID, the latest generation of proximity labeling enzymes can detect PPIs in a minute or less. The APEX2 enzyme is derived from the ascorbate peroxidase of soybeans and its substrate is a biotin derivative, biotin phenol. As a peroxidase, APEX2 will only oxidize biotin phenol in the presence of hydrogen peroxide. The labeling reaction is performed for just one minute and then quenched to neutralize radicals (Roux et al., 2012, Branon et al., 2018, Lam et al., 2015).

Due to the short lifespan of radicals (< 1 ms), activated biotin phenol will covalently attach to electron-rich side chains of proteins within an ~10 nm radius (Mortensen and Skibsted, 1997, Hung et al., 2014, Hung et al., 2016). Due to the short labeling time frame, a snapshot of PPIs can temporally resolve fast-acting cellular processes, such as phosphorylation, that are not captured by conventional PPI detection techniques. Resultant to the dependence of APEX2 on hydrogen peroxide, BioID and the TurboID enzymes are better suited for *in vivo* applications due to the tissue-toxic conditions required for APEX2-based proximity labeling. However, the one-minute labeling period of APEX2 can resolve rapid and time-dependent PPIs.

Proximity labeling reactions are performed at specific time points to spatiotemporally resolve PPIs. APEX2 revealed the dynamic interactions of the GPCR δ-opioid receptor (DOR) upon agonist stimulation (Lobingier et al., 2017). Using organellar proteins as sub-cellular references, identification of WWP2, a HECT family ubiquitin ligase, and TOM1, a ubiquitin binding protein, suggest that the molecular mechanism of DOR down-regulation involves endosomal sorting to the lysosome. APEX2 proximity labeling of angiotensin II type 1 receptor (AT1R) and β2 adrenergic receptor (β2AR) could successfully detect PPIs, both known and novel, during 10 second intervals within the first minute of agonist stimulation (Paek et al., 2017). The MS results suggest that the vast majority of G proteins remain in the membrane during endocytosis, a scenario that contradicts the classical view of GPCR signaling. APEX2 is capable of detecting PPIs that both determine sub-cellular localization and those that may be functionally relevant in rapid GPCR signaling.

APEX2 proximity labeling has successfully detected the interactions of TFs in *D. melanogaster* S2 cells. Proximity labeling verified the nuclear localization of the EcR/Usp

heterodimer, known as the molecular sensor to 20-hydroxyecdysone (20E)-dependent developmental genes (Mazina et al., 2020). The chromatin architectural protein, CP190, was highly enriched in response to 20E treatment from both EcR and Usp identified by APEX2. A combination of co-immunoprecipitation, ChIP-seq, and HiC data revealed that CP190 physically interacts with Ecr, co-localizes with a small portion of sites bound by EcR within the genome, and the CP190-bound sites are not within the differentially accessible regulatory regions of 20E-dependent genes. These data suggest that CP190 binds to EcR via a chromatin looping mechanism. Proximity labeling-MS in combination with PPI validation and chromatin conformation techniques can elucidate gene regulatory mechanisms.

PC12 cell culture as a model to investigate neurite extension

Cell culture is an excellent model to study PPIs within a native environment. Other *in vitro* techniques performed outside of the cellular environment remove the complex variables that occur endogenously and profoundly affect PPIs. Immortalized cell lines are especially useful in that they are well characterized, easy to culture, and expand indefinitely. Many cell lines have been used for decades across many labs and their use is well established. In comparison to primary cell culture, immortalized cells are straightforward to grow, and necessary reagents are widely available. Due to their robust and rapid expansion, cells are easy to collect in amounts required for protein analysis by MS. While PPIs detected in cell lines may not reflect the exact PPIs that occur in intact tissue, they provide a good model for optimizing the molecular tools that can be subsequently used to detect PPIs under more native conditions. This is especially evident for studying neurons that are usually encased within the skull or spinal cord, exemplifying cell culture for neurological research.

In my studies, I have utilized a rat pheochromocytoma cell line (PC12) to model neuronal differentiation. PC12 cells originated from adrenal cells for their ability to spontaneously form neurites. In 1976, a single cell clonal line derived from the tumor cells was established and characterized for various properties as they respond to nerve growth factor (NGF) (Greene and Tischler, 1976). From the American Type Culture Collection (ATCC), the chromaffin cells are either adherent or suspension and will extend neurites after three days of NGF exposure (Wiatrak et al., 2020). Neurites continue to grow when continuously exposed to NGF and will eventually form functional synapses with one another (Fig. 2). The NGF-induced differentiation into sympathetic-like ganglion neurons is characterized by neuronal morphology, synapse formation, and electrical excitability. After removal of NGF, cells return to a proliferative state, lose their neuronal properties, and function once again as neuroendocrine cells (Greene and Tischler, 1982). This model has been used successfully to study both the effects of various toxins on neuronal differentiation and also the pathophysiology neurodegenerative diseases.

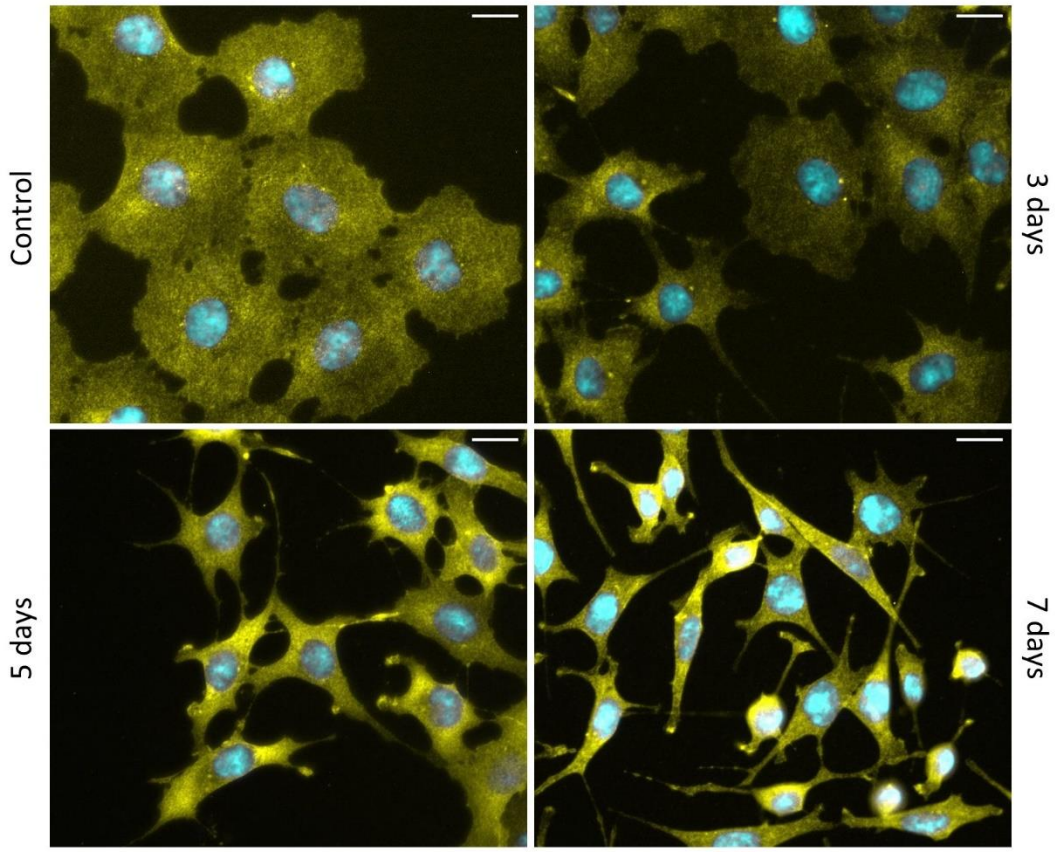

Figure 2: NGF-induced neuronal differentiation of PC12 cells. PC12 cells adopt a neuronal morphology when continuously exposed to nerve growth factor (NGF). *Control*: Cells with no NGF that have been cultured for three days. *3 days*: Cells cultured for three days with constant NGF. The cell bodies begin to contract, and neurites extend from some cells. *5 days*: Soma contraction and neurite extension/elongation continue. *7 days*: Cells adopt a neuronal morphology and search for synaptic connections. Media exchange was performed every other day either with or without 100 ng/µL NGF. Yellow pseudo-coloring marks the cell membrane while cyan is DAPI staining for the nucleus. Scale bar is 10 µm.

PC12 cells have been utilized for mechanistic studies as models for developmental neurotoxicity. For example, evidence suggests that early environmental exposure to many chemicals and metals may predispose one to developmental disorders ranging from ADHD to cerebral palsy (Szpir, 2006). Using PC12 cells, both undifferentiated and differentiating cells were exposed to different pesticides and nickel, then evaluated for short- and long-term exposures (Slotkin et al., 2007). With only one hour of exposure at 5 μM concentrations, a statistically significant reduction of cell replication was observed with increasing concentrations further exacerbating DNA synthesis (Slotkin et al., 2007). In differentiated PC12 cells, membrane receptors favored a catecholaminergic phenotype over cholinergic, consistent with the role of organophosphates as cholinesterase inhibitors (Slotkin et al., 2007). A similar study examined the effect of nontoxic silver levels on PC12 cell differentiation (Powers et al., 2010). One hour exposure to 10 μM silver in undifferentiated cells significantly inhibited DNA synthesis with longer exposures increasing oxidative stress and leading to reduced viability (Powers et al., 2010). Upon NGF-induced differentiation, DNA inhibition and oxidative stress were further exacerbated, and neurite formation was compromised and again favored dopaminergic phenotypes over cholinergic (Powers et al., 2010). PC12 cells have also been used to study neurodevelopment outside of toxicology. While PTEN is usually implicated in tumor development, overexpression studies in undifferentiated PC12 cells showed significant changes in the expression of several genes that mediate the neuronal phenotype, including the NGF receptors, suggesting that it may influence neuronal development (Musatov et al., 2004). The inducible neuronal differentiation ability of PC12 cells provides an easy-to-use model for *in vitro* neurodevelopmental studies.

To model many neurodegenerative diseases, PC12 cells have been instrumental in elucidating neurobiological mechanisms underlying disease progression. A hallmark of Alzheimer's disease is the formation of Aβ plaques. The small molecule Artemisinin was shown to prevent amyloid β-peptide-induced cell death associated with Alzheimer's disease (Zeng et al., 2017). These cells also provide a useful model to study the effects of small molecule treatments to better understand the pathophysiology of neurodegenerative diseases. A key characteristic of amyotrophic lateral sclerosis (ALS) is the progressive loss of motor neurons. Several cyclohexane-1,3-dione (CHD) derivatives have been developed as possible therapeutics for ALS using a familial G93A superoxide dismutase (SOD1) mutant of PC12 cells (Zhang et al., 2012b). A main feature of Parkinson's disease is a loss of dopaminergic neurons leading to motor deficiencies. Conserved dopamine neurotrophic factor (CDNF) increased cell viability in the 6-hydroxydopamine (6-OHDA) PC12 model of Parkinson's disease as evaluated by TUNEL staining and MTT assays (Mei and Niu, 2015). The neuronal morphology of PC12 cells provides an excellent platform for studying diverse cellular mechanisms in the development of neurological disease.

The role of cJun in neuronal differentiation

Many proteins appear to function in both cell death and regeneration, and PC12 cells have been instrumental for elucidating their roles in activating regeneration pathways and inhibiting apoptotic signals. The dichotomous role of Jun in preventing and executing cell death exemplifies this. The expression of cJun is increased in response to NGF stimulation of PC12 which induces their neuronal differentiation (Ham et al., 1995) (Fig. 3). The PC12 cells require NGF to survive once differentiated, and NGF deprivation leads to cJun-mediated apoptosis

(Leppa et al., 2001). In undifferentiated PC12 cells, however, over-expression of cJun protects PC12 cells from undergoing apoptosis (Leppa et al., 2001). The chromatin landscape plays a large role in gene expression between different cell types, cell cycle, and states of differentiation. Consequently, the proteome also varies in each situation. Both chromatin configuration and potential protein interactors will have a significant impact on the available DNA binding sites and available dimerization partners and therefore the activity and effect of cJun.

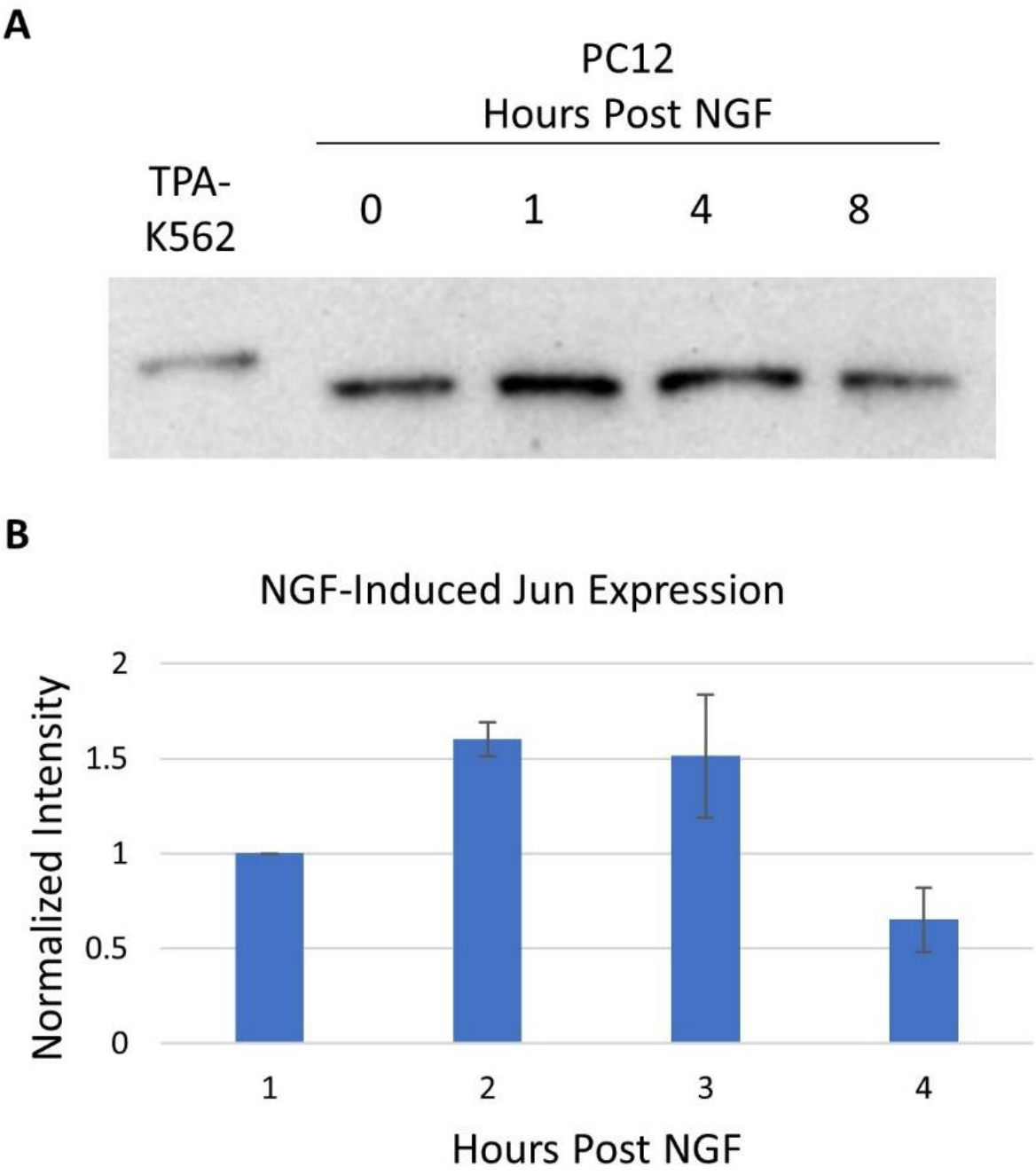

Figure 3: Jun protein expression in PC12 cells. (A) Jun protein expression is induced by NGF in PC12 cells. K562 cells are known to increase Jun expression when exposed to tissue plasminogen activator (TPA) and was used as a positive control. **(B)** Quantified band intensity of Jun protein expression after NGF incubation. N=3

Jun is an essential TF that mediates the neuronal differentiation of PC12 cells (Leppä et al., 1998, Eriksson et al., 2007). As a member of the basic leucine zipper family, Jun functions as an obligate dimer and its binding partners share similarities in their DNA binding and leucine zipper domains. While cJun mRNA is induced within 15 min and peaks at 1 hour in PC12 cells (Wu et al., 1989), Jun protein expression is up-regulated after exposure to NGF, peaking at 1 hour, and returning to baseline levels by 8 hours after exposure (Ham et al., 1995, Eriksson et al., 2007). During this period, known Jun heterodimer partners also vary in protein concentrations (Eriksson et al., 2007). The changing concentrations of potential bZIP partners may suggest that Jun dimerizes with different proteins to progress PC12 differentiation into neurons.

The role of bZIPs in NGF-induced PC12 cell differentiation was investigated using Western blotting, EMSAs, and inhibitor assays. NGF induced robust expression of cFos in PC12 cells within one hour which was preceded by its increased phosphorylation (Eriksson et al., 2007). Protein levels of Fra-2 and cJun also peaked at 1 hour of NGF incubation and were maintained for at least 6 hours (Eriksson et al., 2007). EMSAs revealed that AP-1 activity induced with one hour of NGF stimulation was due to cJun and cFos (Eriksson et al., 2007). As dominant negative cJun had previously been demonstrated to inhibit NGF- induced PC12 neuronal differentiation, siRNA-mediated knockdown of either cJun or cFos also decreased neurite sprouting while Fra-2 siRNA had no discernible effect (Eriksson et al., 2007). The changing bZIP protein levels and consequently AP-1 activity direct PC12 cells towards neuronal differentiation.

Jun activity is regulated by post-translational modifications within its transactivation domain which are known to affect transcription output (Boyle et al., 1991, Meng and Xia, 2011). Not only is cJun protein expression is upregulated in NGF-stimulated PC12 cells, but also the phosphorylation of cJun is induced (Ham et al., 1995, Leppä et al., 1998, Eriksson et al., 2007). Furthermore, exogenous expression of cJun can induce neurite sprouting in PC12 cells (Leppä et al., 1998, Dragunow et al., 2000). In comparison to wild type cJun, the number of cells extending neurites nearly doubled when a phosphate-mimic of cJun was expressed, but decreased with a phospho-null cJun mutant (Leppä et al., 1998). The phosphorylation of serine 73 is likely the main driver of this effect, as 95% of wild type cJun-transfected PC12 cells were phosphorylated on serine 73 as opposed to 13% on serine 63 (Dragunow et al., 2000). The phosphorylation state of cJun plays an important role in PC12 cell differentiation.

Post-translational modifications to cJun are commonly mediated by kinases. The interaction of cJun with ERK directs PC12 cells towards a neuronal cell fate (Leppä et al., 1998). cJun protein levels were suppressed by MEK inhibition (an upstream regulator of ERK), but not p38 or JNK inhibition (Eriksson et al., 2007). However, NGF-induced neurite outgrowth was partially blocked by inhibition of MEK, p38, and JNK activity (Eriksson et al., 2007). cJun is also required for NGF-induced neuronal differentiation of PC12 cells (Leppä et al., 1998, Eriksson et al., 2007). Co-expression of ERK2 and constitutively active MEK results in robust phosphorylation of cJun on serines 63 and 73, but expression of either alone produces only moderate phosphorylation (Leppä et al., 1998). Outside of the RAF/MEK/ERK pathway, the MAPK cascade of MEKK/SEK/JNK is also known to phosphorylate cJun, but appears to regulate cell death as opposed to differentiation (Leppä et al., 1998, Leppa et al., 2001, Xia et al., 1995,

Le-Niculescu et al., 1999). NGF withdrawal from differentiated PC12 cells increases both JNK activity and Jun protein levels (Xia et al., 1995, Maggirwar et al., 2000). Supporting the apoptotic role of the MEKK/JNK pathway, co-expression of two dominant negative forms of cJun decreased cell death induced by either NGF withdrawal or constitutively active MEKK1 in differentiated PC12 cells (Xia et al., 1995). The interactions of cJun with various kinases dictates both its activity and cell fate.

Thesis Statement

Damage to the axons of the mammalian central nervous system (CNS) is irreversible and leads to permanent disability. Transcription factors (TFs) function as an important class of proteins involved in axon regeneration based on their ability to regulate the expression of downstream target genes. Jun is a TF known to be necessary for axon regrowth in neurons capable of regeneration, but it is not sufficient on its own to promote functional regeneration. Jun functions as a homo- or hetero-dimer and its binding partner determines both its transcriptional activity and binding affinity for a given DNA sequence. However, the proteins with which Jun interacts over the time course of successful axon regeneration remain unknown. I hypothesize that Jun interacts with different proteins at different times during axon extension to initiate changes in gene expression necessary for progressing axon growth. To test this, I developed a proximity labeling fusion protein construct of Jun tethered to the APEX2 peroxidase. The work presented here describes the design, validation, and proof of concept for identifying the putative protein-protein interactions of Jun as PC12 cells were stimulated with nerve growth factor. Control and treated cells were analyzed with mass spectrometry to distinguish the Jun-interacting proteome.

Chapter Two Development and Validation of Fusion Protein Construct

Abstract

The diverse interactions of transcription factors govern gene expression throughout the lifetime of a cell. Investigating how these low-abundance proteins interact with other proteins is essential to understanding how they control the timing of regulatory events. Jun is a transcriptional regulator and obligate dimer whose activity is modulated by post-translational modifications. These critical transient interactions are not detected in traditional methods to investigate protein-protein interactions. To address this gap in knowledge, we have created a new tool: a fusion protein of Jun tethered to a proximity labeling ligase, APEX2. In this technique, proteins are biotinylated within a small radius of the transcription factor of interest, regardless of time of interaction. This fusion construct is easily manipulated to modulate expression levels, the protein of interest, and tag. Here, we discuss the validations required to ensure proper functioning of the transcription factor proximity labeling tool. As proof of concept, the protein-protein interactions of Jun were identified by mass spectrometry in neuronally differentiating cells.

Introduction

Transcription factors (TFs) are proteins that bind to genomic DNA to regulate transcription and play important roles in regulating gene programming during development and in mature cells in response to external stimuli. TFs are modular in structure with domains that bind to specific sequences of nucleotides, known as binding motifs, and transactivation domains that interact with a variety of other cellular components to affect transcription, transcription machinery, or chromatin regulators. The DNA binding and dimerization domains

are often similar amongst members of a TF family. Many TFs function as obligate dimers and are often components of larger multimeric complexes. TFs are low-abundance proteins and their relative concentrations will determine the composition of the preferred dimer. It is rare for a dimer to function on its own, so many dimers interact with or form larger quaternary structures. The composition of a dimer or multimeric complex will affect its affinity for a given sequence of DNA, thereby affecting the relative transcriptional output for a gene (Hai and Curran, 1991, Yoshida and Yasuda, 2002). The differences in the transactivation domain of TFs will also have a large effect on the transcription of a gene. The transcriptional capabilities of TFs are modulated by post-translational modifications that induce conformational changes to alter affinity or co-operativity with DNA or other proteins, respectively. Furthermore, certain kinases show preferential activity towards specific dimer compositions and whether or not those dimers are bound to DNA (Abate et al., 1993). To understand transcription in a cell, it is important to understand protein-protein interactions (PPIs) under various conditions. Such transient interactions are important to fine-tune the expression of genes.

Traditional methods to investigate PPIs, such as co-immunoprecipitation and affinity purification, will only identify proteins that interact with a high affinity, such as those directly bound to the protein of interest or within a larger multimeric complex. Other techniques such as the yeast two-hybrid system are capable of identifying the interaction of only two proteins (Fields and Song, 1989). Such techniques are biased towards high affinity interactions and/or slow dissociation kinetics as well as proteins of high abundance (Von Mering et al., 2002). This is particularly problematic for TFs as they are in such low abundance either requiring large amounts of sample or their detection being overwhelmed by others. Ensuring that the protein

of interest is expressed at physiological levels is especially important for TFs as they are naturally in low abundance, thus the over-expression that is typical of many techniques may not reflect the true endogenous PPIs (Gingras et al., 2005). Transcription is tightly regulated and therefore requires the interactions of many proteins within the promoter/enhancer as well as post-translational modifications to those proteins (Qin et al., 2021). These are important interactions necessary for transcription and such transient or further distance interactions are missed by traditional methods for investigating PPIs.

The proximity labeling technique detects endogenous protein interactions as they are occurring in the cell. The composition of a cell is dense with a variety of macromolecules, so the binding affinity of proteins is drastically different from an *in vitro* environment of dilute buffers. As the interacting proteins are labeled *in vivo*, low affinity or transient interactions are retained and not removed at later purification steps with stringent washes. In this technique, an engineered enzyme is genetically tagged to a protein of interest which will covalently tag neighboring proteins with an activated substrate within an ~10 nm radius. The enzymes have evolved from biotin ligases (e.g. BioID and TurboID) with long labeling periods that occur over 24 hours, to the fastest generation of APEX2 with a 1 min labeling period (Roux et al., 2012, Branon et al., 2018, Lam et al., 2015). While interactomes of TFs such as Hox, EcR/USP, Sox2 have been investigated, they were identified using BioID which records the PPIs over many hours which favors stable interactions and high abundance proteins (Carnesecchi et al., 2020, Mazina et al., 2020, Kim et al., 2017). Due to the short 1 min labeling period, a snapshot of PPIs can temporally resolve fast-acting cellular processes, such as phosphorylation, but has yet to be implemented on TFs over a time course (Paek et al., 2017, Lobingier et al., 2017, Mazina et al.,

2020). Furthermore, transient and stable interactions identified by APEX2 labeling can be distinguished when using quantitative mass spectrometry (MS).

To address this gap, we have developed a TF proximity labeling construct to investigate the dynamic and fast-paced PPIs in response to extracellular signals. As a model, we used a PC12 cell line that can differentiate into neurons when exposed to nerve growth factor (NGF) and a key TF mediating this process is Jun. Jun is a component of the AP-1 transcription complex and plays a role in development, regeneration, and cell cycle progression (Hilberg et al., 1993, Herdegen et al., 1991, Angel and Karin, 1991). As a member of the basic leucine zipper family, Jun functions as an obligate dimer and its binding partners share similarities in their DNA binding and leucine zipper domains. In PC12 cells, Jun protein expression is up-regulated after exposure to NGF, peaking at 1 hour and returning to baseline levels by 8 hours after exposure (Ham et al., 1995, Eriksson et al., 2007). During this period, known Jun heterodimer partners also vary in protein concentrations (Eriksson et al., 2007). Jun activity is regulated by post-translational modifications within its transactivation domain which are known to affect transcription output (Boyle et al., 1991, Meng and Xia, 2011). Jun phosphorylation is increased in response to NGF and its interaction with ERK directs PC12 cells towards a neuronal cell fate (Leppä et al., 1998). As proof of principle, the PPIs of Jun-APEX2 were identified using proximity labeling-MS in NGF-stimulated PC12 cells during neuronal differentiation (Fig. 4).

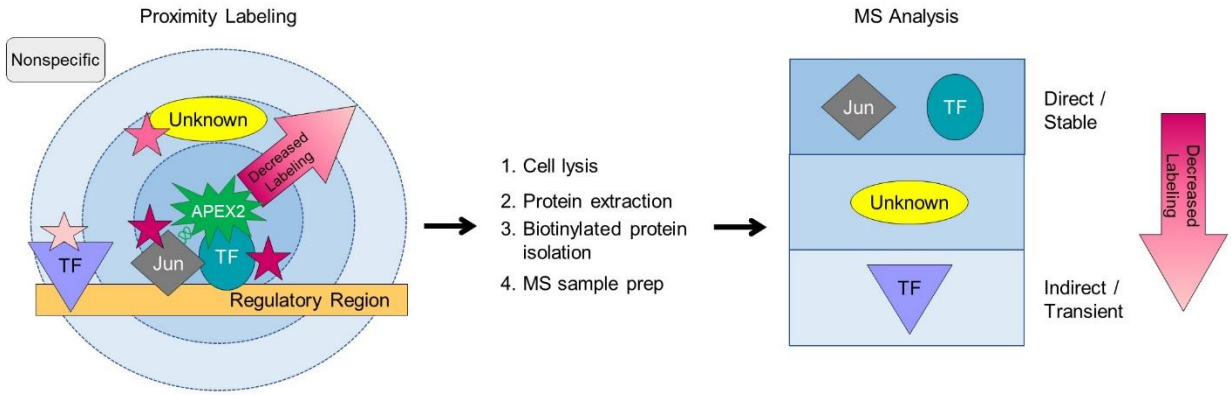

Figure 4: **Schematic and workflow of Jun-APEX2 proximity labeling technique**. *Left*: The engineered peroxidase enzyme (APEX2) is genetically tagged to the transcription factor (TF) of interest (Jun). When exposed to hydrogen peroxide, APEX2 will covalently tag neighboring proteins with the radicalized exogenous substrate, biotin phenol (pink stars). Activated biotin phenol will covalently bond to proteins within an ~10 nm radius (radius of outer blue circle). The extent of tagging of a particular protein will depend upon both the stability of its interaction with Jun and its distance from the peroxidase active site (decreasing blue intensity of "bull's eye" emphasized by pink ombre arrow). The proteins that are farther away from the catalytic site are less likely to be labeled (fewer tags represented by lighter pink stars). The proteins with the most tags (darkest pink stars) will be within close proximity of Jun and have stable interactions. *Middle*: After proximity labeling is performed, cells are lysed and the total protein is extracted. The biotinylated (tagged or labeled) proteins are isolated and prepared for analysis by mass spectrometry (MS). *Right*: Following analysis of MS data, the identified proteins are ranked to determine direct versus indirect protein-protein interactions. Based on their proximity to Jun, it is predicted that direct interactors will include Jun itself along with any direct dimerization partners. Indirect interactions will include both proteins bound nearby on the DNA and also transient interactions, such as those by modifying enzymes.

Materials and methods

pW1-ef1α-jun-linker-APEX2 plasmid synthesis

Double-stranded DNA coding for *ef1α*-linker-*APEX2* (1382 base pairs) was commercially synthesized by GeneWiz Azenta Life Sciences. The *ef1α* promoter sequence was obtained from the *xenopus laevis* genome (GenBank: M25697.1). The lyophilized DNA was re-suspended in water and used as the template for PCR using *Taq* DNA polymerase (Promega Cat No M3001) and the primers 5'-TATGAGCTCCATATGCCG-3' and 5'-TAACTAGTCTCGAGCTGCAGA-3'. The fragment was ligated into the pCR®II vector using the TA Cloning Kit, Dual Promoter (Invitrogen™ Cat No K207040). The ligated plasmid was transformed into One Shot™ MAX Efficiency™ DH5α-T1R Competent Cells for propagation (Invitrogen™Cat No 12297016). Using the *SpeI* and *SacI* restriction enzymes (New England Biolabs), the *ef1α*-linker-*APEX2* fragment was removed from the pCR®II vector and ligated into the pW1 cloning vector using T4 DNA ligase (Invitrogen™ Cat No 15224017). The pW1 vector contains the SV40 small t intron and poly-adenylation site (Linney and Udvadia, 2004). The pW1 vector was treated with Antarctic Phosphatase to prevent self-ligation (New England Biolabs Cat No M0289S). Plasmid DNA was extracted using the PureYield™ Plasmid Midiprep System (Promega® Cat No A2492).

The zebrafish sequence for *jun* was chosen for its 70% homology to human and rodent Jun protein. The difference in sequence can be distinguished from endogenous Jun in MS results. To obtain the sequence for the *jun* gene, RNA isolated from two days post-fertilization EK wild type *danio rerio* larvae was used as a template to create cDNA with the qScript® Flex cDNA Synthesis Kit (Quantabio Cat No 95049-025). Using the cDNA as a template, *Taq* DNA polymerase (Promega Cat No M3001) was used in PCR to amplify the 927 base pair sequence of

the *jun* gene flanked by *NcoI* and *MluI* restriction sites using the primers 5'-CCATGGTTCTATGTCTACCAAGATGG-3' and 5'-ACGCGTGAAGGTTTGCAGCTGT-3'. The fragment was ligated into the pCR®II vector using the TA Cloning Kit, Dual Promoter (Invitrogen™ Cat No K207040). The ligated plasmid was transformed into One Shot™ MAX Efficiency™ DH5α-T1R Competent Cells for propagation (Invitrogen™ Cat No 12297016). The *jun* gene was sequenced for integrity using the Sp6 and T7 promoters within the pCR®II vector. This sequence was subcloned in-frame into the pW1-*ef1α*-linker-*APEX2* plasmid using the restriction sites *NcoI* and *MluI*. The resulting plasmid (pW1-*ef1α*-*jun*-linker-*APEX2*) was verified by Sanger sequencing. Plasmid DNA was extracted using PureYield™ Plasmid Midiprep System (Promega® Cat No A2492)

Cell culture

The PC-12 Adh CRL-1721.1™ cells were purchased from American Type Culture Collection (ATCC). Cells were cultured according to the handling information provided by the ATCC using sterile techniques. Cells were incubated at 37°C and 5% CO_2 in Ham's F-12K Medium (Gibco™ Cat No 21127022) supplemented to 10% horse serum (Sigma-Aldrich Cat No H1138), 5% fetal bovine serum (Gibco™ Cat No 10082147), and 1 X pen/strep (Gibco™ Cat No 15070063). Cells were passaged every other day, seeding at 3.0 x 10^4 viable cells/cm^2 in Nunclon™ Delta surface treated flasks (Thermo Scientific™ Cat No 178983).

Plasmid transfection

jetOPTIMUS® DNA transfection reagent (Polyplus Ref No 117-15) was used for all DNA plasmid transfections. The standard transfection protocol recommended by the manufacturer

at a 1:1 DNA:reagent ratio was used for all for all surface areas, adjusting for volumes accordingly.

Imaging transfected PC12 cells for plasmid cellular localization

PC12 cells were seeded in 12-well plates at 3.0 x 10^4 viable cells/cm^2 and transfected with DNA plasmid 24 hours after plating at 75% confluency. After an additional 24 h post-transfection, cells were placed on ice for ~ 5 min to equilibrate media to temperature. The cells were then incubated for 15 min in freshly prepared ice-cold 50 µM Amplex UltraRed solution (Invitrogen™ Cat No A36006) with or without 10 mM hydrogen peroxide (Sigma-Aldrich Cat No H1009). Cells were rinsed with ice-cold Dulbecco's phosphate-buffered saline (DPBS, Sigma-Aldrich Cat No D5773) and then fixed in warm (30–37 °C) 4% (wt/vol) paraformaldehyde (Thermo Scientific™ Cat No 28906) for 15 min at room temperature. Cells were washed with ice-cold DPBS and followed by 0.1% Tween-20 in DPBS. Nuclei were stained with ice-cold 300 nM 4',6-diamidino-2-phenylindole (DAPI) and finally rinsed with ice-cold DPBS. Fluorescence was visualized (excitation 490–550 nm; emission 580–590 nm) on a Nikon Eclipse TE2000-U microscope. Validation was performed on two wells per condition, in triplicate from three distinct biological replicates.

Proximity labeling reactions

After 24 hours post-transfection when cells were ~90% confluent, biotin-phenol labeling was initiated by changing the media to fresh growth media containing 500 µM biotin-phenol (biotin tyramide, Iris-Biotech Cat No LS-3500). This was incubated at 37°C under 5% CO_2 for 30 min. Afterwards, hydrogen peroxide was added to a final concentration of 1 mM and the flask gently agitated for 1 min. The reaction was quenched by exchanging the media for quenching

buffer (10 mM sodium ascorbate (Spectrum Chemical Cat No S1349), 5 mM Trolox (Sigma-Aldrich Cat No 238813-5G), 10 mM sodium azide (Sigma-Aldrich Cat No S2002) in DPBS). Cells were washed with quenching buffer for a total of three times. Cells were scraped and collected in a conical tube, rinsing the flask with quenching buffer to collect remaining cells. The cell suspension was centrifuged at 4°C for 5 min at 500 x *g*. The supernatant was removed, and either whole cell protein lysate or the nuclear fraction was obtained.

Whole cell protein isolation

From proximity labeled, transfected, or untreated cells, the cell pellet was resuspended by gentle pipetting with RIPA lysis buffer (50 mM Tris, 150 mM NaCl, 0.1% SDS, 0.5% sodium deoxycholate, 1% Triton X-100, 1X protease inhibitor cocktail (PIC, Pierce® Cat No 88266), 1 mM PMSF, 10 mM sodium azide, 10 mM sodium ascorbate, and 5 mM Trolox) and incubated for 2 min on ice. Per 150 cm^2 flask, 0.5 mL RIPA buffer was used. Lysates were clarified by centrifugation at 25 x 10^3 x *g* for 10 min at 4°C. The supernatant was transferred to a clean tube and total protein was quantified. The whole cell protein lysate was stored at -80°C until enrichment of biotinylated protein.

Nuclear protein isolation

From proximity labeled, transfected, or untreated cells, the cell pellet was resuspended by gentle pipetting in cell lysis buffer (CLB; 1.5 mM $MgCl_2$, 10 mM NaCl, 0.5% Igepal-CA630, 1 X PIC, and 10 mM Tris-HCl, pH 8.1) and incubated for at least 20 min on ice. Cell membranes were disrupted by pipetting up and down ten times and the lysate was centrifuged for 5 min at 3.4 x 10^3 x *g* at 4°C. The supernatant was transferred to a fresh tube and saved as cytoplasmic lysate. The pellet was resuspended by gentle pipetting in nuclear lysis buffer (NLB; 5 mM EDTA, 1%

SDS, 1 X PIC, and 50 mM Tris-HCl, pH 8.1) and incubated for at least 20 min on ice. Per 75 cm^2 flask, 1 mL CLB and 200 µL NLB were used. The nuclear membrane was disrupted by passing the sample through a 27-gauge syringe ten times. The sample was centrifuged for 10 min at 25 x 10^3 x *g* at 4°C. The supernatant was transferred to a fresh tube and saved as the nuclear lysate. Both cytoplasmic and nuclear fractions were quantified before storage at -80°C until enrichment of biotinylated protein.

Total protein quantification

The Pierce™ 660 nm Protein Assay Kit (Thermo Scientific™ Cat No 22662) was used to measure the total protein content in whole cell lysates. Samples were measured with assay reagent containing Ionic Detergent Compatibility Reagent (Thermo Scientific™ Cat No 22663). Sample cell lysate (10 µL, measured in duplicate) was mixed with 150 µL of the reagent in a 96-well, round bottom plate. Absorbance was measured at 660 nm on an Infinite® M200 Pro (Tecan) multimode microplate reader. Total protein concentration was determined by comparing to the absorbances of a set of bovine serum albumin (BSA) protein pre-diluted standards (Pierce™ Cat No 23208) prepared and analyzed in the same manner (each standard concentration was prepared in triplicate).

Fractionated protein quantification

The DC™ Protein Assay (BioRad Cat No 500-0116) was used to measure the protein content in the cytoplasmic and nuclear samples according to manufacturer's instructions for the microassay protocol in a 96-well, round bottom plate. Samples were prepared and analyzed in duplicate. Absorbance was measured at 750 nm on an Infinite® M200 Pro multimode microplate reader, and protein concentration was determined by to the absorbances of a set of

BSA protein pre-diluted standards (Pierce™ Cat No 23208) prepared and analyzed in the same manner (each standard concentration was prepared in triplicate).

Validation of APEX2 peroxidase activity

PC12 cells transfected with pW1-*ef1α*-*jun*-linker-*APEX2* underwent proximity labeling as described above either with or without biotin-phenol or hydrogen peroxide. Whole cell protein was extracted and quantified for total protein content as described above. Lysates were separated in 10% polyacrylamide gels (Bio-Rad Cat No 4568034) and protein was then transferred to PVDF membrane before blocking with 3% (w/v) BSA in 1 X TBST (0.1% Tween-20 in tris-buffered saline) overnight at 4°C. The membrane was incubated at room temperature for 2 h in 4 ng/mL streptavidin-HRP (Invitrogen™ Cat No S-911), then rinsed with TBST three times for 10 min each. The blot was visualized using SuperSignal™ West Femto Maximum Sensitivity Substrate (Thermo Scientific™ Cat No 34095) on a G:BOX Chemi XRQ (Syngene). Validation was performed in triplicate using three distinct biological replicates.

EMSA

The unlabeled oligonucleotide probes were synthesized by heating sense and antisense primers to 100°C for 5 min in annealing buffer (10 mM Tris-Cl, 100 mM NaCl, 1 mM EDTA, pH 7.5), followed by cooling at room temperature. The sense strands of the oligonucleotide sequences used in EMSA were the following: 5’-CGCTTGATGACTCAGCCGGAA-3’ for wild type AP-1 consensus sequence and 5’-CGCTTGATAGATCTGCCGGAA-3’ for mutant AP-1 consensus sequence. The mutated sequence was previously validated to disrupt binding of the AP-1 complex (Manna et al., 2004).

Protein-DNA binding assays were carried out according to the Odyssey® EMSA Kit manufacturer's instructions (LI-COR® P/N 829-07910). Briefly, 5 µg whole cell lysate were incubated in 20 µL of reaction buffer (10 mM Tris, 50 mM KCl, 25 mM dithiothreitol (DTT), 50 ng/µL poly dIdC, 50 nM EDTA, 0.25% Tween-20; pH 7.5) for 30 min at room temperature. The fluorescent AP-1 DNA probe (LI-COR® P/N 829-07925, 6.25 fmol) was added alone or in the presence of increasing concentrations (20- to 200-fold molar excess) of unlabeled DNA oligonucleotide. Protein-DNA complexes were then subjected to electrophoresis on 10% polyacrylamide gels (Bio-Rad Cat No 4568034) for about 2.5 h at 150 V in 1 X TBE buffer (90 mM Tris-borate, 2 mM EDTA; pH 8.0) protected from light. Gels were removed from the cassette and scanned on a LI-COR® Odyssey Imager at 700 nm with an offset of 0.5 mm. Validation was performed in triplicate using three distinct biological replicates.

Enrichment of biotinylated proteins with streptavidin beads

Streptavidin-coated magnetic beads (Pierce®, Cat No 88817) were prepared by washing twice with RIPA lysis buffer. For every mg of total protein (at 3-5 mg/mL whole cell protein concentration), 100 µL of streptavidin bead slurry was used. Each replicate sample was mixed with washed streptavidin beads and brought to 0.5 mL final volume in RIPA buffer supplemented with PIC (RIPA-PIC). The suspensions were incubated at room temperature for 1 h with gentle rotation. Streptavidin beads were then washed with 0.5 mL volumes as follows: twice with RIPA-PIC, once with 1 M KCl, once with 0.1 M Na_2CO_3, once with 2 M urea in 10 mM Tris-HCl pH 8.0, and twice with RIPA-PIC. All buffers were maintained at 4°C. Biotinylated proteins were digested in-gel for mass spectrometry analysis.

MS sample preparation, LC-MS/MS, and MS data analysis

In-solution and in-gel sample preparation, LC-MS/MS analysis, and MS data analysis was performed at the Mass Spectrometry Core Facility at the University of Wisconsin – Madison. Samples were analyzed on a Thermo Scientific™ Orbitrap Elite mass spectrometer connected to an Agilent 1100 Nano flow HPLC system with flow rates at 300 nL/min and separation achieved using Thermo Scientific™ EasySpray 75 µm i.d. column coupled to a Thermo Scientific™ EasySpray source. All data analysis was performed at false discovery rate (FDR) <1% for proteins represented by at least two identified peptides. For differentially detected in-solution data, Fisher's Exact Test with multiple test correction was used.

Results

To investigate the PPIs of Jun in response to NGF, a DNA plasmid encoding for Jun tethered to APEX2 via a flexible linker (Jun-APEX2) was transfected into undifferentiated PC12 cells. Cells were either treated with NGF for one hour or left un-treated, then proximity labeling reactions were performed. The protein lysates were collected, and the biotinylated proteins were analyzed using liquid chromatography-mass spectrometry (LC-MS/MS).

Concept and design of Jun-APEX2 construct

The Jun-APEX2 fusion protein construct has a modular design that allows the three components to be easily interchangeable to investigate the PPIs of TFs: the promoter, TF, and proximity labeling entity (Fig. 5). The proteins are separated by a flexible 12 amino acid linker (RGGSGGSGGSGS). The *ef1a* promoter enables ubiquitous, strong expression ideal for obtaining adequate amounts of protein from cell culture. There are multiple cloning sites before and after the promoter, as well as after the APEX2 3'-tag. Multiple cloning sites allow for easy removal of

the promoter and tag as well as restriction enzyme directional insertion of the protein of interest. The ability to exchange cassettes facilitates investigation of different pathways, modulating the amount of fusion protein, and varying the tag.

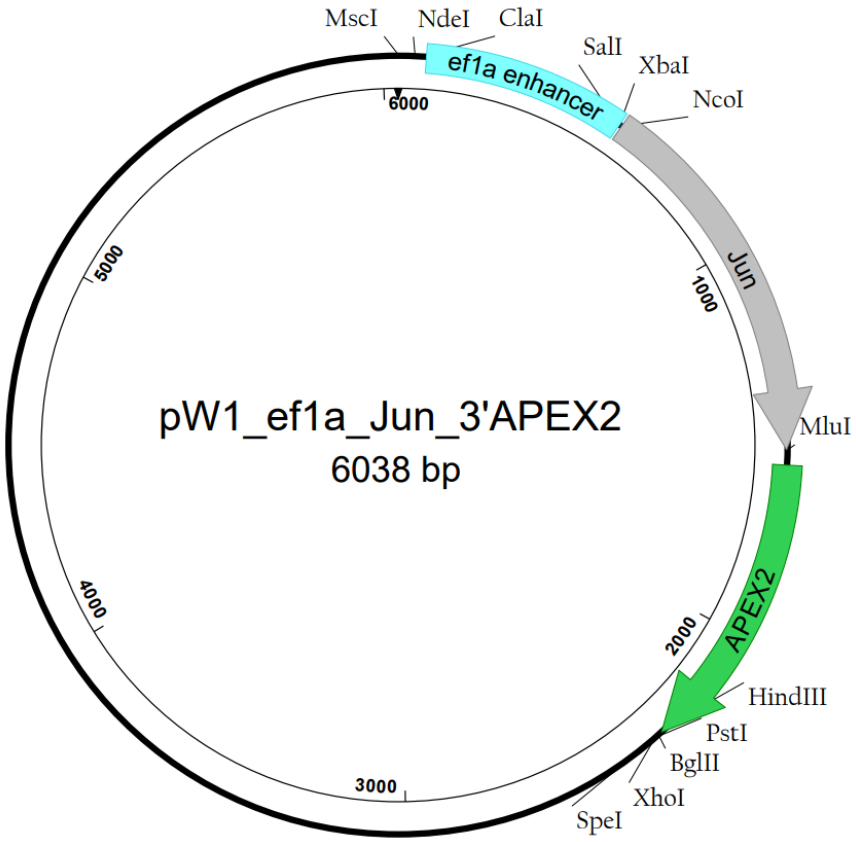

Figure 5: Plasmid map of pW1-*ef1α*-*jun*-linker-*APEX2*. The DNA plasmid that encodes the Jun-APEX2 fusion protein consists of four main cassettes: the *ef1α* promoter (cyan), *jun* gene (grey), linker, and *APEX2* gene (green). There are three multiple cloning sites to facilitate removal of each cassette: on the 3' and 5' termini of the promoter, and the 3' terminal of *APEX2*. The flexible linker arm was cloned in-frame between the *jun* and *APEX2* genes.

Insertion of a single polypeptide chain between the two fusion protein components allows for proper folding after translation and function of the individual proteins. Ten amino acid linkers (~5 nm) of similar composition have been successfully used with APEX or APEX2 within mitochondria to resolve organellar localization (Hung et al., 2014, Hung et al., 2016). A longer 17 amino acid linker tethering together Jun and other bZIP proteins was validated to maintain endogenous functionalities of Jun heterodimers, including transcriptional activation, as well as dimer orientation (3'- versus 5'-terminal tethering) and addition of epitope tags (Bakiri et al., 2002, Danzi et al., 2018). It is of paramount importance to avoid interruption of the normal physiological interactions of the protein of interest to evaluate its true PPIs.

To create the Jun-APEX2 plasmid DNA construct, the *ef1α*-linker-*APEX2* sequence was commercially synthesized and inserted into the pW1 vector using directional restriction enzyme cloning (Balkan et al., 1992, Linney and Udvadia, 2004, Udvadia, 2008). This pW1-*ef1α*-linker-*APEX2* is the base plasmid into which a TF or other protein may be inserted to create a C-terminally tagged proximity labeling construct. The zebrafish sequence for *jun* was chosen for its 70% homology to human and rodent Jun protein. The difference in sequence can be distinguished from endogenous Jun in MS results. Using restriction site directional cloning, *jun* was subcloned into the pW1-*ef1α*-linker-*APEX2* plasmid to create the final pW1-*ef1α*-*jun*-linker-*APEX2*.

Further Considerations & Caveats:

There are many variables to consider for adapting the construct to a different protein of interest. Review the literature to see if the protein of interest functions as expected with tags at the intended sites. It may be time efficient to create fusion constructs tagged at either the 5'-

or 3’-terminal in the case where one orientation may not pass a validation assay. APEX2 has been shown to remain active when attached at either terminal or when inserted internally (Hung et al., 2016). While not featured in the base plasmid, addition of an epitope tag will expand the utility of the construct by enabling fusion protein precipitation or recognition by conjugated fluorophores for spatial localization as visualized with light microscopy. Additionally, if the protein of interest does not have a validated antibody, an antibody against the epitope can be utilized for confirmation of fusion protein expression by molecular weight as assessed by western blotting. In HEK cells, the V5 tag successfully detects APEX2 and Jun can tolerate a 3xFlag tag to its N-terminus, but the HA tag should be avoided as its prone to tyrosine oxidative damage (Hung et al., 2016, Danzi et al., 2018). While fluorescence is convenient for visualizing protein localization, it is not advised to include a fluorophore in the fusion protein for two reasons: (1) larger plasmids are more difficult to transfect and (2) the function of the TF and APEX2 are more likely to be perturbed. Determine whether the protein of interest is post-translationally cleaved at either terminal to avoid APEX2 mistargeting. It is best to empirically test fusion protein orientation and epitope tag tolerance by following the validation steps in this protocol.

To maintain protein expression levels near that of TFs, it may be beneficial to use a weaker promoter. Transient protein expression in cultured cells enables fast validation of the fusion protein construct and can be completed in parallel with stable line generation. The plasmid transfection protocol should be optimized for each promoter and vector type as efficiency varies. The *ef1a* promoter was used in this proof-of-concept model for high expression to compensate for low transfection efficiency. Some promoters are susceptible to

silencing in different species (Battulin et al., 2022). Ideally, stable cell lines in which the fusion protein replaces the endogenous counterpart would be best for obtaining adequate amounts of protein and producing the most physiologically relevant PPIs for MS analysis.

When choosing restriction sites to use for cloning a protein of interest into the pW1-*ef1a*-linker-*APEX2* base plasmid, take note of naturally occurring sites in the protein of interest sequence. To avoid multi-step digests, the multiple cloning sites in the base plasmid utilize restriction enzymes that share the same buffer. Using automated sequencing software greatly aids in developing the fusion construct with features such as primer design, virtual digests, and visualizing sequencing data.

Fusion protein validation

Both the TF and proximity labeling enzyme must be validated to ensure they maintain their proper functions under physiological conditions. The APEX2 peroxidase must maintain its ability to label proteins only in the presence of its two required substrates (Fig. 6). The cellular localization and DNA sequence-specific binding of Jun must be validated as important functions of TFs. The following validation assays can be performed in parallel for time efficiency if one is proficient in handling cell culture and sterile technique.

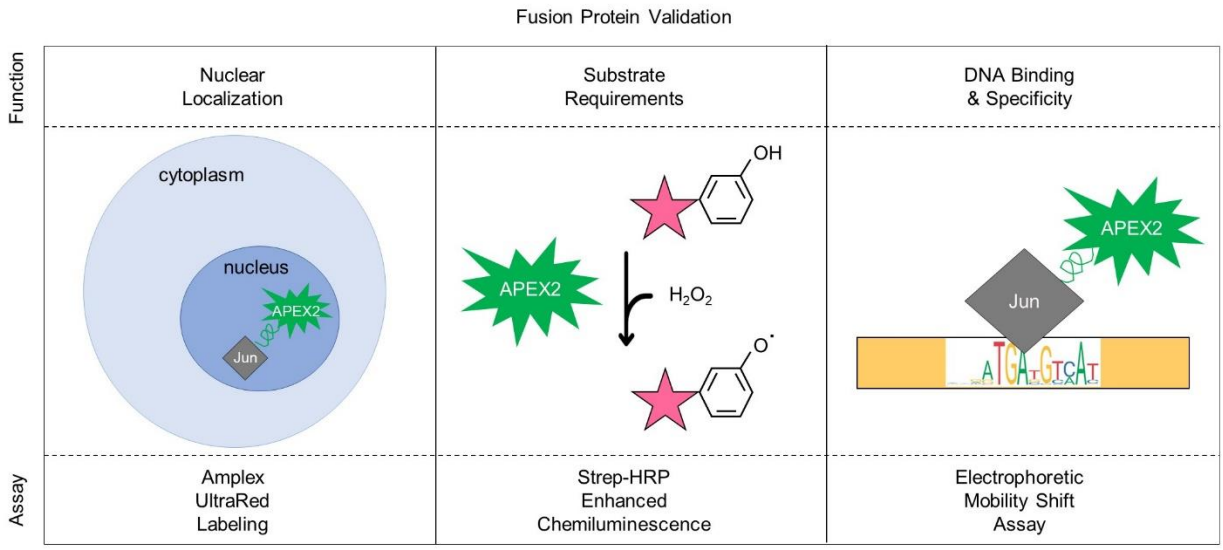

Figure 6: **Workflow for proximity labeling construct validation**. After constructing a TF proximity labeling fusion protein, several core characteristics must be validated. *Left*: Fluorescence microscopy shows the nuclear localization of the TF-proximity labeling enzyme (Jun-APEX2, grey diamond attached to green explosion via green coil). Cells expressing the fusion construct are labeled with Amplex UltraRed reagent which is converted to the red fluorescent resorufin in the presence of peroxidases, e.g. APEX2. *Middle*: To biotinylate proteins, APEX2 requires both of its substrates: hydrogen peroxide and biotin phenol (pink star with phenol group). Proximity labeling reactions are performed with or without either substrate on cells expressing the fusion protein. The protein lysates are collected, separated on polyacrylamide gels, and probed with streptavidin-HRP to specifically detect biotinylated proteins using enhanced chemiluminescence (ECL). *Right*: The fusion protein binds DNA in a sequence-specific manner. Electrophoretic mobility shift assays (EMSA) are performed on protein lysates containing the fusion protein using fluorescent DNA probes or of consensus binding sequence. Binding specificity is confirmed by competition with unlabeled DNA oligomers of the consensus binding sequence.

Cellular localization

The localization of the Jun-APEX2 fusion protein was visualized using Amplex UltraRed. This reagent passes through non-permeabilized cells and is converted to a red fluorophore in the presence of peroxidases and hydrogen peroxide (Fig. 7A). The fluorophore remains localized to the site of production for approximately one hour which enables spatial resolution. As APEX2 is a peroxidase, it will convert the Amplex UltraRed reagent into a red fluorophore in the presence of hydrogen peroxide which can be visualized with fluorescence microscopy.

PC12 cells were transfected with either Jun-APEX2 (pW1-*ef1a*-*jun*-linker-*APEX2*) or APEX2 (pW1-*ef1a*-linker-*APEX2*) alone and compared to un-transfected cells as a control (Fig. 7B). The nuclear localization signal in Jun was expected to target the Jun-APEX2 fusion protein to the nucleus. One day after transfection, Amplex UltraRed was used to visualize peroxidase activity with or without hydrogen peroxide. Cells were also treated with DAPI to label the nucleus. In cells treated with hydrogen peroxide, peroxidase activity was detected in the cytoplasm of cells that were either untreated or expressing APEX2 (Fig. 7C). Cells expressing the Jun-APEX2 fusion protein showed red fluorescence only in the nucleus.

For the remaining validation assays, protein lysates are obtained from proximity labeled, transfected cells. In conjunction with the APEX2 function assay, nuclear localization can be confirmed by comparing cytoplasmic and nuclear fractions. Mammalian cells have endogenously biotinylated proteins at 72, 78, and 130 kDa and will be detected in the cytoplasmic lysates (Chapman-Smith and Cronan, 1999).

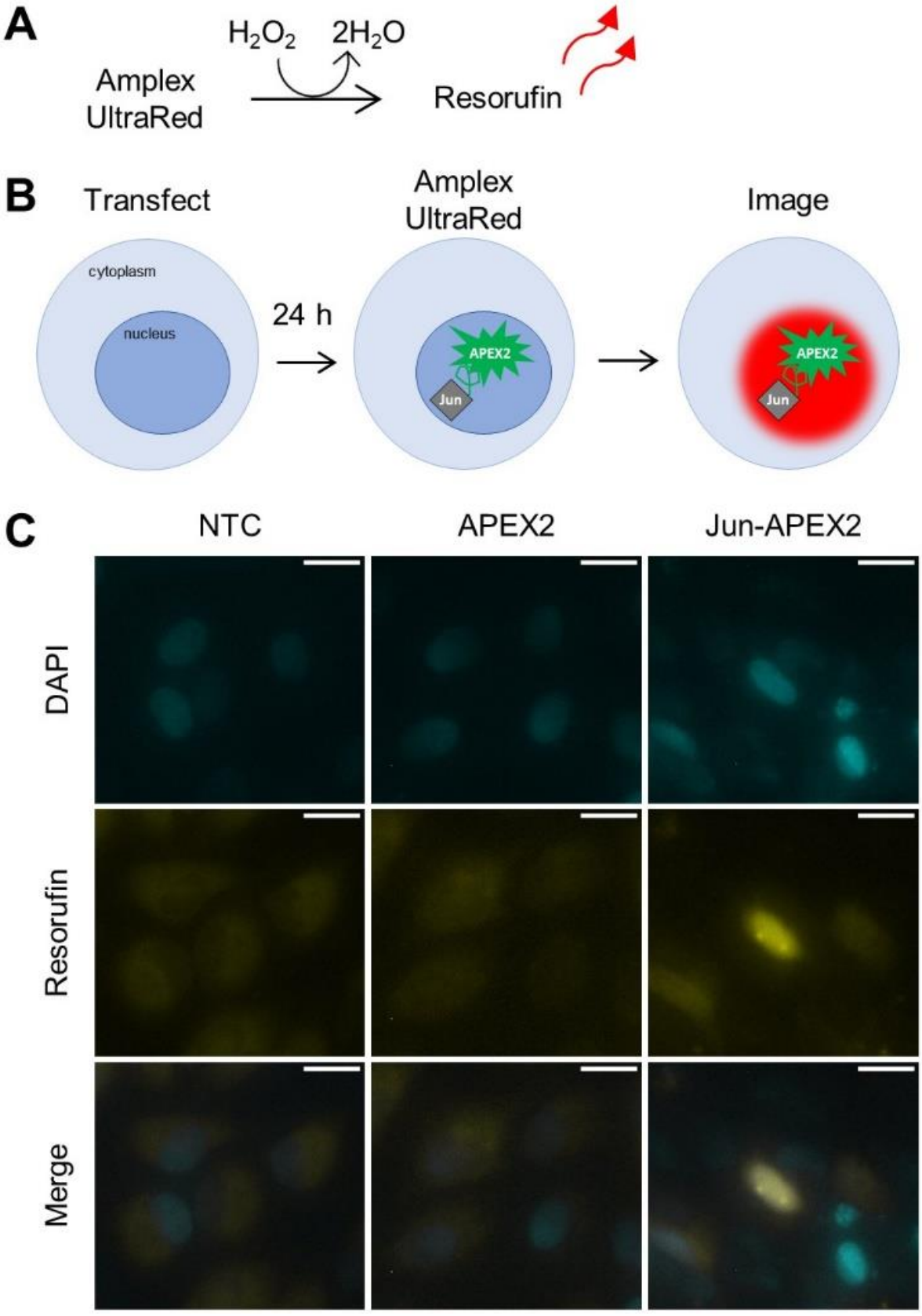
A
H_2O_2
$2H_2O$
Amplex
UltraRed
Resorufin
B
Transfect
Amplex
UltraRed
Image
cytoplasm
nucleus
24 h
APEX2
Jun
APEX2
Jun
C
NTC
APEX2
Jun-APEX2
DAPI
Resorufin
Merge

Figure 7: The Jun-APEX2 fusion protein localizes to the nucleus. (A) When in the presence of hydrogen peroxide (H_2O_2), Amplex UltraRed oxidizes to red fluorescent resorufin. **(B)** Undifferentiated PC12 cells were either transfected with pW1-*ef1α-jun*-linker-*APEX2* or pW1-*ef1α*-linker-*APEX2,* or left untreated. Twenty-four hours after transfection, cells underwent Amplex UltraRed labeling either with or without H_2O_2. DAPI was used to visualize the nucleus. **(C)** Untreated or non-transfected cells (NTC), or those transfected with pW1-*ef1α*-linker-*APEX2* (APEX2) or pW1-*ef1α-jun*-linker-*APEX2* (Jun-APEX2) underwent Amplex UltraRed labeling with or without H_2O_2. All cells without H_2O_2 treatment showed minimal red background (not shown). NTC treated with H_2O_2 appeared similar to those without H_2O_2, but with a higher background, likely due to the harsh conditions of peroxide-exposure. Cells expressing APEX2 showed fluorescence only in the cytoplasm. Cells expressing Jun-APEX2 displayed fluorescence in the nucleus, as visualized by overlapping DAPI staining. Two technical replicates were performed per condition, from three distinct biological replicates. The contrast of the images was increased to enhance visualization. Scale bar is 10 µm.

Further Considerations & Caveats:

When using Amplex UltraRed, it is advised to plan the reactions and imaging prior to performing the experiments to prevent reagent diffusion from cellular compartments. Alternatively, 3,3'-diaminobenzidine (DAB) staining can be performed and detected using light microscopy. This reagent remains tightly localized to the site of production and will not diffuse through cellular compartments. DAB staining is compatible with electron microscopy for precise spatial resolution. DAB staining requires optimization of peroxide incubation period to prevent damage to cell structure which is especially important if electron microscopy will be utilized for sub-compartmental localization. In our hands, DAB staining was not successfully detected using light microscopy. Due to the high background of cellular structures generated by electron microscopy, intense DAB staining by APEX2 may be less sensitive than fluorescence-based methods for spatial resolution. Unlike Amplex UltraRed, fusion proteins containing an epitope tag can be immuno-labeled using fluorophore-conjugated antibodies and stored for subsequent analysis.

APEX2 function

The APEX2 enzyme enables biotinylation of proteins through a peroxidase reaction that can only occur in the presence of its substrates, biotin phenol and hydrogen peroxide. In the presence of hydrogen peroxide, APEX2 will catalyze the one-electron oxidation of biotin phenol into a radical. This radical can then bind to an electron-rich side chain of a protein within an ~10 nm radius of the APEX2 active site (Kim et al., 2014). The total protein can be extracted from the cells, separated in a polyacrylamide gel, and transferred to a membrane. Light collected

from a luminol reaction with streptavidin-horseradish peroxidase (HRP) will specifically visualize the biotinylated proteins in the lysates.

To verify that proteins are biotinylated only in the presence of hydrogen peroxide and biotin phenol, proximity labeling reactions were performed on Jun-APEX2 transfected PC12 cells that were incubated with or without one of the necessary substrates (Fig. 8). In the presence of only biotin phenol, APEX2 cannot catalyze its oxidation and therefore no labeling occurred (Lane 1). Two low-intensity bands were detected around 40 and 50 kDa that are likely self-biotinylation of Jun-APEX2 by endogenous peroxides (Mair et al., 2019). In the presence of only hydrogen peroxide, there is no biotin phenol to tag the proteins, and no bands were detected in the protein lysates (Lane 2). In the presence of both substrates, a smear of bands over a large range of molecular weights was observed (Lane 3). These results confirm that APEX2 labelled proteins only when both substrates are present.

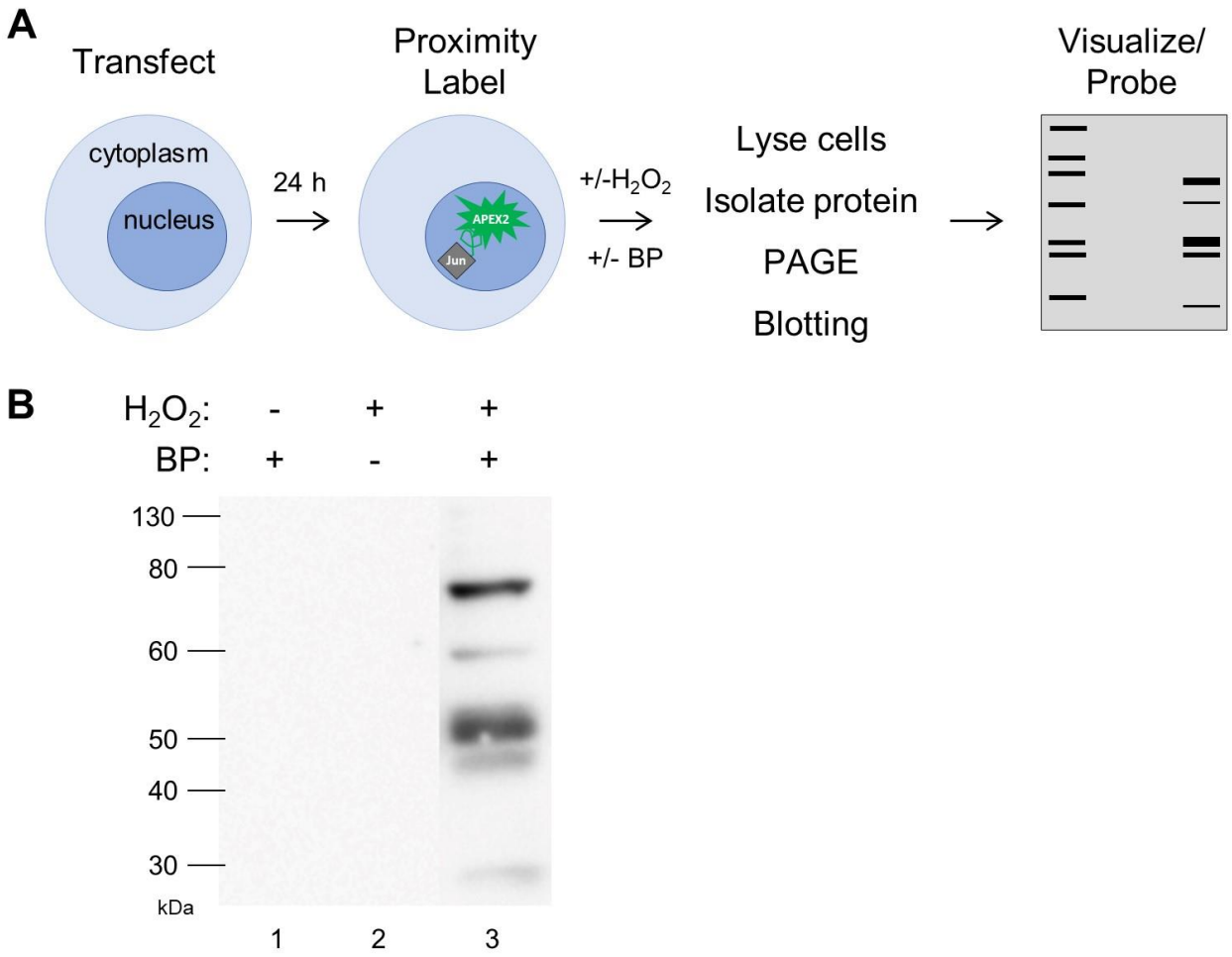

Figure 8: **APEX2 is dependent upon its substrates to biotinylate proteins**. **(A)** PC12 cells were transfected with pW1-*ef1α*-*jun*-linker-*APEX2* and proximity labeling reactions were performed on cells incubated with or without one of the substrates: biotin phenol or hydrogen peroxide. Nuclear lysates (24 µg) were separated using polyacrylamide gel electrophoresis (PAGE), transferred to PVDF membranes, and probed with streptavidin-horseradish peroxidase (HRP) to specifically detect biotinylated proteins. **(B)** Without hydrogen peroxide, biotin phenol cannot be radicalized and therefore no bands are detected (Lane 1). Without biotin phenol, there is no reagent to label proteins and therefore no bands were detected (Lane 2). In the presence of both substrates, a range of proteins were detected at multiple molecular weights (Lane 3). Equal protein loading across lanes was verified by total protein visualization (not shown). Experiment was performed in triplicate from three distinct biological replicates. The sample lanes were moved to group together pertinent samples.

Further Considerations & Caveats:

The procedure for the streptavidin bead pull-down should be optimized for small and large scales. Vary the amount of proximity labeling protein lysate (whole cell, cytoplasmic, or nuclear) and incubate with a constant amount of beads. After the initial incubation to bind the biotinylated protein, save the supernatant as the "flow through". Compare the lysate, the eluate, and the flow through for biotinylated proteins as described above for the streptavidin-HRP membrane. For optimal pull-down efficiency, the maximal amount of lysate per volume of beads is determined when no bands are detected in the lane containing flow-through. Mammalian cells have endogenously biotinylated proteins at 72, 78, and 130 kDa and will be detected in the cytoplasmic lysates (Chapman-Smith and Cronan, 1999). Consequently, the cytoplasmic and whole cell lysates may require a larger volume of beads relative to sample.

APEX2 requires heme as a cofactor for proper functioning. For cell types in which heme biosynthesis is restricted, it may be necessary to supplement the culture media (Lam et al., 2015). This may be the case if no bands are seen in lanes containing lysate incubated with both substrates. If no bands are seen after addition of heme, it may be necessary to change the orientation of APEX2 relative to the protein of interest, especially for internal insertions. Biotin phenol has low penetrance for some cell types which may result in no detected bands. A protocol has been developed to address this (Tan et al., 2020).

DNA binding specificity

TFs bind to specific sequences of DNA in promoters and enhancers of genes to induce conformational changes, recruit transcriptional machinery, or prevent binding of proteins (Panne et al., 2007, Jolma et al., 2015, Frietze and Farnham, 2011, Neubauer and Calef, 1970).

DNA-binding specificity of the TF proximity labeling construct can be tested through *in vitro* DNA binding and competition assays. Electromobility shift assays (EMSA) were performed to test TF-DNA binding specificity. In these assays, a fluorescently labeled DNA probe was incubated with protein lysate and the mixture separated in polyacrylamide gels to resolve interactions by weight. Unbound probes traveled quickly through the gel while bound probes were retarded by interaction with the fusion protein. The binding specificity was tested through competition with unlabeled oligomers.

Jun expression was induced by NGF in PC12 cells, demonstrating probe specificity (Fig. 9, Lanes 1 and 2) (Ham et al., 1995). Cells expressing APEX2 without Jun showed no defined band (Lane 3). Cells expressing Jun-APEX2 (Lane 4) showed a higher molecular weight band that decreased intensity with increasing concentration of unlabeled AP-1 oligomer (Lanes 5-7). The Jun-APEX2 band did not change intensity as unlabeled, mutated AP-1 oligomer concentration was increased (Lanes 8-10). These data confirm that Jun-APEX2 bound DNA in a sequence-specific manner.

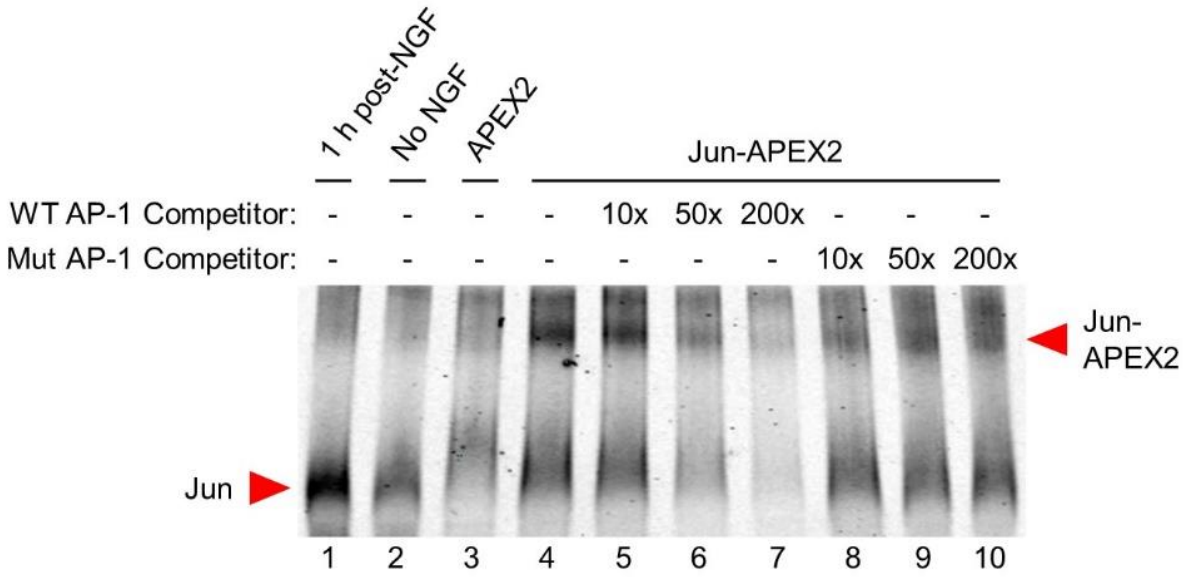

Figure 9: **Jun-APEX2 binds DNA in a sequence-specific manner.** PC12 cells were either un-transfected (Lanes 1 and 2) or transfected with pW1-*ef1α*-linker-*APEX2* (:ane 3) or pW1-*ef1α*-*jun*-linker-*APEX2* (Lanes 4-10). Whole cell lysates (5 µg) were incubated with only fluorescently labeled probe of the AP-1 DNA sequence (Lanes 1-4) or also with unlabeled DNA oligomers (lanes 5-10). Jun protein was induced with 100 ng/µL NGF (Lanes 1 and 2, band denoted by red arrowhead). APEX2 did not bind AP-1 DNA (Lane 3). Jun-APEX2 was detected at a higher molecular weight than Jun alone (Lane 4, red arrowheads). The specificity of binding was tested by adding increasing concentrations of unlabeled AP-1 oligomer (WT, wildtype AP-1 competitor; 10-, 50-, and 200-fold molar excess, Lanes 5-7). In contrast, unlabeled mutant AP-1 oligomer (Mut, mutant AP-1 competitor; 10-, 50-, and 200-fold molar excess, Lanes 8-10) did not diminish the binding of either Jun or Jun-APEX2 to the labeled probe. These results were repeated in three distinct biological replicates.

Further Considerations & Caveats:

For commercially available fluorescent probes, it is important to titrate the amount of probe used per assay before performing experiments. In our hands, crisp bands were obtained using 16 times less probe per reaction than recommended by manufacturer while remaining within linear range. This probe was chosen for its ease of use to avoid protein transfer to a membrane; reactions were measured in-gel.

When choosing a mutated TF binding motif, first search the literature for a validated sequence known to abolish TF-DNA interaction. If none are validated, it is important to test several mutated sequences to ensure that TF-DNA binding is disrupted as the affinity for a specific sequence will vary.

Proximity labeled protein analysis

After validating the Jun-APEX2 construct, we used silver staining and MS to reveal proteins specifically interacting with the modified Jun. Three biological replicates were collected from PC12 cells transfected with either the control APEX2 (pW1-*ef1a*-linker-APEX2) or experimental Jun-APEX2 (pW1-*ef1a*-linker-*jun*-APEX2) plasmids. In addition to untreated cells, we also looked at an NGF-induced fraction to visualize any changes in PPIs between the control and experimental conditions.

Biotinylated proteins were collected on magnetic beads and were analyzed either with polyacrylamide gel electrophoresis (PAGE) silver stain or sent for MS analysis (Fig. 10A). One replicate was analyzed fresh (R1) and the remaining (R2-3) were stored at -80°C (Fig. 10A). We compared the silver-stained gels in three different trials performed on different days (Fig. 10B,C,E). The first trial used R1 of the proximity labeled lysates collected the same day as the

analysis (Fig. 10B, Fig. 11A). There was an observable difference in protein expression between both control and experimental samples as well as untreated and induced conditions. Three specific regions showed more intense staining in the Jun-APEX2 samples. However, after freeze-thaw, repeated silver stain analysis of the same R1 lysates did not replicate the results (Fig. 10C, Fig. 11B). In fact, no visible differences in interacting protein bands were observed between Jun-APEX and control after freeze-thaw in R1, R2 or R3 lysates (Fig. 10E, Fig. 11C). We performed MS analysis on the bands cut from the regions of interest in the fresh lysate gel (Fig. 10B). We also performed MS analysis on interacting proteins from the freeze-thawed lysate that remained in solution and were not separated by gel electrophoresis (Fig. 10D). These experiments and their differing outcomes will be discussed in detail below.

Silver stain analysis

There were clearly distinguishable differences in proteins interacting with Jun-APEX2 from the R1 fresh lysate as detected by silver stain (Fig. 11A). There were significant differences in band intensity between APEX2 and Jun-APEX2 samples. Though the APEX2 lanes appear less intensely stained, the total sample loaded was consistent between control/experimental and untreated/induced cells. Three main regions in the gel (~25, ~35, and ~55 kDa) displayed variation in band patterning and intensity (Fig. 10A black arrowheads).

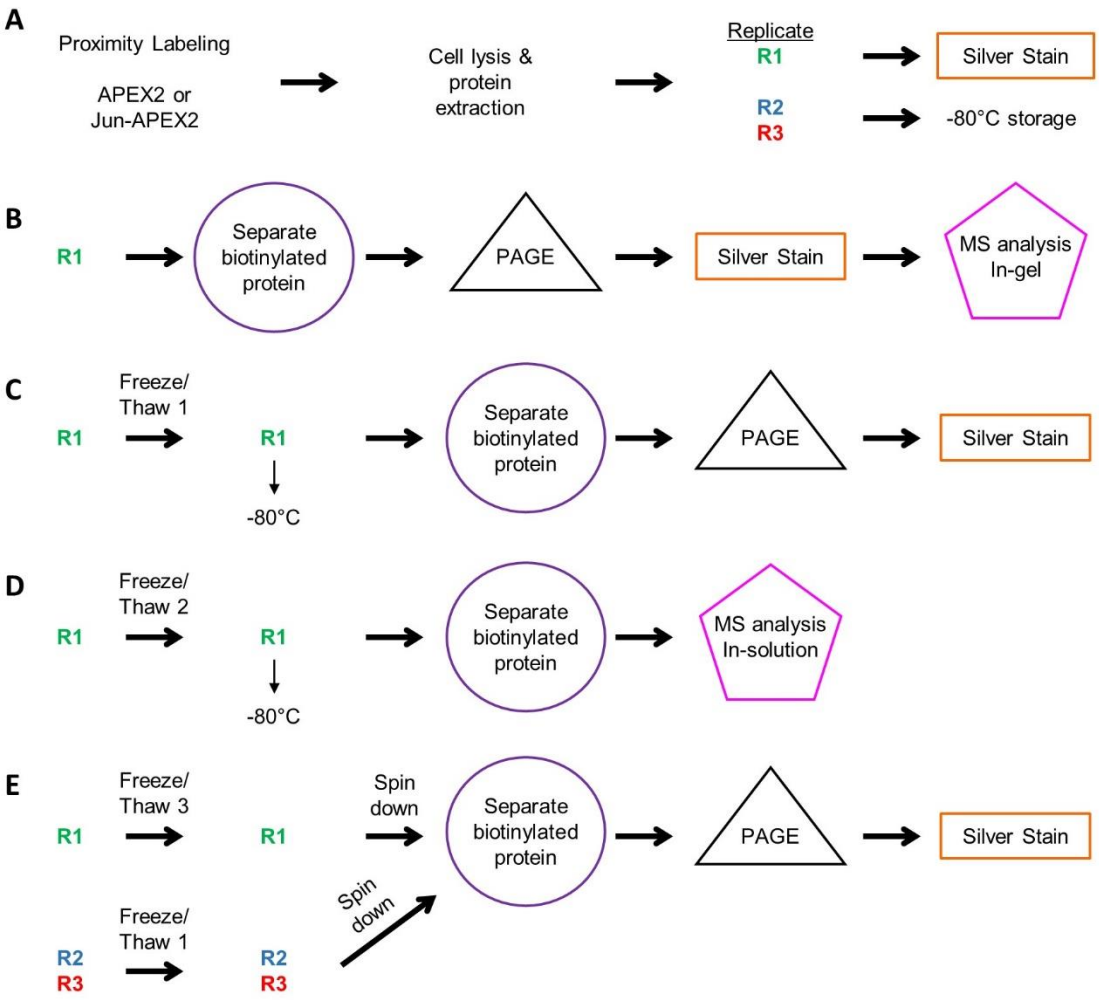

Figure 10: Workflow for biotinylated protein analysis. A: Three biological replicates (R1, R2, and R3) of PC12 cells were transfected with either pW1-*ef1a*-linker-*jun-APEX2* or pW1-*ef1a*-linker-*APEX2*. Twenty-four hours after transfection, the cells were either incubated with 100 ng/mL NGF or left untreated. The cells were then proximity labeled and whole cell protein lysates were prepared and either stored or used immediately. R1 was analyzed by silver stain analysis the same day of sample collection while R2 and R3 were immediately stored at -80°C. **B**: Fresh R1 protein lysate (untreated and stimulated) was subjected to streptavidin-coated magnetic beads to isolate biotinylated proteins. The remaining R1 sample was stored at -80°C. The biotinylated proteins were eluted from beads in denaturing loading dye for 10 min at 95°C. The biotinylated proteins were separated by polyacrylamide gel electrophoresis (PAGE) in a 10% gels and silver stained. The gel was stored at 4°C for two months, then in-gel mass spectroscopy (MS) analysis was performed. **C**: R1 lysate (untreated and stimulated) stored at -80°C was thawed on ice and resuspended by gentle vortexing. The sample was analyzed in the same manner as B. R1 lysate was returned to -80°C storage. **D**: R1 lysate (untreated and stimulated) stored at -80°C was thawed on ice and resuspended by gentle vortexing. Biotinylated proteins were isolated and sent for in-solution MS analysis. The remaining R1

sample was stored at -80°C. **E**: All three NGF-stimulated replicates stored at -80°C were thawed at room temperature, then analyzed as described for C, with the exception that the samples were thawed at room temperature, vortexed, and then centrifuged to bring down aggregates. The portion of lysate used for biotinylated protein isolation was carefully removed from the portion of the sample closest to the surface to avoid any aggregates. R1 had gone through three freeze-thaw cycles while R2/3 had freeze-thawed once. After biotinylated protein was isolated, they were separated by PAGE and silver stained.

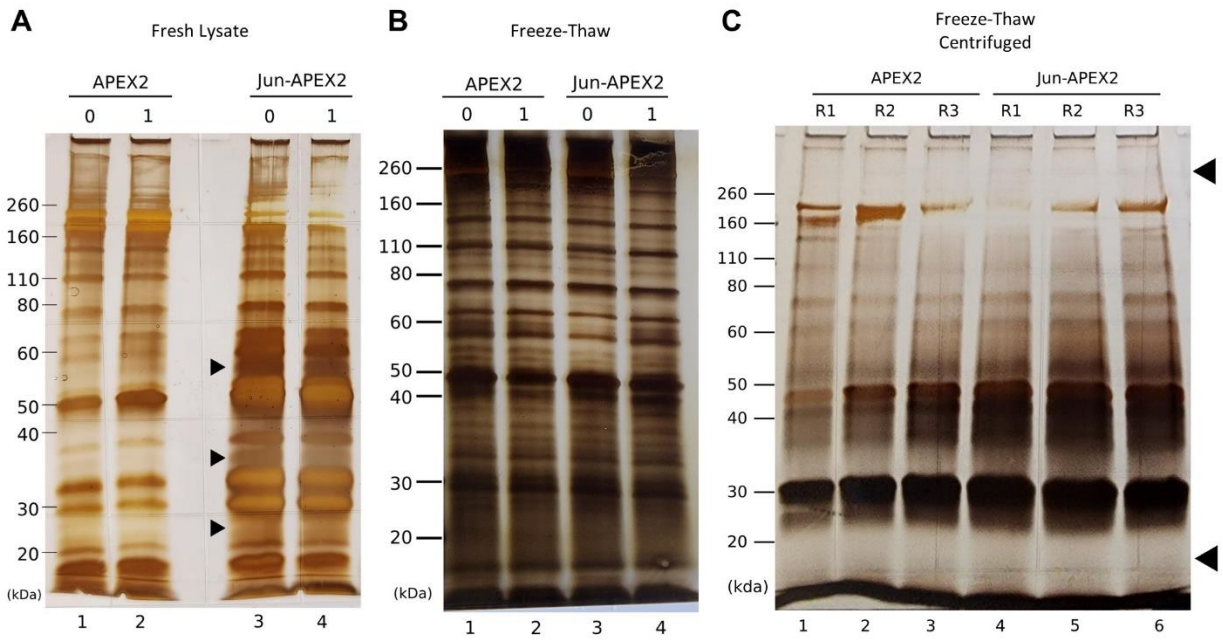

Figure 11: Silver stain analysis of proximity-labeled Jun-APEX2 or APEX2 transfected cells. A: Significant differences in band intensity were seen between APEX2 and Jun-APEX2 samples. Though the APEX2 lanes appear less intensely stained, the total sample loaded was consistent between control/experimental and untreated/induced cells. Three main regions in the gel (~25, ~35, and ~55 kDa) displayed variation in band patterning and intensity between Jun-APEX2 and APEX2 samples (black arrowheads). Refer to Fig. 10B for sample prep. **B**: The three regions of interest from A no longer showed distinct patterning between control and experimental lanes when analyzed after one freeze-thaw cycle. There is significantly more staining in the highest molecular weight region (>260 kDa) and all lanes have intense, diffuse staining at lower molecular weights (20-30 kDa). Distinct bands were seen between 30-40 kDa. Refer to Fig. 10C for sample prep. **C**: After centrifuging the lysates before isolating biotinylated protein, no major differences were seen between Jun-APEX2 or APEX2, all six lanes showed similar banding patterns and relative intensities. Unlike A and B, there was the clear lack of staining at molecular weights >260 kDa and ≤25 kDa (black arrowheads). Refer to Fig. 10E for sample prep.

To test for repeatability, additional silver stain analyses were performed using the same R1 lysate after storage at -80°C for approximately one month (Fig. 10C). The sample was thawed, biotinylated proteins were isolated on magnetic beads, and isolated proteins were separated by PAGE. Silver staining revealed significant differences between the proteins isolated from the fresh lysate when compared with those isolated from frozen lysate (Fig. 11 A & B, respectively). The three regions of interest (~25, ~35, and ~55 kDa) seen in the fresh lysate no longer showed distinct patterning between control and experimental lanes when analyzed after one freeze-thaw cycle. There was significantly more staining in the highest molecular weight region (>260 kDa) and all samples showed more intense, diffuse staining at lower molecular weight regions (20-30 kDa). Additionally, distinct bands appeared between 30-40 kDa after one freeze-thaw cycle. Protein degradation is a byproduct of thawing samples that have been frozen which may account for the appearance of lower molecular weight products (Franks, 1995, Mitchell et al., 2005). Furthermore, protein aggregation can be caused by freeze-thaw cycles due to protein denaturing and renaturing induced by thermodynamic changes of temperature and phase changes (Zhang et al., 2011). The denaturing conditions of PAGE analysis may not be able to overcome the bonds formed in soluble aggregates once large enough structures are formed, hence the observance of high molecular weight products in the silver stain after freeze thaw.

To determine if the differences in banding patterns and intensity between replicates were a result of protein aggregation, we repeated the experiment on all three biological replicates after freeze-thaw (Fig. 10E). We hypothesized that pre-clearing the thawed lysates via centrifugation before isolating the biotinylated protein fraction would remove the high

molecular weight aggregates. We compared samples of interacting proteins from centrifuged Jun-APEX2 and control APEX2 lysates in all three biological replicates (Fig. 11C). The sample preparation remained unchanged from the previous analyses, but the sample used for magnetic bead separation was taken from lysate that was centrifuged. We hypothesized that centrifugation would pellet aggregates at the bottom of the tube, leaving soluble protein in the remaining sample. All six lanes showed similar banding patterns and relative intensities. The major difference from the first two analyses was the clear lack of staining at molecular weights >260 kDa and ≤25 kDa. This suggests that pre-clearing the sample successfully removed the high molecular weight protein aggregate, but also obscured the differential PPIs seen at the lower molecular weights. It is possible that the lower molecular weight products separated from the aggregates during PAGE in the previous two silver stains. However, protein denaturation and degradation increase with each additional freeze-thaw cycle which may contribute to their disappearance in the third silver stain (Mitchell et al., 2005). Further analysis should be completed to determine the underlying reason for the discrepancies seen between replicate silver stains.

In-solution MS analysis

To reveal the putative Jun PPIs, in-solution digest and MS analysis of R1 was performed at the UW-Madison Biotechnology Center (Fig. 10D). Nearly 550 unique peptides were identified between all four conditions (minimum two peptides, FDR < 1.0%). However, only two Jun-APEX2 peptides were detected, and only in the untreated cells. This may indicate a transfection efficiency too low for detection and likely suggests that the identified proteins are those of high abundance, nonspecific interactions. As a consequence of these nonspecifically

binding proteins, any differences detected between control/experimental samples and time points may not be biologically relevant. Additional biological replicates of all samples should be analyzed by MS to evaluate any statistically significant and replicable interactions.

Of the ten most abundant in-solution proteins, six were associated with cell architecture, three with the endoplasmic reticulum, and one was known to be endogenously biotinylated in mammalian cells (Table 2). AHNAK is 581 kDa and it along with other high molecular wight proteins may be artifacts of protein aggregation. While the data do not reveal that Jun-APEX2 was expressed at levels detectable by MS, recombinant protein over-expression can induce large amounts of heat-shock proteins and chaperones due to protein misfolding (Gingras et al., 2005). Endoplasmic reticulum chaperone BiP/heat shock protein 70 was also detected by MS in a two-dimensional gel electrophoresis analysis of unstimulated PC12 whole cell lysate (Yang et al., 2006). The authors detected this protein associated with the unfolded protein response in 19 different spots and attributed the heterogeneity of this abundant protein to variation in post-translational modifications or truncation/degradation products (Yang et al., 2006). In the data presented here, however, the detection of the endoplasmic reticulum-associated protein is similar between the APEX2 and Jun-APEX2 samples as well as between and no treatment and stimulated cells.

Table 2: Most highly abundant proteins identified from in-solution MS analysis.

Rank	Identified Proteins	Accession Number	Alternate ID	Molecular Weight	Total Spectrum Count			
					No NGF		1 h	
					Control	Jun	Control	Jun
1	Myosin, heavy polypeptide 9, non-muscle	G3V6P7	Myh9	226 kDa	959	774	1534	1118
2	Pyruvate carboxylase	A0A0G2JTL5	Pc	140 kDa	158	144	149	122
3	Endoplasmin	A0A0A0MY09	Hsp90b1	93 kDa	128	125	124	120
4	ER chaperone BiP	P06761	Hspa5	72 kDa	138	141	121	107
5	UDP-glucose:glycoprotein glucosyltransferase 1	Q9JLA3	Uggt1	176 kDa	92	96	97	80
6	Myosin heavy chain 14	F1LNF0	Myh14	229 kDa	39	36	82	68
7	Cluster of Actin, cytoplasmic 2	P63259	Actg1	42 kDa	50	60	80	83
8	AHNAK nucleoprotein	A0A0G2JUA5	Ahnak	581 kDa	64	68	67	47
9	Protein disulfide-isomerase	A0A0H2UHM5	Pdia3	57 kDa	60	66	63	51
10	Cytoskeleton-associated protein 4	D3ZH41	Ckap4	36 kDa	66	61	60	51

Proteins highlighted in different colors correspond to different cellular terms. Light blue = cell architecture/cytoskeleton. Green = endogenously biotinylated protein. Orange = endoplasmic reticulum.

As the most abundant protein from the in-solution MS analysis, changes in myosin variants may play a role in cytoskeletal changes induced by NGF. The β and γ actin and myosin light chains 2 and 3 all increase in mRNA expression by 1 day after NGF stimulation (Henke et al., 1991). Myosin V is also known to play a role in fibroblast growth factor (FGF-2)-induced PC12 differentiation (Wolff et al., 1999). The G protein-coupled receptors (GPCRs) can interact with microtubules to regulate cytoskeletal dynamics associated with neurite outgrowth, particularly the α and βγ subunits of heterotrimeric G proteins (Yu et al., 2009, Sachdev et al., 2007). In primary hippocampal neurons, the G-protein (Gβγ) and a component of the dynein motor complex affect neurite outgrowth (Sachdev et al., 2007). Furthermore, Gβγ interacts with microtubules to rearrange the cytoskeleton during PC12 neurite outgrowth and differentiation (Sierra-Fonseca et al., 2014). In our data, myosin was also found to be differentially regulated between APEX2 and Jun-APEX2 samples.

From the proteins that were differential between Jun and control samples from untreated to 1 hour post NGF, one is known to be endogenously biotinylated (Fisher's test with multiple test correction, $p<0.00010$, Table 3). The top nine were associated with cell architecture in which seven are significantly up-regulated in Jun at 1 hour post NGF in comparison to untreated cells. At 0.5 and 1 h after NGF-induction in PC12 cells, another temporal MS study of JNK-interacting proteins identified many actin-binding cytoskeletal proteins and numerous members of the myosin family known to be involved in cytoskeletal reorganization and cargo shuttling along microfilaments (Sury et al., 2015). As these data represent one biological replicate, additional analyses must be completed to demonstrate replicability.

Of interest in the differentially detected proteins was the cytoskeletal/membrane adaptor protein stratifin. There was no change in spectral counts for stratifin in the control samples with two peptides detected, however, it increased over 7-fold (23 peptides) in Jun samples at 1 hour post NGF compared to untreated cells. Stratifin or 14-3-3 proteins act as adaptors between membrane/channel proteins and their interactors or modifiers. Stratifin is rigid in structure and evidence suggests that its binding to the carboxy terminus of the plant plasma membrane H^+-ATPase (PMA) leads to the activation of its ATPase activity through assembly of six PMA proteins into a hexagonal structure (Kanczewska et al., 2005). In cardiac cells, stratifin binding to hERG channels is promoted by PKA-mediated phosphorylation (Kagan et al., 2002). This interaction protects hERG channels from desphosphorylation which augments the potassium currents and decreases action potential duration (Kagan et al., 2002). At post-synaptic clusters, stratifin is believed to recruit additional subunits to the nicotinic acetylcholine receptor (nAChR) (Rosenberg et al., 2008). As a member of the multi-subunit cytoskeletal-anchoring complex, stratifin is believed to bridge the microtubules to the α-3 subunit of the nicotinic acetylcholine receptor which stabilizes those interactions and ultimately the synapse (Rosenberg et al., 2008). Stratfin may play important roles in cytoskeletal interactions as well as channel activity initiated by NGF.

Table 3: Differentially detected proteins identified from in-solution MS analysis.

Identified Proteins	Accession Number	Alternate ID	Molecular Weight	Total Spectrum Count			
				No NGF		1 h	
				Control	Jun	Control	Jun
Desmoplakin	F1LMV6	Dsp	332 kDa	39	13	6	170
Cluster of Myosin heavy chain 2	A0A0G2K484	Myh1	223 kDa	5	4	7	87
Cluster of Keratin, type II cytoskeletal 1b	Q6IG01	Krt77	57 kDa	27	20	20	80
Cluster of Myosin, heavy polypeptide 9, non-muscle	G3V6P7	Myh9	226 kDa	959	774	1534	1118
Plakophilin 1	D3ZY51	Pkp1	67 kDa	2	0	0	21
Cluster of Junction plakoglobin	Q6P0K8	Jup	82 kDa	12	7	5	41
Plectin	Q6S3A0	Plec	534 kDa	40	62	30	30
Latent transforming growth factor-β binding protein 2	A0A0G2K1G5	Ltbp2	197 kDa	10	21	8	3
Stratifin	G3V9A3	Sfn	28 kDa	2	2	3	23
Methylcrotonoyl-CoA carboxylase subunit α	F1LP30	Mccc1	79 kDa	39	50	38	23

Proteins highlighted in different colors correspond to different cellular terms. Light blue = cell architecture/cytoskeleton. Green = endogenously biotinylated protein.

In-gel MS analysis

As the in-solution MS data did not reveal many nuclear proteins as predicted, the areas of interest (~25, ~35, and ~55 kDa) from the fresh lysate silver stain were sent for MS analysis at the UW-Madison Biotechnology Center (Fig. 10B). MS is sensitive enough to detect differences in protein content in gel pieces that are not discernible by silver stain. We hypothesized that the three visually distinguishable regions would yield differentially detected Jun-interacting proteins. Additionally, using the silver stain of the fresh sample would circumvent the complications associated with possible degradation/aggregation due to sample freeze-thaw.

The in-gel analysis was performed on three regions per lane (APEX2 and Jun-APEX2, untreated and NGF stimulated) for a total of 12 gel pieces. Each was digested individually, but each region (~25, ~35, and ~55 kDa) for either condition (untreated or NGF-stimulated) was combined for MS analysis for only APEX2- or Jun-APEX2 interacting proteins (three samples per control or experimental sample). This sample preparation excludes differentiation between untreated and NGF-induced proteins but includes differences at the regions of interest between control APEX2 and experimental Jun-APEX2 samples. This method of preparation and analysis was chosen to ensure instrument sensitivity of the sample peptides.

A total of 825 unique peptides were identified between the six samples. Of the top five most abundant proteins in all three regions of interest (~25 = low, ~35 = mid, and ~55 kDa = high), ribosomal proteins represented at least 2 members (Table 4). Other proteins detected in the bands were vesicular trafficking proteins Rabs and the endocytosis-associated activator protein 2 complex which will be discussed below. Of the differentially detected proteins (FDR<1%), four were associated with ribosomes and two were Rabs.

Table 4: High abundance and differentially detected proteins identified from in-gel MS analysis.

	Rank	Identified Proteins	Accession Number	Alternate ID	Molecular Weight	Total Spectrum Count	
						Control	Jun
Low	1	Cluster of 60S ribosomal protein L24	A0A0H2UH99	Rpl24	18 kDa	117	96
	2	Cluster of 60S ribosomal protein L17	A0A0H2UHQ1	Rpl17	22 kDa	75	60
	3	Cluster of 60S ribosomal protein L21	D3Z9G3		19 kDa	65	54
	4	Cluster of 60S ribosomal protein L18a	P62718	Rpl18a	21 kDa	56	39
	5	Cluster of RAB10, member RAS oncogene family	Q5RKJ9	Rab10	23 kDa	33	38
	23*	Ras-related protein Rab-13	P35286	Rab13	23 kDa	5	9
	26*	Ras-related protein Rab-21	Q6AXT5	Rab21	24 kDa	5	8
Mid	1	Cluster of Histone H1.4	P15865	H1-4	22 kDa	109	116
	2	Cluster of 60S ribosomal protein L6	F1LQS3	Rpl6-ps1	34 kDa	138	85
	3	60S ribosomal protein L7	B0K031	Rpl7	30 kDa	50	63
	4	40S ribosomal protein S3	P62909	Rps3	27 kDa	67	57
	5	40S ribosomal protein S3a	P49242	Rps3a	30 kDa	32	36
	26*	Cluster of 40S ribosomal protein S2	D3ZT78		29 kDa	6	12
High	1*	60S ribosomal protein L4	Q6P3V9	Rpl4	47 kDa	65	118
	2	Adaptor protein 2 complex subunit μ	P84092	Ap2m1	50 kDa	88	62
	3	Cluster of Tubulin beta-5 chain	P69897	Tubb5	50 kDa	102	55
	4	Protein disulfide-isomerase A6	A0A0G2JSZ5	Pdia6	49 kDa	59	40
	5	Cell growth-regulating nucleolar protein	Q6AYK5	Lyar	44 kDa	40	40
	9*	Eukaryotic translation initiation factor 2 subunit β	Q6P685	Eif2s2	38 kDa	25	35
	19*	Cluster of RNA helicase	Q6P3V8	Eif4a1	46 kDa	10	23

An asterisk (*) denotes differentially detected proteins (FDR<1%). Proteins highlighted in different colors correspond to different cellular terms. Light purple = ribosomal. Light pink = G-proteins. Aqua = nuclear. Yellow = vesicular transport. Light blue = cell architecture/cytoskeleton. Orange = endoplasmic reticulum. Low = ~25 kDa, mid = ~35 kDa, and high = ~55 kDa from regions of silver stain gel in Fig. 10B.

Rab proteins are small, monomeric GTPases whose numerous and heterogeneous members localize to discrete intracellular compartments and largely regulate vesicular transport between organelles (Novick and Zerial, 1997). Rab GTPases are “switched” on and off through the cycling of interactions with guanine nucleotide exchange factors (GEFs) and GTPase-activating proteins (GAFs). Some Rabs have been linked to neuronal differentiation. For example, Vps9 domain and ankyrin-repeat-containing protein (Varp) is a GEF of Rab21 (Burgo et al., 2009). In differentiating murine hippocampal neurons, tetanus neurotoxin-insensitive vesicle-associated membrane protein (TI-VAMP), Varp, and Rab21 all co-localize and regulate vesicular transport in neurites (Burgo et al., 2009). Rab proteins mainly function in vesicular transport, but some belong to the family of Ras GTPases that function in signal transduction.

The three Rabs identified in this data (Rab10, Rab13, and Rab21) are all members of the larger Ras superfamily of GTPases. Ras is generally associated with the activation of signal transduction pathways through plasma membrane receptors for growth factor and adhesion molecules (Hall and Lalli, 2010). Ras has been shown to activate ERK and MAPK signaling cascades which have been implicated in neurite extension in PC12 cells (Markus et al., 2002). Signal transduction plays an important role during axon guidance which is mediated by proteins in the cell membrane of the growth cone.

Adaptor protein complex (AP-2) is commonly associated with synaptic vesicle recycling. AP-2 mediates endocytosis through its interaction with clathrin and clathrin-coated vesicles (Schmid and McMahon, 2007). However, AP-2 may also play an important role in neuronal development. Clathrin-mediated endocytosis regulates cell surface expression of receptors for axon guidance cues and AP-2 plays a role in chemotaxis and conveying directional cues during

axonogenesis (Tojima et al., 2010, Raman et al., 2014). Furthermore, in developing rat hippocampal neurons *in vitro*, the shRNA-knockdown of AP-2 significantly decreased axon growth (Kyung et al., 2017). However, the role of AP-2 during the very early stages of PC12 neuronal differentiation remains unclear.

Ribosomal biogenesis varies throughout the developmental stages of the brain. The nucleolus synthesizes ribosomal RNA. As a model for post-mitotic neurons, the nucleoli from chicken cerebellar Purkinje neurons from embryonic day 13 to post-hatching day 7 were used to approximate the ribosomal changes that occur during neuronal maturation (Lafarga et al., 1995). The number of nucleoli increased during this period, corresponding to times of dramatic structural changes (Lafarga et al., 1995). In the rat forebrain, ribosome biogenesis and total protein content steadily increase as the forebrain develops from post-natal days 7-42 (Slomnicki et al., 2016). However, in rat callosal projection neurons, a decrease in ribosomes is mediated by the proteasome in axons undergoing synaptogenesis (Costa et al., 2019). The ribosomal content varies as a neuron progresses to maturation.

The eukaryotic translation initiation factor 2 (eIF2) is associated with ribosomes for its role in translation initiation. The initiator methionyl-tRNA is brought to the 40 S ribosomal subunit by eIF2. The presence of these ribosome-associated proteins (e.g. eIF2 and the various subunits of both the 40S and 60S ribosomal components) in the stimulated PC12 cells is congruent with the increased requirement of new protein synthesis for neuronal differentiation to initiate neurite extension.

The Jun-APEX2 fusion protein was not detected in any of the gel pieces. However, this does not preclude its presence in the sample. Post-translational modifications may cause

significant variation in gel migration pattern, so Jun-APEX2 may be present elsewhere in the sample lane. To determine where the fusion protein is migrating within the lane, an anti-APEX2 antibody would reveal its localization while multiple bands would suggest several states of post-translational modifications.

Further Considerations & Caveats:

In our experience, the proximity labeled PC12 whole cell lysate demonstrated different banding patterns when analyzed by silver stain after freeze-thaw in comparison to fresh lysate. This could be a result of degradation, aggregation, or protein-refolding induced by thermal stress (Vasconcelos et al., 2021, Mitchell et al., 2005, Hawe et al., 2009). Therefore, it is recommended to proximity label, isolate biotinylated protein, and begin preparation for MS analysis on the same day. For in-gel analysis, separation by gel electrophoresis should maintain true interactions, but in-solution samples should be subjected to trypsin digestion the same day as protein isolation.

The silver stain analysis can reveal differences in PPIs between sample conditions, but hundreds of proteins may be represented in each band. Two-dimensional gel electrophoresis would provide another level of separation to reveal protein expression differences that are obscured within a single band as analyzed by traditional one-dimensional PAGE. Post-translational modifications to proteins can cause proteins to migrate in a different pattern based on hydrophobicity, changes in protein structure, overall charge, or isoelectric point. Taking advantage of such differences, two-dimensional gel electrophoresis has helped reveal differentially detected proteins that were later identified by MS (Yang et al., 2006).

Discussion

The Jun-APEX2 fusion protein was validated for functionality in cellular localization, substrate requirements, and DNA binding specificity. Silver stain visualization of the proximity labeled protein showed differences between control APEX2 and experimental Jun-APEX2 samples that were either untreated or stimulated for 1 hour with NGF. However, this observation was not repeatable. A silver stain of the same replicate that underwent showed no differences in staining patterns or intensity. Hypothesizing that protein aggregation induced by freeze-thaw obscured the initial differential patterning, the samples were pre-cleared before biotinylated proteins were isolated using streptavidin magnetic beads. A silver stain of this sample preparation showed decreased high molecular weight protein, indicating that the aggregates were successfully removed. However, a concurrent decrease in staining intensity was seen in the region ≤25 kDa. The discrepancies between silver stain analyses are unclear, but we hypothesize that freeze-thaw induced changes in protein structure may underly these observations.

There are a few possibilities that could lead to these phenomena in which protein aggregation and degradation may play a role. During freeze-thaw cycles of sample storage, proteins undergo phase changes that subject them to mechanical damage and denaturing conditions in part due to changes in pH (Mitchell et al., 2005, Benjakul and Bauer, 2000). Furthermore, protein aggregation can result from structural changes induced by freeze-thaw that internalize hydrophilic residues that would otherwise be exposed to the surface (Zhang et al., 2011). To reduce the degradation of freeze-thaw, slow freezing and fast thawing prevents damage to proteins that is seen with fast freezing and slow thawing, even preserving enzymatic

activity (Cao et al., 2003, Jain et al., 2021). The silver stain analyses of the biological replicates were not replicable. We hypothesize that freeze-thaw cycles caused degradation and aggregation of the proteins. More analysis is required to determine if the root cause of the variability in silver stain results between freeze-thaw cycles.

Contrary to our hypothesis that mostly nuclear proteins were detected, the majority of proteins identified either in-solution or in-gel MS analyses were cytoplasmic. The most abundant in-solution proteins were associated with cellular architecture and the endoplasmic reticulum. The differentially detected proteins were exclusively cytoskeletal apart from one endogenously biotinylated protein. The neuronally differentiating PC12 cell drastically changes in structure and morphology, and these identified proteins may reflect the initiation of those events.

The in-gel MS data revealed a more varied proteome. Of the top five most abundant proteins across the three regions of interest, nearly half were associated with ribosomes. Also present were Rab GTPases and the clathrin-associated activator protein complex (AP-2). Rabs play a role in vesicular trafficking while AP-2 is associated with endocytic events. As the PC12 cell responds to NGF, newly synthesized proteins will need transport to their appropriate cellular compartments.

We predicted that Jun interacts with different proteins at different times during NGF-induced neuronal differentiation of PC12 cells. While the MS analyses were successful in detecting proteins, mostly cytoplasmic or membrane proteins were detected. We interpret that this is due to a low transfection efficiency in which too little of the Jun-APEX2 fusion protein was expressed for its PPIs to be identified by MS. Without enough of the Jun-APEX2 construct,

too few proteins were biotinylated and thus the nonspecific proteins overwhelmed the MS signal. Furthermore, the masking effect of the nonspecific proteins is exacerbated by the already very low abundance of TF within cells. More replicates would reveal if the identified, likely nonspecific, proteins were statistically significant. To address this deficiency, there are a few options to increase the amount of Jun-APEX2 protein.

Higher expression of the Jun-APEX2 fusion protein both across the total cell population and in the cells themselves would increase the probability of successful MS detection of putative PPIs. This deficiency could be addressed by increasing transfection efficiency to bolster the number of Jun-APEX2-expressing cells. Better optimization of transfection reagent and efficiency would increase the percent of starting material that contained Jun-APEX2 and therefore increase downstream analysis sensitivity to proximity labeling. Another option to increase recombinant protein production in transfected cells is to use a different promoter. We used the *xenopus laevis ef1a* promoter which may not be as highly expressed in the mammalian cells. By changing the promoter to one optimized for mammalian expression, the amount of translated recombinant protein could be increased. Furthermore, additional replicates are necessary for greater power in the statistical analysis of protein identifications.

As there are few MS analyses evaluating the changing proteome during PC12 neuronal differentiation, more studies that reveal the PPIs throughout this event would provide great insight into the underlying cellular processes. While induction of PC12 differentiation by NGF is well established, the molecular mechanisms by which this occurs are not well understood. A co-immunoprecipitation-MS analysis of the Shc adaptor protein revealed some important PPIs. NGF activates a MAPK cascade that is mediated by the Shc (Cohen et al., 1995, Pelicci et al.,

1992). PC12 cells stimulated with NGF for four hours and the Shc-interacting proteins were separated using PAGE and subjected to MALDI-MS (Patterson et al., 1996). Providing further evidence that Shc interacts with the cytoskeleton, three direct interacting proteins were identified as β/γ-actin, α-actinin, and neuronal myosin heavy chain (Patterson et al., 1996). This approach provided valuable information for the PPIs of Shc, but its interactions are a very small part of the signaling initiated by NGF.

A more exhaustive analysis of the PC12 proteome was evaluated in undifferentiated cells using two-dimensional gel electrophoresis. A total of 1080 protein spots were selected and analyzed with MALDI TOF/TOF MS (Yang et al., 2006). Many proteins were present in multiple spots including heat shock cognate 71 kDa protein, pyruvate kinase, and heat shock 70 kDa protein 5. The heterogeneity of these proteins' presence may be attributed to post-translational modifications that affect their migration patterns. Additionally, their abundance may be a result of fragmentation. From the 1080 spots, 474 gene products were represented (Yang et al., 2006). Gene ontology analysis revealed that the proteins involved in binding and catalytic activity comprised 59.0% of all proteins while structural proteins followed at 10.3%. While this analysis was more comprehensive than co-immunoprecipitation-MS, two-dimensional gel electrophoresis-MS is still inherently biased in protein identification through the choice of spots.

An unbiased and quantitative approach to examine proteomic changes employs quantitative MS techniques. To evaluate the neuronal differentiation proteome, two separate MS instruments were used to analyze differentiating PC12 cells with the isobaric tagging system iTRAQ. Both MALDI and ESI-MS/MS were used to quantitatively reveal differentially detected

proteins in iTRAQ-labeled whole cell lysate (Kobayashi et al., 2009). In total, 1482 proteins were identified with 580 unique identities by MALDI and 158 by ESI with an overlap of 744 between the two. (Kobayashi et al., 2009) In comparison to untreated PC12 cells, 39 proteins were up-regulated while 33 were down-regulated in cells stimulated with NGF for 48 hours (Kobayashi et al., 2009). According to gene ontology analysis, proteins most represented in the up-regulated category were those associated with cell morphogenesis and apoptosis (cell survival) while the down-regulated category included cellular metabolic processes (Kobayashi et al., 2009). By combining data from parallel MS analysis, an increased number of unique peptides were identified. Even though PC12 cells have been a popular neuronal differentiation model for nearly 50 years, there are few MS studies that examine proteomic changes over that time course.

Proximity labeling techniques are excellent tools to identify potential PPIs both *in vitro* and *in vivo.* However, additional steps are required to verify if the interaction is direct or indirect, stable or transient. Any direct-interacting proteins from the MS data can be further resolved using methods such as surface plasmon resonance. This technique measures the angle of reflected light produced from the binding of the protein in question with a protein of interest to determine affinity constants and dissociation rates (Barberis et al., 1995, Corr et al., 1994). For proteins with validated antibodies, stable complex formation between two known proteins can be confirmed using co-immunoprecipitation (Zhou et al., 2022, Chung et al., 2017). Yeast two hybrid assays have been used to confirm the physical interaction of proximity labeling-identified proteins as well (Mair et al., 2019). To resolve larger complexes of unknown content, affinity purification or tandem affinity tagging techniques in combination with MS will reveal

the makeup of the components (Liu et al., 2018, Liu et al., 2020). Furthermore, comparing the data between two different proximity labeling enzymes can identify putative stable interactions or contribute to the likelihood of the interaction (Mazina et al., 2020, Rosenthal et al., 2021). Proximity labeling-MS can serve as a hypothesis-generating machine to investigate the importance of PPIs with functional validations.

Proximity labeling is sensitive enough to detect transient interactions, such as post-translational modifications by enzymes, and those PPIs can be probed using functional assays. The impact of Jun phosphorylation by MAPKs was tested using kinase inhibitors and the effect was quantified by changes in protein expression and neurite extension. Inhibition of MEK, p38, and JNK moderately attenuated NGF-induced neurite outgrowth (Eriksson et al., 2007). The expression of cJun was decreased by MEK inhibitors, cFos was decreased by MEK and JNK, and JunD was unaffected (Eriksson et al., 2007). Furthermore, inhibition of MAPKs had no discernible effect on apoptosis mediated by anisomycin (Eriksson et al., 2007). The significance of PPIs resulting in phosphorylation can be evaluated by small molecule kinase inhibitors and measured as cellular and molecular changes.

Combining PPIs validated from proximity labeling-MS data with deep sequencing data is a powerful analysis to investigate the role of TFs in gene regulation. For example, a multi-omics study was looking at TF interactions in drosophila. In S2 cells, co-immunoprecipitation confirmed the interactions of several proteins with the EcR/USP heterodimer while chromatin immunoprecipitation (ChIP)-seq data of EcR and the confirmed complexing protein CP190 revealed that only a fraction of all identified sites were bound by both factors (Mazina et al., 2020). Further comparison to capture chromatin conformation (Hi-C) data showed areas highly

enriched in CP190 often interacted with promoters/enhancers of 20E-responsive developmental genes and that the CP190 sites facilitated chromatin interactions between multiple regulatory regions of those genes (Mazina et al., 2020). Gene expression is controlled not only by TFs but is also influenced by chromatin structure and accessibility. The combination of transcriptomic, PPI, and chromatin conformation will elucidate the spatial-temporal regulation of gene expression.

More detailed PPIs identified with proximity labeling over a time course and/or in response to a treatment are revealed when using quantitative MS analysis. Quantitative analysis greatly reduces the likelihood of false positive discovery rate by identifying nonspecific binders which are generally in high abundance. This is achieved by using methods such as stable isotope labeling by amino acids in cell culture (SILAC) or tandem mass tagging (Ong et al., 2002, Thompson et al., 2003). Both methods determine the identity of peptides and their relative abundance in multiple samples simultaneously. SILAC is performed in cell culture and therefore requires very few additional steps for preparing samples. Tandem mass tags have a high sensitivity which is beneficial for low-abundance proteins like TFs but requires larger amounts of protein than SILAC and thus more sample material. Care must be taken in general handling technique and sample preparation to ensure high labeling efficiency and signal as the labeling reaction is pH-sensitive (Zecha et al., 2019, Hutchinson-Bunch et al., 2021). Label-free methods have been shown to detect more phosphorylated peptides in addition to superior overall coverage but are less quantifiable (Stepath et al., 2020). Quantitative MS analysis can provide a wealth of potential PPIs in many different contexts and experimental conditions.

Revealing the protein interactomes of multiple TFs could be the key to understanding how temporal gene expression is regulated. The availability of TF binding sites within the open regulatory regions of genes changes throughout development and in response to extracellular signals. The interactions and co-operation of hundreds of proteins control the dynamic chromatin landscape and subsequently transcription. Proximity labeling-MS data of TFs can be combined with chromatin conformation, ChIP- and RNA-seq data to reveal which TFs control the expression of specific genes. This type of information will greatly aid in our understanding of the complex protein-protein and protein-DNA interactions that facilitate cell processes.

Chapter 3 General Discussion

Summary of key findings

A proximity labeling transcription factor construct was designed and functionally validated. The Jun-APEX2 fusion protein localized to the nucleus of PC12 cells and bound DNA in a sequence-specific manner (Fig. 7, Fig. 9). The APEX2 peroxidase biotinylated nuclear proteins only when both of its substrates were present (Fig. 8). As proof of principle to demonstrate that the proximity labeling construct would detect putative PPIs, APEX2 control and Jun-APEX2 experimental samples were evaluated for any visual differences in biotinylation patterns using silver staining (Fig. 10). Fresh protein lysates showed distinct differences between APEX2 and Jun-APEX2 as well as between untreated and stimulated cells (Fig. 11A). Variations in banding and band intensity were visible, particularly in three molecular weight ranges ~25, ~35, and ~55 kDa.

The silver stain analysis was repeated twice more to test for replicability. When using the same replicate sample that had undergone freeze-thaw, the silver stain results did not match those of the first gel (Fig. 10C). When repeated, all time points and conditions shared similar band patterns and intensity (Fig. 11B). Staining was increased in the area >260 kDa and there were more bands at lower molecular weights between 20-30 kDa. We hypothesized that these differences were due to protein aggregation and degradation due to sample freeze-thaw. Therefore, the sample preparation was modified to remove aggregates through brief centrifugation before isolating the biotinylated proteins with magnetic beads (Fig. 10E). A silver stain of all three biological replicates of stimulated samples revealed that the high molecular weight products were significantly reduced in all samples, but there was a concurrent decrease

in staining in the area ≤25 kDa (Fig. 11C). Increasing freeze-thaw cycles have been shown to increase protein denaturation, aggregation, and degradation, but further research must be performed to determine the root cause of the discrepancies in repeatability (Mitchell et al., 2005, Vasconcelos et al., 2021, Zhang et al., 2011).

MS analysis was performed both for samples prepared in-solution and also in-gel. In-solution MS analysis returned over 550 unique protein identifications (Table 2). However, only two peptides for the Jun-APEX2 fusion protein were detected. Several reasons could contribute to this observation which will be discussed in the next section. As TFs are low abundance proteins and the transfection efficiency was low, we hypothesize that the biotinylated Jun-protein interactors were masked by the far more abundant cytosolic proteins. Therefore, the MS data may not be of biological relevance. These are the results of only one replicate, so inter-replicate statistical significance cannot confirm that the detected proteins were nonspecifically binding.

Contrary to our hypothesis that mostly nuclear proteins would be detected, the majority of proteins yielded by MS analysis were cytoplasmic. Different cytoplasmic protein populations were represented in either the in-gel and in-solution data. From the latter, the most abundant proteins were cytoskeletal or associated with the endoplasmic reticulum. Of the differentially detected proteins, most were involved in cell architecture such as cytoskeletal, membrane adaptors, or extracellular matrix proteins (Table 3). This is in accordance with the architectural changes that a cell must undergo to prepare for neurite extension.

The in-gel MS analysis of the three differentially stained regions detected a variety of proteins (Table 4). Common amongst all three molecular weight classes were ribosome-

associated proteins which were also four of the six differentially detected proteins. Also present were Rab GTPases and the adaptor protein complex (AP-2).

Critical evaluation of the current approach

A potential limitation to the data presented here is the lack of proof that Jun-APEX2 is transcriptionally active. This luciferase validation for transcriptional activity of Jun-APEX2 was unsuccessful. Initial investigation using luciferase assays (CMV-ELuc::6xAP-1-Ren) was inconclusive due to an AP-1 site in the CMV promoter. Due to this site, the control Eluc (enhanced luciferase) enzyme is also transcribed by Jun-APEX2 binding to the CMV promoter. As the amount of control luciferase should remain unchanged between experimental conditions, this rendered the data inconclusive. Attempts to remove or mutate the site were unsuccessful. However, the data obtained indicated that Jun-APEX2 is likely transcriptionally functional as the Renilla luciferase signal changed as the amount of Jun-APEX2 was varied in comparison to control luciferase.

Whole cell protein lysate was used for silver stain analysis. A more suitable negative control could be APEX2 with nuclear localization signal (NLS). This would rule out any non-specific nuclear proteins in the Jun-APEX2 sample lysates. Furthermore, the nuclear protein content of a cell makes up a fraction of the whole cell protein. A more targeted sample consisting of only nuclear protein extract would remove all of the endogenously labeled cytosolic proteins in addition to the non-specific cytosolic binding proteins. However, because the nuclear content is a small portion of the whole cell, a larger amount of initial sample material would be required for sufficient protein analysis. Together, the APEX2-NLS would likely

deliver more reliable putative PPI identifications with the caveat of requiring a larger sample amount.

A caveat to the approach taken here is the variability of transfection efficiency. As evaluated by Jun-GFP transfection, the amount of PC12 cells that successfully took up the *ef1α*-Jun-GFP plasmid was <5%. This is also supported by Amplex UltraRed assays in which peroxidase activity served as a read-out for Jun-APEX2 expression. Furthermore, only two Jun-APEX2 peptides were detected in the MS in-solution data. Therefore, the MS analyses likely do not show true identifications due to the nonspecific binding of other proteins overwhelming the biotinylated proteins of interest. To address this, transfection efficiency could be further optimized, or a reagent better suited for PC12 transfection could provide better results. In our hands, both electroporation and nucleofection caused overwhelming cell death with no increase in transfection efficiency. The best option may be to genetically modify a line of PC12 cells to replace endogenous Jun with Jun-APEX2. With the fusion protein under control of the endogenous Jun promoter, Jun-APEX2 would be expressed in all cells and would change in response to NGF as would endogenous Jun. The amount of protein required would be significantly less than under transfection conditions. Furthermore, only nuclei would be collected if APEX-NLS was the negative control, thus limiting the sample collection to only nuclear protein and minimizing non-specific binding at later isolation steps.

The knowledge obtained for protein function in one species is often assumed for other species. This type of thinking is deceptive, however, as significant homology does not equate to similar function. Due to differences in chaperone proteins, protein folding, and tertiary structure can vary between species. The surface-accessible amino acids will interact with other

molecules, so their position-based availability will influence the protein's function. Evidence against sequence homology inferring functional similarity is seen between cell types within the same species. The variation in proteomic content and DNA conformation dictates cell fate and type. Therefore, the presence or absence of one or more proteins can affect the function of a single TF as the combined interactions of many TFs and proteins determine whether or not a gene is transcribed. It is possible that the zebrafish Jun may not function the same as mammalian cJun in PC12 cells. This may not reflect the true interactions of Jun due to variations in amino acid sequence despite their 73% homology.

To obtain the best data, it is important to choose the MS instrument that best fits the sample and type of analysis desired. A mass spectrometer detects the mass-to-charge ratio (m/z) of molecules present in a sample. To separate its components, the sample is loaded into the MS instrument using a liquid chromatographer (i.e., HPLC). The sample is ionized, sorted by m/z, and measured by abundance. For our purposes, the peptides were analyzed on the Thermo Scientific™ Orbitrap Elite. The nano-level sample separation paired with the Orbitrap instrument provides well-separated data with high sensitivity (60,000 full width at half maximum (FWHM) at m/z 400, Thermo Scientific™ Orbitrap Elite). In comparison to the Orbitrap, a quadrupole time-of-flight (Q-TOF) has lower resolving power (30,000 FWHM at m/z 1,972, Shimadzu LCMS-9030) and a lower dynamic range of resolution, thus lower mass accuracy in detection. While the Q-TOF is sufficient to detect peptides, an Orbitrap is better suited for discovery methods due to its ability to both separate and distinguish between m/z values.

Freeze-thaw effect on protein stability

Protein denaturation, loss of biological activity, and generation of high molecular weight species are well-established effects of temperature on protein structure and activity. Because of this, the number of freeze-thaw cycles to a protein sample should be restricted as much as possible to limit the effects of phase change. The consequences this process has on the identification of putative PPIs by MS should be better investigated, but what is known about the effects of freeze-thaw and analysis of protein is reviewed here.

MS is used to reveal biomarkers in patient samples, many of which are stored frozen until the time of analysis to reduce protein degradation. Little is known about how sample handling impacts the proteins within these samples and how that may affect the fidelity of biomarker identification. A study investigated the effects of multiple freeze-thaw cycles and long-term storage on the MALDI-TOF MS scans of blood plasma samples (Mitchell et al., 2005). As for the latter, little difference was seen between peak number, mass distribution, or coefficient of variation. However, the effects of repeated freeze-thaw cycles generally trended toward decreased peak intensity. A small change in median peak intensity between 2-5 freeze-thaw cycles suggests that the plasma proteins are relatively stable. However, the high range of intensity change was striking. After 4 freeze-thaw cycles, for example, 1% of the proteins had changed by at least 67%. There was also a general trend in m/z range with peaks greater than 20,000 and between 10,000-20,000 m/z reducing in median peak intensity while the 5,000-10,000 m/z range increasing in peak intensity. This suggests that either the charge of peptides was increasing or the mass is decreasing with the latter indicating protein degradation. Taken together, these results showed that increased freeze-thaw cycles have a significant impact on

the range of MS peak intensity and mass to charge ratio, indicating protein degradation with temperature variance.

Less technically- and time-demanding methods to detect biomarkers are used to study neurodegenerative diseases. The Tau protein is highly implicated in Alzheimer's disease and referred to as "neurofibrillary tangles" (Medeiros et al., 2011). It helps to stabilize microtubules in neurons and its activity is controlled by phosphorylation. A simple and common technique to evaluate Tau phosphorylation and degradation is Western blotting. A study investigated the effect of freeze-thaw cycles on whole cell protein lysates from both rodent and human brain (Vasconcelos et al., 2021). Blots for overall Tau protein showed an additional ~25 kDa band that was not present in fresh rat brain lysate. This was also observed for mouse samples, but not human. MS analysis of this band revealed 9 peptides located near the C-terminal of Tau, indicating Tau degradation. This could be due to the differences in amino acid sequence between species in which there is a protective effect against proteolysis observed in humans. This was further explored by observing the denaturing effect of adding SDS/PAGE loading buffer to rat samples before freezing. This procedure significantly reduced the appearance of the lower molecular weight product, suggesting that the Tau site was more prone to lysis in its native conformation, or that a protease inhibitor was inactivated. These results suggest that freeze-thaw may lead to protein degradation which may vary between species, but also that enzymatic activity may change.

The effect of freeze-thaw on quality of meat is a topic of interest in the food industry. The freeze-thaw process not only mechanically damages the muscle cells, but also releases enzymes into contact with proteins that would not occur naturally. A study examining the

effects of freeze-thaw on enzymatic activity used the exudate from fish that had undergone a set number of freeze-thaw cycles (Benjakul and Bauer, 2000). Enzyme assays indicated that the activity of α-glucosidase, β-N-acetyl-glucosaminidase, and magnesium-dependent EGTA-ATPase increased as the number of cycles increased. However, the activity of calcium-dependent ATPase and magnesium/calcium-dependent ATPase decreased with increasing freeze-thaw cycles. Furthermore, there was an ~60% loss of protein solubility after 5 cycles of freeze-thaw. A possible contributing factor to enzyme stability and activity may be the presence of di-sulfide bonds. The overall sulfhydryl content of proteins did not change, but the surface sulfhydryl group content decreased as freeze-thaw cycles increased. These data suggest that freeze-thaw fish exudate exhibit changes in enzyme activity, and lower total protein content that may be resultant of changes in protein stability.

The precise effects of freeze-thaw cycles on protein structure and stability remains unclear. Hydrogen deuterium exchange has been used successfully in solution phase for analysis of protein conformation and structural changes upon folding/unfolding, ligand binding, and self-association (Cierpicki et al., 2009, Zhang et al., 2009, Lu et al., 2007). In a study to investigate the effects of freeze-thaw versus aggregation on protein structure, lactate dehydrogenase was frozen in a 90% deuterium buffer with liquid nitrogen, and then stored at −10°C for 10 min to 4 days (Zhang et al., 2011). Using hydrogen-deuterium exchange MS, 21.8% of lactate dehydrogenase incorporated deuterium at 10 min, but increased to 68% at 4 days. To determine which regions most highly incorporated deuterium, peptide-level hydrogen-deuterium exchange MS identified three regions of lactate dehydrogenase, including the residues just adjacent to the most solvent-exposed amino acids, as the labile regions

susceptible to freeze-thaw. After 10 cycles of freeze-thaw, only ~4% of the native lactate dehydrogenase was remaining in the solution at 0.1 mg/mL in comparison to 92% at 1.0 mg/mL. The increased aggregation with increasing freeze-thaw cycles was supported by dynamic light scattering results of a hydrodynamic radius of from ~300 increasing to ~2,500 nm with increasing freeze-thaw cycles. Furthermore, analysis of 8-anilino-1-naphthalenesulfonic acid (ANS) dye binding suggesting more hydrophobic residues were exposed in the aggregated than native state. These results indicate that freeze-thaw induces protein denaturation and aggregation, preferentially affecting hydrophobic residues.

Protein aggregation and denaturation are major hurdles to successful protein analysis by MS due to the significant effects that they impose on protein structure and stability. MS relies on precise protein cleavage by specific proteases, the most popular being trypsin. Databases for MS data analysis are created based on the peptides generated by specific proteases from native, full-length proteins. Protein degradation induced by freeze-thaw is not as precise and will likely affect the peptides generated by proteases like trypsin. Therefore, fewer peptides will be identified in freeze-thaw samples as they will differ from the known trypsin-induced peptides in a database. Furthermore, in human serum samples, all free aromatic amino acids are sensitive to storage temperature and freeze-thaw (An et al., 2021). In proximity labeling techniques, these are the electron-rich amino acids to which biotin/biotin phenol covalently bonds. It is possible that derivatization of these amino acids could change the mass to charge ratio and therefore influence peptide identification, especially with increased freeze-thaw cycles. The exact effects of freeze-thaw on protein structure remain unknown, but it appears that many obstacles would be avoided using fresh protein lysate. However, this is not

practical for high throughput analysis of many samples or for samples that require a large amount of starting material that is collected over a long time period. Until further research elucidates this gap in knowledge, freeze-thaw cycles should be limited when sample handling for best results.

Next Steps

Jun-APEX2 proximity labeling fusion protein has the potential to be a useful tool in many models and cellular contexts. Several different methods will be discussed in the following section. For confirming putative PPIs, a few techniques to validate direct and indirect interactions will be examined. Also, several functional assays will be considered to test the importance of putative PPIs. Lastly, the benefits of using Jun-APEX2 proximity labeling in combination with quantitative MS will be discussed.

Validate Interactions

While the Jun-APEX2 fusion protein is useful for generating potential PPIs, additional verification is required to determine if the interaction is direct or indirect, stable or transient. Direct-interacting proteins identified by MS can be further resolved using surface plasmon resonance. This technique measures the angle of reflected light produced from the binding of the protein in question with the protein of interest to determine affinity constants and dissociation rates (Barberis et al., 1995, Corr et al., 1994). SPR spectroscopy has demonstrated estrogen receptor α is capable of binding to its cognate DNA recognition site alone within the progesterone receptor gene, but can also stably interact with the TF Sp1 bound to its DNA binding site (Neo et al., 2009). However, the reverse was not true in which Sp1 did not bind to

DNA-bound estrogen receptor α. Such SPR studies contribute to a better understanding of how progesterone receptor is regulated.

Stable complexes formed between two known proteins can be confirmed using co-immunoprecipitation. This is a common method used to verify direct PPIs for proteins with validated antibodies. For example, BioID identified the transcription factor 20 (TCF20) complex as a putative interactor of X-linked methyl-CpG–binding protein 2 (MECP2) (Zhou et al., 2022). Co-immunoprecipitation confirmed the interaction of TCF20 with MECP2 in mouse cortical brain extracts (Zhou et al., 2022). Yeast two hybrid assays have been used to confirm the physical interaction of proximity labeling-identified proteins as well (Mair et al., 2019, Chung et al., 2017). APEX2 revealed 225 putative PPIs of α-synuclein in rat cortical neurons and yeast two-hybrid assays verified the physical interaction with the vesicular proteins clathrin, dynamin, and VPS20, but also the retromer-associated protein SNX1 (Chung et al., 2017). These validation methods can support the direct interaction between two proteins.

To resolve larger complexes of unknown content, immuno- and fluorescence-based techniques can be used. Affinity purification or tandem affinity tagging methods in combination with MS can reveal the makeup of the components in multi-protein complexes. Lists of high-confidence interactions were generated from BioID and affinity-MS data sets of 18 subcellular markers (Liu et al., 2018, Liu et al., 2020). Another technique to verify PPIs is termed fluorescence resonance energy transfer (FRET). This method detects energy transfer from a donor fluorophore to an acceptor fluorophore if both are appropriately positioned. The efficiency of energy transfer is limited to a short range of 1-10 nm, so any significant FRET signal implies a physical or direct interaction between two proteins (Kenworthy, 2001). Researchers

have successfully used this technique to reveal the subcellular localization and mobility of tissue-specific basic helix-loop-helix (bHLH) TFs using confocal microscopy (Wang et al., 2006). Immunological and fluorescence methods can identify the composition of multi-protein complexes.

Furthermore, comparing the data between two different proximity labeling enzymes can identify putative stable interactions or contribute to the likelihood of the interaction. For example, in zebrafish embryos, the proximate proteins of transiently expressed Lamin A fused to either TurboID or miniTurbo were evaluated at either 12- or 24-hours post fertilization (Rosenthal et al., 2021). TurboID consistently labeled ~25% more proteins, regardless of condition. After analysis to determine high-confidence proteins, 89 and 144 unique proteins were identified at 12- and 48- hours post fertilization, respectively, for TurboID and 37 and 34 proteins for miniTurbo. At either time point, 40 proteins were shared between the enzyme data sets and 34-54% were previously identified in BioGRID. Furthermore, over half of the miniTurbo high-confidence proteins and 24-33% for TurboID were associated with the gene ontology nuclear envelope term. Proteins that overlap between the enzymes have a higher probability of being true interactions, whether those are direct or indirect.

Functional Interactions

Proximity labeling is sensitive enough to detect transient interactions, such as post-translational modifications by enzymes, and those PPIs can be probed using functional assays. The impact of Jun phosphorylation by MAPKs was tested using kinase inhibitors and the effect was quantified by changes in protein expression and neurite extension. Inhibition of MEK, p38,

and JNK moderately attenuated NGF-induced neurite outgrowth (Eriksson et al., 2007). The expression of cJun was decreased by MEK inhibitors, cFos was decreased by MEK and JNK, and JunD was unaffected (Eriksson et al., 2007). Furthermore, inhibition of MAPKs had no discernible effect on apoptosis mediated by anisomycin (Eriksson et al., 2007). The significance of PPIs resulting in phosphorylation can be evaluated by small molecule kinase inhibitors and measured as cellular and molecular changes.

Potential downstream effectors of TFs can be investigated using knockdown experiments. For example, Jun was expected to be a regulator of nitric oxide synthase (NOS) expression, an enzyme that is known to promote survival of differentiated PC12 cells (Schonhoff et al., 2001). NOS protein levels were decreased by siRNA-mediated knockdown of cJun (Cheng et al., 2012). Inhibition of NOS had no effect on cJun expression, confirming the role of cJun as an upstream regulator of NOS (Cheng et al., 2014). The associations and crosstalk of proteins with one another can be revealed using knockdown techniques.

Point mutations to a TF can elucidate the significance of specific functional domains. While cJun can rescue PC12 cells from apoptosis, dimerization and DNA-binding mutants of cJun showed that deletion of either domain was not required for this capability (Leppa et al., 2001). In cJunMUT^{14}, mutations to two of the amino acids within the DNA binding domain of cJun render it incapable of binding DNA (Leppa et al., 2001). Withing the dimerization domain of cJun, mutations to two amino acids in cJunMUT$^{22–23}$ eliminate its ability to dimerize with other proteins (Leppa et al., 2001). Unlike wild type cJun, both mutants neither increase MEKK-induced AP-1 promoter luciferase activity nor promote neuronal differentiation (Leppa et al., 2001). However, both mutants maintain the ability to significantly inhibit MEKK1-induced

apoptosis (Leppa et al., 2001). These results suggest that the conventional AP-1 activity of cJun does not facilitate its anti-apoptotic function, but perhaps it is mediated through other PPIs.

Quantitative MS

Quantitative MS analysis can provide a wealth of PPIs in many different contexts and experimental conditions. In comparison to label-free MS, the false positive discovery rate is significantly reduced when using quantitative analysis through identification of nonspecific binders present amongst all treatments or samples. stable isotope labeling by amino acids in cell culture (SILAC) replaces an endogenous amino acid with one that incorporates a known isotope. Such “light”, “medium”, and “heavy” SILAC media that contains amino acids of varying masses can be distinguished using MS. By using a single amino acid variant per experimental condition (e.g. increasing NGF incubation periods), the samples can be pooled for MS analysis yet remain chemically distinct as shifted m/z values in MS.

SILAC was employed to discover how the JNK-interacting proteome changes in response to NGF in PC12 cells. While JNK is known to induce cell death, this kinase also plays roles in differentiation and neuronal regeneration (Waetzig and Herdegen, 2003, Eminel et al., 2008). JNK-interacting proteins were immunoprecipitated with JNK1/2-specific antibodies and analyzed by MS (Sury et al., 2015). After employing hierarchical clustering of 728 identified proteins, the first group increased expression at 0.5 and 1 hour, decreased from 2 to 6 hours, and then increased again at 24 hours. These proteins were associated with the cytoskeleton such as myosin family members and the motor protein kinesin light chain. A second group of proteins were increased from 0.5 to 2 hours, but then gradually decreased to baseline levels at 24 hours after NGF addition. Large G-proteins and GTPases were amongst this group in which

JNK has been previously shown to interact with a handful of G-proteins in NGF-induced PC12 cells (Heasley et al., 1996). The final group of proteins did not interact with JNK until 2 to 24 hours after NGF was introduced to the media and this included many RNA binding proteins such as RNA helicases. While cJun was not identified in this dataset, this is likely due to the fleeting interaction between a post-translational modifier and its substrate. Immunoprecipitation preferentially detects stable, direct interactions, but use of proximity labeling has the potential to reveal the transient and indirect PPIs of JNK.

Proximity labeling can reveal temporal PPIs when paired with quantitative MS. Using labeling techniques like isobaric iTRAQ tags allows for simultaneous analysis of pooled samples. The different reporter ions attached to samples of different conditions enables both relative and absolute protein quantification. Furthermore, complementary MS analysis using capillary electrophoresis (CE)-ESI-MS/MS and SCX-RPLC-ESI-MS/MS provided higher confidence data with a greater protein sequence coverage (Wojcik et al., 2010, Wang et al., 2012b, Zhu et al., 2013). Differentiating PC12 cells were analyzed at 0, 3, 7, and 12 days following NGF stimulation using the iTRAQ tagging technique (Zhu et al., 2013). CE-MS generated 2,329 unique peptide identifications corresponding to 835 protein groups while SCX-RPLC-MS identified 3,494 peptides which corresponded to 1,369 proteins with an overlap of 762 proteins between the two MS techniques. Interestingly, the authors only investigated differential expression of proteins that were present at all time points, a total of 63 proteins present in both MS approaches. Using complementary MS analysis techniques not only generates more reliable identifications between data sets, but also can reveal proteins that are better separated by different techniques (i.e. isoelectric focusing versus strong cation exchange).

Future Directions

The proximity labeling technique combined with MS is a powerful tool to discover putative PPIs of TFs. Our Jun-APEX2 fusion protein was designed for easy manipulation to investigate the PPIs of other TF in other contexts. The *ef1a* promoter is easily removed with the *NheI* restriction enzyme and the multiple cloning sites enable selection for restriction enzyme site-directed cloning of the promoter of choice. This enables tissue or cell-type selectivity for *in vivo* applications or changing the promoter strength to adjust transcriptional output. APEX2 may be exchanged for a different proximity labeling enzyme such as TurboID if exogenous substrate is not feasible. Furthermore, the orientation of the tethered proteins may be changed, or the linker length modified.

A longer tether between the TF and APEX2 will likely increase the number of identified proteins by proximity labeling-MS. This longer linker length may increase the number of false positives but may also reveal the longer distance interactions involved in large multiprotein complexes. Using an earlier generation ligase, addition of a 25 nm linker between BioID2 and the Nup43 component of the nuclear pore complex increased detection of all proteins within the multi-protein complex, but also detected proteins known to be present in the targeted area (Kim et al., 2016). While a greater coverage of the nuclear pore complex was achieved with linker addition, there was not a significant increase in detection of proteins outside of the complex. This could indicate high spatial specificity, but labeling will depend on the relative protein concentration within the environment, efficiency of radical generation, and additional factors. Therefore, one should consider how the length of the fusion protein tether may affect experimental outcomes.

Deep sequencing

To elucidate the gene regulatory role of TFs, the combination of deep sequencing data with PPI data can reveal molecular level details of transcriptional regulation. For example, proximity labeling MS identified putative EcR/USP heterodimer interactions with several different proteins (Mazina et al., 2020). The authors performed additional multi-omics studies to further probe those TF interactions by pairing co-immunoprecipitation-Western blots with chromatin immunoprecipitation (ChIP)-seq data. EcR-CP190 interaction was confirmed, but only a fraction of all identified TF binding sites were bound by both. Areas highly enriched in CP190 identified by capture chromatin conformation (Hi-C) data were often associated with promoters/enhancers of developmental genes known to be regulated by EcR/USP. This data suggests that the CP190-bound sites may facilitate the interactions between the regulatory regions of the EcR/USP-responsive genes (Mazina et al., 2020). This study not only demonstrates the multi-level complexity of gene expression, but also how the combination of transcriptomic, proteomic, and chromatin conformation data can expose the molecular mechanisms that regulate gene expression.

While information regarding the PPIs of Jun is crucial, combining that knowledge with deep sequencing data would create a more complete picture regarding the role of Jun in the genetic regulation during PC12 neuronal differentiation. An elegant approach is to combine RNA-seq, ATAC-seq, Hi-C, and ChIP-seq data to elucidate the changes in transcription, chromatin availability and conformation, as well as TF-DNA binding. The combination of these techniques would inform potential Jun gene targets and how their expression is modified throughout neuronal differentiation. It has been suspected that Jun can act as a pioneer factor

(Sheffield et al., 2013), so ATAC-seq, Hi-C, and ChIP-seq data could provide evidence for whether or not this is true in PC12 neuronal differentiation. Furthermore, ChIP-seq data of the validated direct interactors of Jun would reveal a more complete understanding of bZIP transcriptional control. Proximity labeling data can help predict targets for deep sequencing and their combination provides a wealth of gene regulatory information.

Post-translational modifications (PTMs)

Post-translational modifications (PTMs) play a major role in regulating enzymatic activity, but the exact mechanisms by which this process is completed remains unclear. Stable isotope dilution (SID)-selective reaction monitoring (SRM) MS technique can determine PTMs to specific residues and levels of protein expression. To monitor the changes in expression of a protein of interest, an isotopically-labeled synthetic peptide is designed to be identical to the endogenous counterpart produced by proteolytic cleavage for MS analysis (Gerber et al., 2003). This peptide serves as an internal standard for quantification during SRM to determine changes in protein levels between treatments or conditions.

The SID-SRM-MS strategy was used to examine the changes in phosphorylation state of ERK in response to NGF in PC12 cells (Lee et al., 2019). A 13-peptide sequence (DHTGFLTEYVATR) is produced from proteolytic cleavage and conserved across ERK homologs. Of the three threonine residues, the second is known to activate ERK by MEK-mediated phosphorylation (Hahn et al., 2013). Producing the possible phosphorylated variants of the peptide can then distinguish those from endogenous ERK phosphorylation to those amino acids. NGF treatment of PC12 cells induced ERK phosphorylation from 10-60 min with SID-SRM-MS revealing that it was on the second threonine residue (Lee et al., 2019). However, there was

no change in the overall protein levels of ERK suggesting that ERK translation is not induced during this time. PTM data can reveal the molecular mechanisms that underly extracellular signal transduction.

The transcriptional activity of Jun is known to be regulated by phosphorylation to its serine residues 63 and 73 within its transactivation domain. Several different kinases are known to modify those serines including ERK, JNK, and other MAPKs (Leppä et al., 1998, Deng and Karin, 1994). SID-SRM-MS/MS of the transactivation fragment containing serines 63 and 73 would reveal which residue(s) are important at specific times during PC12 neuronal differentiation. Once the specific PTMs are identified, ChIP-seq using antibodies specific to the Jun PTMs could suggest which genes are regulated by which Jun PTMs. Outside of the transactivation domain, less is known about the PTMs to the C-terminus of Jun. Residues near the DNA binding domain of Jun are suspected to affect DNA-binding activity and transactivation potential, so SID-SRM-MS/MS could elucidate those mechanisms (Baker et al., 1992). Additional knowledge of the PTMs to Jun could help us understand how Jun activity is regulated.

Genetically modified models

Proximity labeling assays to detect the most biologically relevant PPIs will be performed either *in vivo* or in animal models. Furthermore, proteins of interest should be expressed at endogenous levels for PPIs to accurately reflect native conditions. Therefore, genetically modified models that express the proximity labeling fusion protein of interest in place of the native protein would be incredibly useful. In theory, such an approach would express the fusion protein at endogenous levels, regardless of conditions or stimulus, thus avoiding complications presented by transient expression. For example, recombinant protein over-expression induces

the unfolded protein response or, in the case of bZIP TFs, forced homodimerization which not only do not reflect native cellular conditions, but also create false-positive identifications in MS analysis. Furthermore, consideration should be taken as to which proximity labeling enzyme best suits the model and experiment.

APEX2 is most useful for detecting fast interactions with labeling times as short as 15 seconds, making it appealing for *in vitro* cultures and investigating events such as extracellular signaling. Because APEX2 requires both exogenous biotin phenol substrate and hydrogen peroxide, it is not well suited for *in vivo* purposes. However, if tissue is quickly and easily extracted, the quick labeling period of APEX2 can be performed *ex vivo* for genetically modified animals fed biotin phenol; cellular uptake of biotin phenol must be confirmed prior to proximity labeling. TurboID or miniTurbo are better options for proximity labeling *in vivo* as they do not require an additional substrate other than the easily supplemented biotin.

Both TurboID and miniTurbo will label proximate proteins if biotin is present. Therefore, inducible expression of the proximity labeling fusion protein would be beneficial in cases in which temporal analysis is important. For example, stable transgenic zebrafish were created that express Lamin A-TurboID or Lamin A-miniTurbo under the control of the inducible *hsp70l* heat shock promoter, with negative control fish replacing Lamin A with GFP (Rosenthal et al., 2021). Also incorporated in the transgene was a 3XFLAG tag and GFP under control of the cardiomyocyte-specific *myl7* promoter for easy selection of positive embryos. When labeling at 72 hours post fertilization, TurboID yielded 60 high-confidence proteins with human orthologs of which 40% were previously identified in BioGRID and miniTurbo identified 55 proteins of which 36% were in BioGRID. Given that most PPI databases are generated from analyses that

mostly identify stable protein complex formation, it is likely that many of the PPIs detected by the proximity labeling technique have yet to be verified and may be more dynamic in nature.

As for examining the PPIs of Jun during PC12 neuronal differentiation, the best approach would be to create a stable PC12 line in which endogenous cJun is replaced with cJun-APEX2. Replacing zebrafish Jun (validated in this thesis) with murine cJun to avoid any error attributed to differences in amino acid sequence. Furthermore, cJun-APEX2 under control of the endogenous *cjun* promoter would best reflect the native TF expression levels that are induced by NGF and avoid complications of over-expression or transient expression. Adding a fluorescent protein via an E2A linker would ease detection of successfully incorporated cells. Furthermore, a small epitope tag such as 3XFLAG to the 3' end of APEX2 should not impact its function and would facilitate some downstream functional analyses. The optimal negative control would be a stable PC12 cell line of nuclear localized APEX2. Assuming that the cell lines behave as expected, proximity labeled nuclear protein lysate should contain sufficient levels of biotinylated protein for MS analysis. However, an anit-APEX2 or anti-3XFLAG antibody Western blot could approximate protein expression levels. Furthermore, the antibody could be used in co-immunoprecipitation validations of predicted stable PPIs. A more accurate differential protein expression between time points would be obtained from SILAC quantitative MS analysis. Such an experiment would serve as a good proof of concept model for the hypothesis that cJun interacts with different proteins at different times during NGF-induced neuronal differentiation of PC12 cells.

cJun outside of neuronal differentiation

As a TF, Jun is a key component of gene expression and naturally plays a role in many cell processes outside of neuronal differentiation. Knockout of cJun in mice leads not only to death at mid-gestation, but also defects in hepatogenesis (Hilberg et al., 1993). To better understand the role of cJun in liver development, mice were genetically modified to carry a floxed *cjun* allele in hepatocytes (Behrens et al., 2002). Deletion of *cjun* both decreased hepatocyte proliferation and overall body size. As the liver is capable of regeneration, the mutant mice were subjected to partial hepatectomy resulting in diminished liver regeneration or the death of half of the mice. However, mice lacking only the cJun N-terminal phosphorylation sites did not display impaired liver regeneration. These results suggest that cJun transcriptional activation is an important factor in liver development and regeneration.

cJun is necessary for normal development and its knockout in mice leads to embryonic lethality (Hilberg et al., 1993). While Jun clearly plays a key role, its mechanisms remain unknown. However, using human pluripotent stem cells (hESCs) as a model for cardiomyocyte differentiation, knockout of Jun led to enhanced chromatin accessibility in regulatory regions associated with cardiomyocyte development and improved cardiomyocyte generation (Zhong et al., 2023). In fact, Jun along with the pluripotent TFs Oct4, Nanog, and Smad2/3, bind to enhancers, preventing the differentiation of hESCs to a cardiac endoderm (Li et al., 2019). The precise developmental mechanistic aspects under control of Jun remain unclear.

The dichotomous function of Jun in the cell cycle makes it an intriguing target for studying its role in cancer. The *jun* gene is considered to be proto-oncogenic as it and other AP-1 components are mis-regulated in several tumor types (Eferl and Wagner, 2003). While the cJun homodimer is associated with oncogenic activity, however, the cJun-JunB heterodimer

alters cJun DNA binding, thus changing its transcriptional activity (Deng and Karin, 1993). Furthermore, cJun is known to increase expression of several genes associated with tumor development such cyclin D1, Fas, and CD44 (Eferl and Wagner, 2003, Bakiri et al., 2000, Ivanov et al., 2001). Conversely, in rat sympathetic neurons, cJun also has anticancer effects in which it stimulates BIM expression which in turn promotes apoptosis (Whitfield et al., 2001). With both pro- and anti-tumorigenic properties, the mechanistic actions of cJun remain elusive for its role in cancer.

Some evidence suggests that cJun may be a target of WNT signaling in some types of colon cancer. cJun and TCF4 are known to directly interact in HCT116 colon cancer cells, and serines 63 and 73 within cJun's transactivation domain are required for this binding (Nateri et al., 2005). This could indicate that the binding of cJun and TCF4 is phosphorylation-dependent. Additionally, cJun and TCF4 were dependent upon β-catenin to activate the *cjun* promoter in reporter assays (Nateri et al., 2005). The WNT signaling pathway stimulates growth which is regulated by β-catenin functioning as a cofactor of the TCF (Giles et al., 2003). In HCT116 cells, formation of the cJun-TCF4/β-catenin ternary complex on the *cjun* promoter was dependent upon JNK activation (Nateri et al., 2005). cJun is known to autoregulate its transcription and is also one of the most highly up-regulated TCF/β-catenin target genes in colon cancer cell lines (Stein et al., 1992, Mann et al., 1999). Therefore, cJun may play a role in colon cancer through WNT signaling mediated both the JNK and β-catenin pathways.

In addition to transcriptional up-regulation of *cjun* in intestinal tumor cells, cJun protein accumulation in glioblastoma may be controlled at the level of translation. As mRNA levels of *cjun* did not show a correlation with malignancy, it was proposed that cJun must be regulated

post-transcriptionally (Blau et al., 2012). In human immuno-stained brain sections, the levels of cJun protein had a positive correlation with increasingly invasive grades of glial tumors (Blau et al., 2012). While the cJun was transcriptionally active, reporter gene expression revealed that cJun expressed over 100-fold more protein from a TRE-containing promoter over a 5xAP-1 repeat, suggesting that *cjun* autoregulation does not play a role in U87 cells. Furthermore, the cJun protein stability was comparable between cancer and control cells. Interestingly, cJun protein levels increased in response to depolymerization of either the actin or microtubule networks with no increase in cJun mRNA in glial cells. This translational control is mediated by an area within the 5'UTR that contains an internal ribosomal entry site (IRES), rendering cJun transcripts cap-independent and highly translatable. The dynamic changes in the cytoskeleton during cell proliferation may be important for cJun expression, especially in glioblastoma.

Jun is important in a plethora of different cell processes. Jun is crucial during development and necessary for regeneration in the peripheral nervous system. It also is a key player in the cell cycle and is implicated in both tumorigenesis and apoptotic activities. The involvement of Jun in such a wide array of cellular processes provides an open horizon to display the potential of the Jun-APEX2 proximity labeling construct for putative detection of cJun PPIs in many cell activities.

APEX2 in other contexts

The short labeling period of APEX2 can allow for temporal and spatial resolution of PPIs in response to treatments (Paek et al., 2017). Membrane receptors for steroids respond quickly to ligand binding and the proximity labeling technique has been used to compare the mechanisms of different of these different protein complexes. Steroid hormone receptors are a

class of TFs that control aspects of cell cycle, metabolism, development, and other processes. Inactive glucocorticoid receptor (GR) and androgen receptor (AR) are located in the cytoplasm, and within 30 to 60 min of ligand binding, they are translocated to the nucleus to regulate gene expression (Cato et al., 2002). The GR and AR interactomes were examined, either unstimulated or in response to both activators and inhibitors using BioID (Lempiäinen et al., 2017, Vélot et al., 2021). Notably, the number of interacting proteins increased over five-fold from unstimulated to 24 or 72 h after activation indicating a drastic change in binding partners (Vélot et al., 2021). The PPIs identified in these studies are recorded over a 24-hour period. Proximity labeling with an APEX2 fusion of GR or AR would discern the PPIs at distinct time points which could aid in determining how the receptor is acting within those day-long time windows.

APEX2 was utilized to identify interacting proteins of the membrane (M) protein of the porcine epidemic diarrhea virus, or PEDV, a member of the alphacoronavirus genus. The M proteins of coronaviruses are the main component of the viral envelope and are critical for virus particle assembly, along with the envelope (E) proteins (Wang et al., 2012a). Outside of its stable role in the viral envelope structure, the PEDV M protein is implicated in the host immunity response (Woods et al., 1988), inhibiting the activities of IFN-b and IRF3 at promoters (Zhang et al., 2016), and cell cycle arrest (Xu et al., 2015). To uncover additional functions of PEDV M, APEX2 proximity labeling-MS was performed in the porcine intestinal cell line, IPEC-J2 (Dong et al., 2021). A total of 40 high-confidence (≥2 unique peptides) annotated proteins were identified between three replicates. Five protein interactions were confirmed with co-immunoprecipitation. siRNA knockdown of S100A11 and NHE-RF1 significantly increased PEDV

production. While the mechanistic interaction is not yet clear, APEX2 proximity labeling can reveal novel PPIs that could impact our understanding of the coronavirus.

Potential for therapeutics

Alzheimer's disease model

An important first step of developing therapeutics is the ability to test potential drugs in a cell model. Just in the United States in 2021, Alzheimer's disease (AD) reportedly affects 6.2 million individuals over the age of 65 with a projected increase to 82 million in just seven years (2021, Aminyavari et al., 2019). Current treatments for AD include acetylcholinesterase inhibitors, NMDA receptor antagonists, or a combination of the two, all of which only abate symptoms. As we still do not understand the pathogenesis of AD, a reliable *in vitro* model to study the physiological mechanisms of neurons before testing *in vivo*. PC12 cells can differentiate into neurons and express several membrane receptors, including NDMA and acetylcholine, that are implicated in AD onset (Wiedmer et al., 2019). They are catecholaminergic neurons, so they can synthesize, store, and release dopamine and norepinephrine (Greene and Tischler, 1976). Due to their physiological properties, PC12 cells can serve as neuronal models to investigate AD.

Through transfection of amyloid precursor protein (APP) and presenilin mutants, PC12 cells have been successfully used to model an autosomal-dominant form in early-onset AD (Marques et al., 2003, Guo et al., 1997, Wolozin et al., 1996). A stably transfected APP mutant increased oxidative stress, resulting apoptosis mediated by JNK and caspase-3 with a concurrent reduction in caspase 9 activity (Marques et al., 2003). PC12 cells overexpressing a presenilin-1 or -2 mutant displayed increased levels of oxidative stress and intracellular calcium,

heightening their susceptibility to amyloid β-peptide-induced or trophic factor withdrawal-induced apoptosis (Guo et al., 1997, Wolozin et al., 1996). A more thorough understanding of the molecular mechanisms of AD pathogenesis could be achieved using proximity labeling.

Both tau and amyloid β-peptide aggregation have been implicated in the development of AD. Evidence suggests that amyloid-β oligomers underly the cognitive defects observed in AD (Bjorklund et al., 2012). Neurofibrillary tangles are mainly composed of phosphorylated tau protein and have been found in cholinergic neurons of AD patients post-mortem (Mesulam et al., 2004). An APEX2 fusion protein could reveal the PPIs leading up to oligomeric accumulation during early disease development. Preventing or disrupting the interactions of amyloid plaques or neurofibrillary tangles could delay AD onset or perhaps diminish symptoms. Proximity labeling could identify other putative interactors of APP or tau that may be the key to understanding how their aggregates are formed and elucidate a part of AD pathophysiology.

Concluding remarks

It is well-established that cJun plays an integral role in development and successful axon regeneration (Hilberg et al., 1993, Ruff et al., 2012), but its binding partners and other PPIs over the time course of these events are not fully understood. The Jun-APEX2 proximity labeling construct has the potential to identify important PPIs of the differentiating or regenerating neuron, both stable and transient interactions. Here, a method for developing a TF proximity labeling construct is detailed, highlighting construct features such as the easily exchanged modules (i.e., promoter, protein of interest, proximity labeling enzyme). Furthermore, important design considerations are explained, and caveats are mentioned.

The Jun-APEX2 protein was then functionally validated for cellular localization, substrate dependence, and DNA-binding specificity. As proof of concept that the Jun-APEX2 fusion protein would label putative PPIs, PC12 cells were stimulated with NGF in cells expressing either Jun-APEX2 or the control APEX2. Proximity labeled protein displayed different banding patterns and intensities between control and Jun-APEX2 samples as visualized with silver staining. These results were not repeatable when using freeze/thaw protein lysate. MS analysis was performed to identify the putative Jun-interacting proteins, but the data were inconclusive. However, the results presented here provide a basis for optimization of the Jun-APEX2 fusion construct in many other contexts outside of PC12 cell culture or neuronal differentiation. Jun is implicated in many cellular processes and much remains to be explored of its mechanistic actions.

Functional axonal regeneration is the product of temporally controlled cooperativity of multiple cell types. For example, glial cells are extremely important in successful nerve regeneration as demonstrated by the contribution of essential neurotrophins from Schwann cells in the PNS (Fontana et al., 2012). Many extracellular signals converge onto signaling pathways that ultimately regulate the transcription of distinct genes at specific times. Gene expression is modulated by several multi-protein complexes including many different TFs, the exact combinations of which are yet to be discovered. TF proximity labeling constructs can be a valuable tool to identify those transcriptional proteins which may serve as pharmacological targets for stimulating successful axon growth and re-innervation within the mammalian CNS.

References

2021. 2021 Alzheimer's disease facts and figures. *Alzheimers Dement,* 17**,** 327-406.

ABATE, C., BAKER, S. J., LEES-MILLER, S. P., ANDERSON, C. W., MARSHAK, D. R. & CURRAN, T. 1993. Dimerization and DNA binding alter phosphorylation of Fos and Jun. *Proc Natl Acad Sci U S A,* 90**,** 6766-70.

ACHARYA, A., RUVINOV, S. B., GAL, J., MOLL, J. R. & VINSON, C. 2002. A heterodimerizing leucine zipper coiled coil system for examining the specificity of a position interactions: amino acids I, V, L, N, A, and K. *Biochemistry,* 41**,** 14122-31.

AGUILERA, C., NAKAGAWA, K., SANCHO, R., CHAKRABORTY, A., HENDRICH, B. & BEHRENS, A. 2011. c-Jun N-terminal phosphorylation antagonises recruitment of the Mbd3/NuRD repressor complex. *Nature,* 469**,** 231-5.

AIELLO, L. P., AVERY, R. L., ARRIGG, P. G., KEYT, B. A., JAMPEL, H. D., SHAH, S. T., PASQUALE, L. R., THIEME, H., IWAMOTO, M. A., PARK, J. E. & ET AL. 1994. Vascular endothelial growth factor in ocular fluid of patients with diabetic retinopathy and other retinal disorders. *N Engl J Med,* 331**,** 1480-7.

AIGNER, L. & CARONI, P. 1995. Absence of persistent spreading, branching, and adhesion in GAP-43-depleted growth cones. *J Cell Biol,* 128**,** 647-60.

AMATO, R., CATALANI, E., DAL MONTE, M., CAMMALLERI, M., CERVIA, D. & CASINI, G. 2022. Morpho-functional analysis of the early changes induced in retinal ganglion cells by the onset of diabetic retinopathy: The effects of a neuroprotective strategy. *Pharmacol Res,* 185**,** 106516.

AMINYAVARI, S., ZAHMATKESH, M., FARAHMANDFAR, M., KHODAGHOLI, F., DARGAHI, L. & ZARRINDAST, M. R. 2019. Protective role of Apelin-13 on amyloid beta25-35-induced memory deficit; Involvement of autophagy and apoptosis process. *Prog Neuropsychopharmacol Biol Psychiatry,* 89**,** 322-334.

AN, Z., SHI, C., LI, P. & LIU, L. 2021. Stability of amino acids and related amines in human serum under different preprocessing and pre-storage conditions based on iTRAQ((R))-LC-MS/MS. *Biol Open,* 10.

ANDREWS, E. M., RICHARDS, R. J., YIN, F. Q., VIAPIANO, M. S. & JAKEMAN, L. B. 2012. Alterations in chondroitin sulfate proteoglycan expression occur both at and far from the site of spinal contusion injury. *Exp Neurol,* 235**,** 174-87.

ANDREWS, M. R., SOLEMAN, S., CHEAH, M., TUMBARELLO, D. A., MASON, M. R., MOLONEY, E., VERHAAGEN, J., BENSADOUN, J. C., SCHNEIDER, B., AEBISCHER, P. & FAWCETT, J. W. 2016. Axonal Localization of Integrins in the CNS Is Neuronal Type and Age Dependent. *eNeuro,* 3.

ANGEL, P., IMAGAWA, M., CHIU, R., STEIN, B., IMBRA, R. J., RAHMSDORF, H. J., JONAT, C., HERRLICH, P. & KARIN, M. 1987. Phorbol ester-inducible genes contain a common cis element recognized by a TPA-modulated trans-acting factor. *Cell,* 49**,** 729-39.

ANGEL, P. & KARIN, M. 1991. The role of Jun, Fos and the AP-1 complex in cell-proliferation and transformation. *Biochim Biophys Acta,* 1072**,** 129-57.

ARTHUR-FARRAJ, P. J., LATOUCHE, M., WILTON, D. K., QUINTES, S., CHABROL, E., BANERJEE, A., WOODHOO, A., JENKINS, B., RAHMAN, M., TURMAINE, M., WICHER, G. K., MITTER, R., GREENSMITH, L., BEHRENS, A., RAIVICH, G., MIRSKY, R. & JESSEN, K. R. 2012. c-Jun

reprograms Schwann cells of injured nerves to generate a repair cell essential for regeneration. *Neuron,* 75**,** 633-47.

ASCHERIO, A. 2013. Environmental factors in multiple sclerosis. *Expert Rev Neurother,* 13**,** 3-9.

BAKER, S. J., KERPPOLA, T. K., LUK, D., VANDENBERG, M. T., MARSHAK, D. R., CURRAN, T. & ABATE, C. 1992. Jun is phosphorylated by several protein kinases at the same sites that are modified in serum-stimulated fibroblasts. *Molecular and Cellular Biology,* 12**,** 4694-4705.

BAKIRI, L., LALLEMAND, D., BOSSY-WETZEL, E. & YANIV, M. 2000. Cell cycle-dependent variations in c-Jun and JunB phosphorylation: a role in the control of cyclin D1 expression. *EMBO J,* 19**,** 2056-68.

BAKIRI, L., MATSUO, K., WISNIEWSKA, M., WAGNER, E. F. & YANIV, M. 2002. Promoter specificity and biological activity of tethered AP-1 dimers. *Mol Cell Biol,* 22**,** 4952-64.

BALKAN, W., COLBERT, M., BOCK, C. & LINNEY, E. 1992. Transgenic indicator mice for studying activated retinoic acid receptors during development. *Proc Natl Acad Sci U S A,* 89**,** 3347-51.

BANNISTER, A. J. & KOUZARIDES, T. 1996. The CBP co-activator is a histone acetyltransferase. *Nature,* 384**,** 641-3.

BARBERIS, A., PEARLBERG, J., SIMKOVICH, N., FARRELL, S., REINAGEL, P., BAMDAD, C., SIGAL, G. & PTASHNE, M. 1995. Contact with a component of the polymerase II holoenzyme suffices for gene activation. *Cell,* 81**,** 359-368.

BARRES, B. A., JACOBSON, M. D., SCHMID, R., SENDTNER, M. & RAFF, M. C. 1993. Does oligodendrocyte survival depend on axons? *Curr Biol,* 3**,** 489-97.

BARRON, K. D. 1995. The microglial cell. A historical review. *J Neurol Sci,* 134 Suppl**,** 57-68.

BASS, A. J., WATANABE, H., MERMEL, C. H., YU, S., PERNER, S., VERHAAK, R. G., KIM, S. Y., WARDWELL, L., TAMAYO, P., GAT-VIKS, I., RAMOS, A. H., WOO, M. S., WEIR, B. A., GETZ, G., BEROUKHIM, R., O'KELLY, M., DUTT, A., ROZENBLATT-ROSEN, O., DZIUNYCZ, P., KOMISAROF, J., CHIRIEAC, L. R., LAFARGUE, C. J., SCHEBLE, V., WILBERTZ, T., MA, C., RAO, S., NAKAGAWA, H., STAIRS, D. B., LIN, L., GIORDANO, T. J., WAGNER, P., MINNA, J. D., GAZDAR, A. F., ZHU, C. Q., BROSE, M. S., CECCONELLO, I., RIBEIRO, U., JR., MARIE, S. K., DAHL, O., SHIVDASANI, R. A., TSAO, M. S., RUBIN, M. A., WONG, K. K., REGEV, A., HAHN, W. C., BEER, D. G., RUSTGI, A. K. & MEYERSON, M. 2009. SOX2 is an amplified lineage-survival oncogene in lung and esophageal squamous cell carcinomas. *Nat Genet,* 41**,** 1238-42.

BATTULIN, N., KORABLEV, A., RYZHKOVA, A., SMIRNOV, A., KABIROVA, E., KHABAROVA, A., LAGUNOV, T., SEROVA, I. & SEROV, O. 2022. The human EF1a promoter does not provide expression of the transgene in mice. *Transgenic Research,* 31**,** 525-535.

BEHRENS, A., SIBILIA, M., DAVID, J. P., MOHLE-STEINLEIN, U., TRONCHE, F., SCHUTZ, G. & WAGNER, E. F. 2002. Impaired postnatal hepatocyte proliferation and liver regeneration in mice lacking c-jun in the liver. *EMBO J,* 21**,** 1782-90.

BENJAKUL, S. & BAUER, F. 2000. Physicochemical and enzymatic changes of cod muscle proteins subjected to different freeze-thaw cycles. *Journal of the Science of Food and Agriculture,* 80**,** 1143-1150.

BERNSTEIN, J. J., GETZ, R., JEFFERSON, M. & KELEMEN, M. 1985. Astrocytes secrete basal lamina after hemisection of rat spinal cord. *Brain Res,* 327**,** 135-41.

BIDDIE, S. C., JOHN, S., SABO, P. J., THURMAN, R. E., JOHNSON, T. A., SCHILTZ, R. L., MIRANDA, T. B., SUNG, M. H., TRUMP, S., LIGHTMAN, S. L., VINSON, C., STAMATOYANNOPOULOS, J. A. & HAGER, G. L. 2011. Transcription factor AP1 potentiates chromatin accessibility and glucocorticoid receptor binding. *Mol Cell,* 43**,** 145-55.

BJORKLUND, N. L., REESE, L. C., SADAGOPARAMANUJAM, V. M., GHIRARDI, V., WOLTJER, R. L. & TAGLIALATELA, G. 2012. Absence of amyloid beta oligomers at the postsynapse and regulated synaptic Zn2+ in cognitively intact aged individuals with Alzheimer's disease neuropathology. *Mol Neurodegener,* 7**,** 23.

BLACK, M. M. & LASEK, R. J. 1979. Slowing of the rate of axonal regeneration during growth and maturation. *Exp Neurol,* 63**,** 108-19.

BLACKSHAW, S. 2022. Why Has the Ability to Regenerate Following CNS Injury Been Repeatedly Lost Over the Course of Evolution? *Front Neurosci,* 16**,** 831062.

BLAU, L., KNIRSH, R., BEN-DROR, I., OREN, S., KUPHAL, S., HAU, P., PROESCHOLDT, M., BOSSERHOFF, A. K. & VARDIMON, L. 2012. Aberrant expression of c-Jun in glioblastoma by internal ribosome entry site (IRES)-mediated translational activation. *Proc Natl Acad Sci U S A,* 109**,** E2875-84.

BOIVIN, A., PINEAU, I., BARRETTE, B., FILALI, M., VALLIERES, N., RIVEST, S. & LACROIX, S. 2007. Toll-like receptor signaling is critical for Wallerian degeneration and functional recovery after peripheral nerve injury. *J Neurosci,* 27**,** 12565-76.

BOYER, D. S., YOON, Y. H., BELFORT, R., JR., BANDELLO, F., MATURI, R. K., AUGUSTIN, A. J., LI, X. Y., CUI, H., HASHAD, Y., WHITCUP, S. M. & OZURDEX, M. S. G. 2014. Three-year, randomized, sham-controlled trial of dexamethasone intravitreal implant in patients with diabetic macular edema. *Ophthalmology,* 121**,** 1904-14.

BOYLE, W. J., SMEAL, T., DEFIZE, L. H., ANGEL, P., WOODGETT, J. R., KARIN, M. & HUNTER, T. 1991. Activation of protein kinase C decreases phosphorylation of c-Jun at sites that negatively regulate its DNA-binding activity. *Cell,* 64**,** 573-84.

BRACKEN, C., CARR, P. A., CAVANAGH, J. & PALMER, A. G., 3RD 1999. Temperature dependence of intramolecular dynamics of the basic leucine zipper of GCN4: implications for the entropy of association with DNA. *J Mol Biol,* 285**,** 2133-46.

BRADBURY, E. J., MOON, L. D., POPAT, R. J., KING, V. R., BENNETT, G. S., PATEL, P. N., FAWCETT, J. W. & MCMAHON, S. B. 2002. Chondroitinase ABC promotes functional recovery after spinal cord injury. *Nature,* 416**,** 636-40.

BRANON, T. C., BOSCH, J. A., SANCHEZ, A. D., UDESHI, N. D., SVINKINA, T., CARR, S. A., FELDMAN, J. L., PERRIMON, N. & TING, A. Y. 2018. Efficient proximity labeling in living cells and organisms with TurboID. *Nat Biotechnol,* 36**,** 880-887.

BROWN, A. L., WILKINS, O. G., KEUSS, M. J., HILL, S. E., ZANOVELLO, M., LEE, W. C., BAMPTON, A., LEE, F. C. Y., MASINO, L., QI, Y. A., BRYCE-SMITH, S., GATT, A., HALLEGGER, M., FAGEGALTIER, D., PHATNANI, H., CONSORTIUM, N. A., NEWCOMBE, J., GUSTAVSSON, E. K., SEDDIGHI, S., REYES, J. F., COON, S. L., RAMOS, D., SCHIAVO, G., FISHER, E. M. C., RAJ, T., SECRIER, M., LASHLEY, T., ULE, J., BURATTI, E., HUMPHREY, J., WARD, M. E. & FRATTA, P. 2022. TDP-43 loss and ALS-risk SNPs drive mis-splicing and depletion of UNC13A. *Nature,* 603**,** 131-137.

BRUSHART, T. M. & MESULAM, M. M. 1980. Alteration in connections between muscle and anterior horn motoneurons after peripheral nerve repair. *Science,* 208**,** 603-5.

BURGO, A., SOTIRAKIS, E., SIMMLER, M. C., VERRAES, A., CHAMOT, C., SIMPSON, J. C., LANZETTI, L., PROUX-GILLARDEAUX, V. & GALLI, T. 2009. Role of Varp, a Rab21 exchange factor and TI-VAMP/VAMP7 partner, in neurite growth. *EMBO Rep,* 10**,** 1117-24.

CAMPOCHIARO, P. A., BROWN, D. M., PEARSON, A., CIULLA, T., BOYER, D., HOLZ, F. G., TOLENTINO, M., GUPTA, A., DUARTE, L., MADREPERLA, S., GONDER, J., KAPIK, B., BILLMAN, K., KANE, F. E. & GROUP, F. S. 2011. Long-term benefit of sustained-delivery fluocinolone acetonide vitreous inserts for diabetic macular edema. *Ophthalmology,* 118**,** 626-635 e2.

CAO, E., CHEN, Y., CUI, Z. & FOSTER, P. R. 2003. Effect of freezing and thawing rates on denaturation of proteins in aqueous solutions. *Biotechnol Bioeng,* 82**,** 684-90.

CARMICHAEL, S. T., ARCHIBEQUE, I., LUKE, L., NOLAN, T., MOMIY, J. & LI, S. 2005. Growth-associated gene expression after stroke: evidence for a growth-promoting region in peri-infarct cortex. *Exp Neurol,* 193**,** 291-311.

CARNESECCHI, J., SIGISMONDO, G., DOMSCH, K., BAADER, C. E. P., RAFIEE, M. R., KRIJGSVELD, J. & LOHMANN, I. 2020. Multi-level and lineage-specific interactomes of the Hox transcription factor Ubx contribute to its functional specificity. *Nat Commun,* 11**,** 1388.

CARONI, P. & SCHWAB, M. E. 1988. Two membrane protein fractions from rat central myelin with inhibitory properties for neurite growth and fibroblast spreading. *J Cell Biol,* 106**,** 1281-8.

CATO, A. C., NESTL, A. & MINK, S. 2002. Rapid actions of steroid receptors in cellular signaling pathways. *Sci STKE,* 2002**,** re9.

CAVALLI, V., KUJALA, P., KLUMPERMAN, J. & GOLDSTEIN, L. S. 2005. Sunday Driver links axonal transport to damage signaling. *J Cell Biol,* 168**,** 775-87.

CHANDRAN, V., COPPOLA, G., NAWABI, H., OMURA, T., VERSANO, R., HUEBNER, E. A., ZHANG, A., COSTIGAN, M., YEKKIRALA, A., BARRETT, L., BLESCH, A., MICHAELEVSKI, I., DAVIS-TURAK, J., GAO, F., LANGFELDER, P., HORVATH, S., HE, Z., BENOWITZ, L., FAINZILBER, M., TUSZYNSKI, M., WOOLF, C. J. & GESCHWIND, D. H. 2016. A Systems-Level Analysis of the Peripheral Nerve Intrinsic Axonal Growth Program. *Neuron,* 89**,** 956-70.

CHAPMAN-SMITH, A. & CRONAN, J. E., JR. 1999. Molecular biology of biotin attachment to proteins. *J Nutr,* 129**,** 477S-484S.

CHENG, X., LIU, S., WANG, Y. Q., LI, Y. Q., FU, R., TANG, Y., ZHENG, W. H. & ZHOU, L. H. 2012. Suppression of c-jun influences nNOS expression in differentiated PC12 cells. *Mol Med Rep,* 6**,** 750-4.

CHENG, X., LUO, H., HOU, Z., HUANG, Y., SUN, J. & ZHOU, L. 2014. Neuronal nitric oxide synthase, as a downstream signaling molecule of c-jun, regulates the survival of differentiated PC12 cells. *Mol Med Rep,* 10**,** 1881-6.

CHINENOV, Y. & KERPPOLA, T. K. 2001. Close encounters of many kinds: Fos-Jun interactions that mediate transcription regulatory specificity. *Oncogene,* 20**,** 2438-52.

CHO, Y., SLOUTSKY, R., NAEGLE, K. M. & CAVALLI, V. 2013. Injury-induced HDAC5 nuclear export is essential for axon regeneration. *Cell,* 155**,** 894-908.

CHOI-RHEE, E., SCHULMAN, H. & CRONAN, J. E. 2004. Promiscuous protein biotinylation by Escherichia coli biotin protein ligase. *Protein Sci,* 13**,** 3043-50.

CHRONIS, C., FIZIEV, P., PAPP, B., BUTZ, S., BONORA, G., SABRI, S., ERNST, J. & PLATH, K. 2017. Cooperative Binding of Transcription Factors Orchestrates Reprogramming. *Cell,* 168**,** 442-459 e20.

CHUNG, C. Y., KHURANA, V., YI, S., SAHNI, N., LOH, K. H., AULUCK, P. K., BARU, V., UDESHI, N. D., FREYZON, Y., CARR, S. A., HILL, D. E., VIDAL, M., TING, A. Y. & LINDQUIST, S. 2017. In Situ Peroxidase Labeling and Mass-Spectrometry Connects Alpha-Synuclein Directly to Endocytic Trafficking and mRNA Metabolism in Neurons. *Cell Syst,* 4**,** 242-250 e4.

CIERPICKI, T., BIELNICKI, J., ZHENG, M., GRUSZCZYK, J., KASTERKA, M., PETOUKHOV, M., ZHANG, A., FERNANDEZ, E. J., SVERGUN, D. I., DEREWENDA, U., BUSHWELLER, J. H. & DEREWENDA, Z. S. 2009. The solution structure and dynamics of the DH-PH module of PDZRhoGEF in isolation and in complex with nucleotide-free RhoA. *Protein Sci,* 18**,** 2067-79.

COFFILL, C. R., MULLER, P. A., OH, H. K., NEO, S. P., HOGUE, K. A., CHEOK, C. F., VOUSDEN, K. H., LANE, D. P., BLACKSTOCK, W. P. & GUNARATNE, J. 2012. Mutant p53 interactome identifies nardilysin as a p53R273H-specific binding partner that promotes invasion. *EMBO Rep,* 13**,** 638-44.

COHEN, G. B., REN, R. & BALTIMORE, D. 1995. Modular binding domains in signal transduction proteins. *Cell,* 80**,** 237-48.

COMPSTON, A. & COLES, A. 2002. Multiple sclerosis. *Lancet,* 359**,** 1221-31.

CORR, M., SLANETZ, A. E., BOYD, L. F., JELONEK, M. T., KHILKO, S., AL-RAMADI, B. K., KIM, Y. S., MAHER, S. E., BOTHWELL, A. L. & MARGULIES, D. H. 1994. T cell receptor-MHC class I peptide interactions: affinity, kinetics, and specificity. *Science,* 265**,** 946-949.

COSTA, R. O., MARTINS, H., MARTINS, L. F., CWETSCH, A. W., MELE, M., PEDRO, J. R., TOME, D., JEON, N. L., CANCEDDA, L., JAFFREY, S. R. & ALMEIDA, R. D. 2019. Synaptogenesis Stimulates a Proteasome-Mediated Ribosome Reduction in Axons. *Cell Rep,* 28**,** 864-876 e6.

COULPIER, M., ANDERS, J. & IBANEZ, C. F. 2002. Coordinated activation of autophosphorylation sites in the RET receptor tyrosine kinase: importance of tyrosine 1062 for GDNF mediated neuronal differentiation and survival. *J Biol Chem,* 277**,** 1991-9.

CRAIG, R. A. & LIAO, L. 2007. Phylogenetic tree information aids supervised learning for predicting protein-protein interaction based on distance matrices. *BMC Bioinformatics,* 8**,** 6.

D'SOUZA, S. D., BONETTI, B., BALASINGAM, V., CASHMAN, N. R., BARKER, P. A., TROUTT, A. B., RAINE, C. S. & ANTEL, J. P. 1996. Multiple sclerosis: Fas signaling in oligodendrocyte cell death. *J Exp Med,* 184**,** 2361-70.

DAI, T., RUBIE, E., FRANKLIN, C., KRAFT, A., GILLESPIE, D., AVRUCH, J., KYRIAKIS, J. & WOODGETT, J. 1995. Stress-activated protein kinases bind directly to the delta domain of c-Jun in resting cells: implications for repression of c-Jun function. *Oncogene,* 10**,** 849-855.

DANZI, M. C., MEHTA, S. T., DULLA, K., ZUNINO, G., COOPER, D. J., BIXBY, J. L. & LEMMON, V. P. 2018. The effect of Jun dimerization on neurite outgrowth and motif binding. *Mol Cell Neurosci,* 92**,** 114-127.

DAVALOS, D., GRUTZENDLER, J., YANG, G., KIM, J. V., ZUO, Y., JUNG, S., LITTMAN, D. R., DUSTIN, M. L. & GAN, W. B. 2005. ATP mediates rapid microglial response to local brain injury in vivo. *Nat Neurosci,* 8**,** 752-8.

DAVID, S. & AGUAYO, A. J. 1981. Axonal elongation into peripheral nervous system "bridges" after central nervous system injury in adult rats. *Science,* 214**,** 931-3.

DENG, T. & KARIN, M. 1993. JunB differs from c-Jun in its DNA-binding and dimerization domains, and represses c-Jun by formation of inactive heterodimers. *Genes Dev,* 7**,** 479-90.

DENG, T. & KARIN, M. 1994. c-Fos transcriptional activity stimulated by H-Ras-activated protein kinase distinct from JNK and ERK. *Nature,* 371**,** 171-5.

DEVARY, Y., GOTTLIEB, R. A., SMEAL, T. & KARIN, M. 1992. The mammalian ultraviolet response is triggered by activation of Src tyrosine kinases. *Cell,* 71**,** 1081-91.

DEWAN, M. C., RATTANI, A., GUPTA, S., BATICULON, R. E., HUNG, Y. C., PUNCHAK, M., AGRAWAL, A., ADELEYE, A. O., SHRIME, M. G., RUBIANO, A. M., ROSENFELD, J. V. & PARK, K. B. 2018. Estimating the global incidence of traumatic brain injury. *J Neurosurg***,** 1-18.

DHARA, S. P., RAU, A., FLISTER, M. J., RECKA, N. M., LAIOSA, M. D., AUER, P. L. & UDVADIA, A. J. 2019. Cellular reprogramming for successful CNS axon regeneration is driven by a temporally changing cast of transcription factors. *Sci Rep,* 9**,** 14198.

DIAMOND, M. I., MINER, J. N., YOSHINAGA, S. K. & YAMAMOTO, K. R. 1990. Transcription factor interactions: selectors of positive or negative regulation from a single DNA element. *Science,* 249**,** 1266-72.

DONG, S., WANG, R., YU, R., CHEN, B., SI, F., XIE, C. & LI, Z. 2021. Identification of cellular proteins interacting with PEDV M protein through APEX2 labeling. *J Proteomics,* 240**,** 104191.

DRAGUNOW, M., XU, R., WALTON, M., WOODGATE, A.-M., LAWLOR, P., MACGIBBON, G. A., YOUNG, D., GIBBONS, H., LIPSKI, J. & MURAVLEV, A. 2000. c-Jun promotes neurite outgrowth and survival in PC12 cells. *Molecular brain research,* 83**,** 20-33.

DUYNDAM, M. C., VAN DAM, H., SMITS, P. H., VERLAAN, M., VAN DER EB, A. J. & ZANTEMA, A. 1999. The N-terminal transactivation domain of ATF2 is a target for the co-operative activation of the c-jun promoter by p300 and 12S E1A. *Oncogene,* 18**,** 2311-21.

EDVINSSON, L., BRODIN, E., JANSEN, I. & UDDMAN, R. 1988. Neurokinin A in cerebral vessels: characterization, localization and effects in vitro. *Regul Pept,* 20**,** 181-97.

EFERL, R. & WAGNER, E. F. 2003. AP-1: a double-edged sword in tumorigenesis. *Nat Rev Cancer,* 3**,** 859-68.

EL BEJJANI, R. & HAMMARLUND, M. 2012. Neural regeneration in Caenorhabditis elegans. *Annu Rev Genet,* 46**,** 499-513.

ELLENBERGER, T. E., BRANDL, C. J., STRUHL, K. & HARRISON, S. C. 1992. The GCN4 basic region leucine zipper binds DNA as a dimer of uninterrupted alpha helices: crystal structure of the protein-DNA complex. *Cell,* 71**,** 1223-37.

EMINEL, S., ROEMER, L., WAETZIG, V. & HERDEGEN, T. 2008. c-Jun N-terminal kinases trigger both degeneration and neurite outgrowth in primary hippocampal and cortical neurons. *J Neurochem,* 104**,** 957-69.

ERIKSSON, M., TASKINEN, M. & LEPPA, S. 2007. Mitogen activated protein kinase-dependent activation of c-Jun and c-Fos is required for neuronal differentiation but not for growth and stress response in PC12 cells. *J Cell Physiol,* 210**,** 538-48.

ERTURK, A., HELLAL, F., ENES, J. & BRADKE, F. 2007. Disorganized microtubules underlie the formation of retraction bulbs and the failure of axonal regeneration. *J Neurosci,* 27**,** 9169-80.

ESTUS, S., ZAKS, W. J., FREEMAN, R. S., GRUDA, M., BRAVO, R. & JOHNSON, E. M., JR. 1994. Altered gene expression in neurons during programmed cell death: identification of c-jun as necessary for neuronal apoptosis. *J Cell Biol,* 127**,** 1717-27.

FAN, X., MASAMSETTI, V. P., SUN, J. Q., ENGHOLM-KELLER, K., OSTEIL, P., STUDDERT, J., GRAHAM, M. E., FOSSAT, N. & TAM, P. P. 2021. TWIST1 and chromatin regulatory proteins interact to guide neural crest cell differentiation. *Elife,* 10.

FIELDS, S. & SONG, O.-K. 1989. A novel genetic system to detect protein–protein interactions. *Nature,* 340**,** 245-246.

FISCHER, J. A., GINIGER, E., MANIATIS, T. & PTASHNE, M. 1988. GAL4 activates transcription in Drosophila. *Nature,* 332**,** 853-6.

FITCH, M. T., DOLLER, C., COMBS, C. K., LANDRETH, G. E. & SILVER, J. 1999. Cellular and molecular mechanisms of glial scarring and progressive cavitation: in vivo and in vitro analysis of inflammation-induced secondary injury after CNS trauma. *J Neurosci,* 19**,** 8182-98.

FONTANA, X., HRISTOVA, M., DA COSTA, C., PATODIA, S., THEI, L., MAKWANA, M., SPENCER-DENE, B., LATOUCHE, M., MIRSKY, R., JESSEN, K. R., KLEIN, R., RAIVICH, G. & BEHRENS, A. 2012. c-Jun in Schwann cells promotes axonal regeneration and motoneuron survival via paracrine signaling. *J Cell Biol,* 198**,** 127-41.

FRANKS, F. 1995. Protein destabilization at low temperatures. *Adv Protein Chem,* 46**,** 105-39.

FRASER, M. M., BAYAZITOV, I. T., ZAKHARENKO, S. S. & BAKER, S. J. 2008. Phosphatase and tensin homolog, deleted on chromosome 10 deficiency in brain causes defects in synaptic structure, transmission and plasticity, and myelination abnormalities. *Neuroscience,* 151**,** 476-88.

FRIEDE, R. L. & BISCHHAUSEN, R. 1980. The fine structure of stumps of transected nerve fibers in subserial sections. *J Neurol Sci,* 44**,** 181-203.

FRIETZE, S. & FARNHAM, P. J. 2011. Transcription factor effector domains. *Subcell Biochem,* 52**,** 261-77.

FU, S. Y. & GORDON, T. 1997. The cellular and molecular basis of peripheral nerve regeneration. *Mol Neurobiol,* 14**,** 67-116.

FUCHS, S. Y. & RONAI, Z. 1999. Ubiquitination and degradation of ATF2 are dimerization dependent. *Mol Cell Biol,* 19**,** 3289-98.

FUJII, Y., SHIMIZU, T., TODA, T., YANAGIDA, M. & HAKOSHIMA, T. 2000. Structural basis for the diversity of DNA recognition by bZIP transcription factors. *Nat Struct Biol,* 7**,** 889-93.

GAVIN, A. C., BOSCHE, M., KRAUSE, R., GRANDI, P., MARZIOCH, M., BAUER, A., SCHULTZ, J., RICK, J. M., MICHON, A. M., CRUCIAT, C. M., REMOR, M., HOFERT, C., SCHELDER, M., BRAJENOVIC, M., RUFFNER, H., MERINO, A., KLEIN, K., HUDAK, M., DICKSON, D., RUDI, T., GNAU, V., BAUCH, A., BASTUCK, S., HUHSE, B., LEUTWEIN, C., HEURTIER, M. A., COPLEY, R. R., EDELMANN, A., QUERFURTH, E., RYBIN, V., DREWES, G., RAIDA, M.,

BOUWMEESTER, T., BORK, P., SERAPHIN, B., KUSTER, B., NEUBAUER, G. & SUPERTI-FURGA, G. 2002. Functional organization of the yeast proteome by systematic analysis of protein complexes. *Nature,* 415**,** 141-7.

GEORGE, E. B., GLASS, J. D. & GRIFFIN, J. W. 1995. Axotomy-induced axonal degeneration is mediated by calcium influx through ion-specific channels. *J Neurosci,* 15**,** 6445-52.

GEORGE, R. & GRIFFIN, J. W. 1994. Delayed macrophage responses and myelin clearance during Wallerian degeneration in the central nervous system: the dorsal radiculotomy model. *Exp Neurol,* 129**,** 225-36.

GERBER, S. A., RUSH, J., STEMMAN, O., KIRSCHNER, M. W. & GYGI, S. P. 2003. Absolute quantification of proteins and phosphoproteins from cell lysates by tandem MS. *Proc Natl Acad Sci U S A,* 100**,** 6940-5.

GIGER, R. J., HOLLIS, E. R., 2ND & TUSZYNSKI, M. H. 2010. Guidance molecules in axon regeneration. *Cold Spring Harb Perspect Biol,* 2**,** a001867.

GILES, R. H., VAN ES, J. H. & CLEVERS, H. 2003. Caught up in a Wnt storm: Wnt signaling in cancer. *Biochim Biophys Acta,* 1653**,** 1-24.

GINGRAS, A. C., AEBERSOLD, R. & RAUGHT, B. 2005. Advances in protein complex analysis using mass spectrometry. *J Physiol,* 563**,** 11-21.

GIOVANNONI, G., SOELBERG SORENSEN, P., COOK, S., RAMMOHAN, K., RIECKMANN, P., COMI, G., DANGOND, F., ADENIJI, A. K. & VERMERSCH, P. 2018. Safety and efficacy of cladribine tablets in patients with relapsing-remitting multiple sclerosis: Results from the randomized extension trial of the CLARITY study. *Mult Scler,* 24**,** 1594-1604.

GORDON, T., GILLESPIE, J., OROZCO, R. & DAVIS, L. 1991. Axotomy-induced changes in rabbit hindlimb nerves and the effects of chronic electrical stimulation. *J Neurosci,* 11**,** 2157-69.

GREENE, L. A. & TISCHLER, A. S. 1976. Establishment of a noradrenergic clonal line of rat adrenal pheochromocytoma cells which respond to nerve growth factor. *Proc Natl Acad Sci U S A,* 73**,** 2424-8.

GREENE, L. A. & TISCHLER, A. S. 1982. PC12 Pheochromocytoma Cultures in Neurobiological Research.

GUO, Q., SOPHER, B. L., FURUKAWA, K., PHAM, D. G., ROBINSON, N., MARTIN, G. M. & MATTSON, M. P. 1997. Alzheimer's presenilin mutation sensitizes neural cells to apoptosis induced by trophic factor withdrawal and amyloid beta-peptide: involvement of calcium and oxyradicals. *J Neurosci,* 17**,** 4212-22.

GUPTA, S., BARRETT, T., WHITMARSH, A. J., CAVANAGH, J., SLUSS, H. K., DÉRIJARD, B. & DAVIS, R. J. 1996. Selective interaction of JNK protein kinase isoforms with transcription factors. *The EMBO Journal,* 15**,** 2760-2770.

GUTMANN, E., GUTTMANN, L., MEDAWAR, P. B. & YOUNG, J. Z. 1942. The Rate of Regeneration of Nerve. *Journal of Experimental Biology,* 19**,** 14-44.

HAAS, C. A., DONATH, C. & KREUTZBERG, G. W. 1993. Differential expression of immediate early genes after transection of the facial nerve. *Neuroscience,* 53**,** 91-9.

HAAS, C. A., STREIT, W. J. & KREUTZBERG, G. W. 1990. Rat facial motoneurons express increased levels of calcitonin gene-related peptide mRNA in response to axotomy. *J Neurosci Res,* 27**,** 270-5.

HAFTEK, J. & THOMAS, P. 1968. Electron-microscope observations on the effects of localized crush injuries on the connective tissues of peripheral nerve. *Journal of Anatomy,* 103**,** 233.

HAHN, B., D'ALESSANDRO, L. A., DEPNER, S., WALDOW, K., BOEHM, M. E., BACHMANN, J., SCHILLING, M., KLINGMULLER, U. & LEHMANN, W. D. 2013. Cellular ERK phospho-form profiles with conserved preference for a switch-like pattern. *J Proteome Res,* 12**,** 637-46.

HAI, T. & CURRAN, T. 1991. Cross-Family Dimerization of Transcription Factors Fos/Jun and ATF/CREB Alters DNA Binding Specificity. *Proceedings of the National Academy of Sciences of the United States of America,* 88**,** 3720-3724.

HALL, A. & LALLI, G. 2010. Rho and Ras GTPases in axon growth, guidance, and branching. *Cold Spring Harb Perspect Biol,* 2**,** a001818.

HAM, J., BABIJ, C., WHITFIELD, J., PFARR, C. M., LALLEMAND, D., YANIV, M. & RUBIN, L. L. 1995. A c-Jun dominant negative mutant protects sympathetic neurons against programmed cell death. *Neuron,* 14**,** 927-939.

HANDSTAD, T., RYE, M., MOCNIK, R., DRABLOS, F. & SAETROM, P. 2012. Cell-type specificity of ChIP-predicted transcription factor binding sites. *BMC Genomics,* 13**,** 372.

HARUTA, T., TAKAMI, N., OHMURA, M., MISUMI, Y. & IKEHARA, Y. 1997. Ca2+-dependent interaction of the growth-associated protein GAP-43 with the synaptic core complex. *Biochem J,* 325 (Pt 2)**,** 455-63.

HAWE, A., KASPER, J. C., FRIESS, W. & JISKOOT, W. 2009. Structural properties of monoclonal antibody aggregates induced by freeze-thawing and thermal stress. *Eur J Pharm Sci,* 38**,** 79-87.

HEASLEY, L. E., STOREY, B., FANGER, G. R., BUTTERFIELD, L., ZAMARRIPA, J., BLUMBERG, D. & MAUE, R. A. 1996. GTPase-deficient G alpha 16 and G alpha q induce PC12 cell differentiation and persistent activation of cJun NH2-terminal kinases. *Mol Cell Biol,* 16**,** 648-56.

HEINTZMAN, N. D., HON, G. C., HAWKINS, R. D., KHERADPOUR, P., STARK, A., HARP, L. F., YE, Z., LEE, L. K., STUART, R. K., CHING, C. W., CHING, K. A., ANTOSIEWICZ-BOURGET, J. E., LIU, H., ZHANG, X., GREEN, R. D., LOBANENKOV, V. V., STEWART, R., THOMSON, J. A., CRAWFORD, G. E., KELLIS, M. & REN, B. 2009. Histone modifications at human enhancers reflect global cell-type-specific gene expression. *Nature,* 459**,** 108-12.

HENKE, R. C., TOLHURST, O., SENTRY, J. W., GUNNING, P. & JEFFREY, P. L. 1991. Expression of actin and myosin genes during PC12 cell differentiation. *Neurochem Res,* 16**,** 675-9.

HERDEGEN, T., CLARET, F. X., KALLUNKI, T., MARTIN-VILLALBA, A., WINTER, C., HUNTER, T. & KARIN, M. 1998. Lasting N-terminal phosphorylation of c-Jun and activation of c-Jun N-terminal kinases after neuronal injury. *J Neurosci,* 18**,** 5124-35.

HERDEGEN, T., KUMMER, W., FIALLOS, C. E., LEAH, J. & BRAVO, R. 1991. Expression of c-JUN, JUN B and JUN D proteins in rat nervous system following transection of vagus nerve and cervical sympathetic trunk. *Neuroscience,* 45**,** 413-22.

HEUMANN, R., KORSCHING, S., BANDTLOW, C. & THOENEN, H. 1987. Changes of nerve growth factor synthesis in nonneuronal cells in response to sciatic nerve transection. *J Cell Biol,* 104**,** 1623-31.

HIBBARD, E. 1963. Regeneration in the severed spinal cord of chordate larvae of Petromyzon marinus. *Experimental Neurology,* 7**,** 175-185.

HIBI, M., LIN, A., SMEAL, T., MINDEN, A. & KARIN, M. 1993. Identification of an oncoprotein- and UV-responsive protein kinase that binds and potentiates the c-Jun activation domain. *Genes Dev,* 7**,** 2135-48.

HILBERG, F., AGUZZI, A., HOWELLS, N. & WAGNER, E. F. 1993. c-jun is essential for normal mouse development and hepatogenesis. *Nature,* 365**,** 179-81.

HOFFMAN, P. N., GRIFFIN, J. W. & PRICE, D. L. 1984. Control of axonal caliber by neurofilament transport. *J Cell Biol,* 99**,** 705-14.

HOKE, A., CHENG, C. & ZOCHODNE, D. W. 2000. Expression of glial cell line-derived neurotrophic factor family of growth factors in peripheral nerve injury in rats. *Neuroreport,* 11**,** 1651-4.

HOLLAND, J. P., SYDSERFF, S. G., TAYLOR, W. A. & BELL, B. A. 1994. Calcitonin gene-related peptide reduces brain injury in a rat model of focal cerebral ischemia. *Stroke,* 25**,** 2055-8; discussion 2058-9.

HOLLENBECK, J. J., MCCLAIN, D. L. & OAKLEY, M. G. 2002. The role of helix stabilizing residues in GCN4 basic region folding and DNA binding. *Protein Sci,* 11**,** 2740-7.

HOSUR, R., XU, J., BIENKOWSKA, J. & BERGER, B. 2011. iWRAP: An interface threading approach with application to prediction of cancer-related protein-protein interactions. *J Mol Biol,* 405**,** 1295-310.

HUNG, V., UDESHI, N. D., LAM, S. S., LOH, K. H., COX, K. J., PEDRAM, K., CARR, S. A. & TING, A. Y. 2016. Spatially resolved proteomic mapping in living cells with the engineered peroxidase APEX2. *Nat Protoc,* 11**,** 456-75.

HUNG, V., ZOU, P., RHEE, H. W., UDESHI, N. D., CRACAN, V., SVINKINA, T., CARR, S. A., MOOTHA, V. K. & TING, A. Y. 2014. Proteomic mapping of the human mitochondrial intermembrane space in live cells via ratiometric APEX tagging. *Mol Cell,* 55**,** 332-41.

HUTCHINSON-BUNCH, C., SANFORD, J. A., HANSEN, J. R., GRITSENKO, M. A., RODLAND, K. D., PIEHOWSKI, P. D., QIAN, W. J. & ADKINS, J. N. 2021. Assessment of TMT Labeling Efficiency in Large-Scale Quantitative Proteomics: The Critical Effect of Sample pH. *ACS Omega,* 6**,** 12660-12666.

IP, Y. T. & DAVIS, R. J. 1998. Signal transduction by the c-Jun N-terminal kinase (JNK)--from inflammation to development. *Curr Opin Cell Biol,* 10**,** 205-19.

IVANOV, V. N., BHOUMIK, A., KRASILNIKOV, M., RAZ, R., OWEN-SCHAUB, L. B., LEVY, D., HORVATH, C. M. & RONAI, Z. 2001. Cooperation between STAT3 and c-jun suppresses Fas transcription. *Mol Cell,* 7**,** 517-28.

JAIN, K., SALAMAT-MILLER, N. & TAYLOR, K. 2021. Freeze-thaw characterization process to minimize aggregation and enable drug product manufacturing of protein based therapeutics. *Sci Rep,* 11**,** 11332.

JARIEL-ENCONTRE, I., SALVAT, C., STEFF, A. M., PARIAT, M., ACQUAVIVA, C., FURSTOSS, O. & PIECHACZYK, M. 1997. Complex mechanisms for c-fos and c-jun degradation. *Mol Biol Rep,* 24**,** 51-6.

JAYARAMAN, V., KRISHNA, K., YANG, Y., RAJASEKARAN, K. J., OU, Y., WANG, T., BEI, K., KRISHNAMURTHY, H. K., RAJASEKARAN, J. J., RAI, A. J. & GREEN, D. A. 2020. An ultra-high-density protein microarray for high throughput single-tier serological detection of Lyme disease. *Sci Rep,* 10**,** 18085.

JENKINS, R., MCMAHON, S. B., BOND, A. B. & HUNT, S. P. 1993. Expression of c-Jun as a response to dorsal root and peripheral nerve section in damaged and adjacent intact primary sensory neurons in the rat. *Eur J Neurosci,* 5**,** 751-9.

JOHNSON, E. M., JR., TANIUCHI, M., CLARK, H. B., SPRINGER, J. E., KOH, S., TAYRIEN, M. W. & LOY, R. 1987. Demonstration of the retrograde transport of nerve growth factor receptor in the peripheral and central nervous system. *J Neurosci,* 7**,** 923-9.

JOLMA, A., YIN, Y., NITTA, K. R., DAVE, K., POPOV, A., TAIPALE, M., ENGE, M., KIVIOJA, T., MORGUNOVA, E. & TAIPALE, J. 2015. DNA-dependent formation of transcription factor pairs alters their binding specificity. *Nature,* 527**,** 384-8.

KAGAN, A., MELMAN, Y. F., KRUMERMAN, A. & MCDONALD, T. V. 2002. 14-3-3 amplifies and prolongs adrenergic stimulation of HERG K+ channel activity. *EMBO J,* 21**,** 1889-98.

KAKIDANI, H. & PTASHNE, M. 1988. GAL4 activates gene expression in mammalian cells. *Cell,* 52**,** 161-7.

KALLUNKI, T., DENG, T., HIBI, M. & KARIN, M. 1996. c-Jun can recruit JNK to phosphorylate dimerization partners via specific docking interactions. *Cell,* 87**,** 929-39.

KALLUNKI, T., SU, B., TSIGELNY, I., SLUSS, H. K., DERIJARD, B., MOORE, G., DAVIS, R. & KARIN, M. 1994. JNK2 contains a specificity-determining region responsible for efficient c-Jun binding and phosphorylation. *Genes Dev,* 8**,** 2996-3007.

KANCZEWSKA, J., MARCO, S., VANDERMEEREN, C., MAUDOUX, O., RIGAUD, J. L. & BOUTRY, M. 2005. Activation of the plant plasma membrane H+-ATPase by phosphorylation and binding of 14-3-3 proteins converts a dimer into a hexamer. *Proc Natl Acad Sci U S A,* 102**,** 11675-80.

KARIN, M. 1995. The regulation of AP-1 activity by mitogen-activated protein kinases. *J Biol Chem,* 270**,** 16483-6.

KENNEY, A. M. & KOCSIS, J. D. 1998. Peripheral axotomy induces long-term c-Jun amino-terminal kinase-1 activation and activator protein-1 binding activity by c-Jun and junD in adult rat dorsal root ganglia In vivo. *J Neurosci,* 18**,** 1318-28.

KENWORTHY, A. K. 2001. Imaging protein-protein interactions using fluorescence resonance energy transfer microscopy. *Methods,* 24**,** 289-96.

KERPPOLA, T. K. & CURRAN, T. 1991. Fos-Jun heterodimers and Jun homodimers bend DNA in opposite orientations: implications for transcription factor cooperativity. *Cell,* 66**,** 317-26.

KIGERL, K. A., GENSEL, J. C., ANKENY, D. P., ALEXANDER, J. K., DONNELLY, D. J. & POPOVICH, P. G. 2009. Identification of two distinct macrophage subsets with divergent effects causing either neurotoxicity or regeneration in the injured mouse spinal cord. *J Neurosci,* 29**,** 13435-44.

KIM, B. R., COYAUD, E., LAURENT, E. M. N., ST-GERMAIN, J., VAN DE LAAR, E., TSAO, M. S., RAUGHT, B. & MOGHAL, N. 2017. Identification of the SOX2 Interactome by BioID Reveals EP300 as a Mediator of SOX2-dependent Squamous Differentiation and Lung Squamous Cell Carcinoma Growth. *Mol Cell Proteomics,* 16**,** 1864-1888.

KIM, D. I., BIRENDRA, K. C., ZHU, W., MOTAMEDCHABOKI, K., DOYE, V. & ROUX, K. J. 2014. Probing nuclear pore complex architecture with proximity-dependent biotinylation. *Proc Natl Acad Sci U S A,* 111**,** E2453-61.

KIM, D. I., JENSEN, S. C., NOBLE, K. A., KC, B., ROUX, K. H., MOTAMEDCHABOKI, K. & ROUX, K. J. 2016. An improved smaller biotin ligase for BioID proximity labeling. *Mol Biol Cell,* 27**,** 1188-96.

KOBAYASHI, D., KUMAGAI, J., MORIKAWA, T., WILSON-MORIFUJI, M., WILSON, A., IRIE, A. & ARAKI, N. 2009. An integrated approach of differential mass spectrometry and gene ontology analysis identified novel proteins regulating neuronal differentiation and survival. *Mol Cell Proteomics,* 8**,** 2350-67.

KOVARY, K. & BRAVO, R. 1991. Expression of different Jun and Fos proteins during the G0-to-G1 transition in mouse fibroblasts: in vitro and in vivo associations. *Molecular and Cellular Biology,* 11**,** 2451-2459.

KYUNG, J. W., CHO, I. H., LEE, S., SONG, W. K., RYAN, T. A., HOPPA, M. B. & KIM, S. H. 2017. Adaptor Protein 2 (AP-2) complex is essential for functional axogenesis in hippocampal neurons. *Sci Rep,* 7**,** 41620.

LABBADIA, J. & MORIMOTO, R. I. 2013. Huntington's disease: underlying molecular mechanisms and emerging concepts. *Trends Biochem Sci,* 38**,** 378-85.

LAFARGA, M., ANDRES, M. A., FERNANDEZ-VIADERO, C., VILLEGAS, J. & BERCIANO, M. T. 1995. Number of nucleoli and coiled bodies and distribution of fibrillar centres in differentiating Purkinje neurons of chick and rat cerebellum. *Anat Embryol (Berl),* 191**,** 359-67.

LAM, S. S., MARTELL, J. D., KAMER, K. J., DEERINCK, T. J., ELLISMAN, M. H., MOOTHA, V. K. & TING, A. Y. 2015. Directed evolution of APEX2 for electron microscopy and proximity labeling. *Nat Methods,* 12**,** 51-4.

LANDSCHULZ, W. H., JOHNSON, P. F. & MCKNIGHT, S. L. 1988. The leucine zipper: a hypothetical structure common to a new class of DNA binding proteins. *Science,* 240**,** 1759-64.

LAUX, T., FUKAMI, K., THELEN, M., GOLUB, T., FREY, D. & CARONI, P. 2000. GAP43, MARCKS, and CAP23 modulate PI(4,5)P(2) at plasmalemmal rafts, and regulate cell cortex actin dynamics through a common mechanism. *J Cell Biol,* 149**,** 1455-72.

LE-NICULESCU, H., BONFOCO, E., KASUYA, Y., CLARET, F. X., GREEN, D. R. & KARIN, M. 1999. Withdrawal of survival factors results in activation of the JNK pathway in neuronal cells leading to Fas ligand induction and cell death. *Mol Cell Biol,* 19**,** 751-63.

LEAH, J. D., HERDEGEN, T. & BRAVO, R. 1991. Selective expression of Jun proteins following axotomy and axonal transport block in peripheral nerves in the rat: evidence for a role in the regeneration process. *Brain Res,* 566**,** 198-207.

LEE, N., LEE, J. W., KANG, G. Y., PARK, S. H. & KIM, K. P. 2019. Quantification of the Dynamic Phosphorylation Process of ERK Using Stable Isotope Dilution Selective Reaction Monitoring Mass Spectrometry. *Proteomics,* 19**,** e1900086.

LEMPIÄINEN, J. K., NISKANEN, E. A., VUOTI, K.-M., LAMPINEN, R. E., GÖÖS, H., VARJOSALO, M. & PALVIMO, J. J. 2017. Agonist-specific Protein Interactomes of Glucocorticoid and Androgen Receptor as Revealed by Proximity Mapping*. *Molecular & Cellular Proteomics,* 16**,** 1462-1474.

LEPPA, S., ERIKSSON, M., SAFFRICH, R., ANSORGE, W. & BOHMANN, D. 2001. Complex functions of AP-1 transcription factors in differentiation and survival of PC12 cells. *Mol Cell Biol,* 21**,** 4369-78.

LEPPÄ, S., SAFFRICH, R., ANSORGE, W. & BOHMANN, D. 1998. Differential regulation of c-Jun by ERK and JNK during PC12 cell differentiation. *The EMBO journal,* 17**,** 4404-4413.

LI, G. L., FAROOQUE, M., HOLTZ, A. & OLSSON, Y. 1999. Apoptosis of oligodendrocytes occurs for long distances away from the primary injury after compression trauma to rat spinal cord. *Acta Neuropathol,* 98**,** 473-80.

LI, L., YANG, H., HE, Y., LI, T., FENG, J., CHEN, W., AO, L., SHI, X., LIN, Y., LIU, H., ZHENG, E., LIN, Q., BU, J., ZENG, Y., ZHENG, M., XU, Y., LIAO, Z., LIN, J. & LIN, D. 2018. Ubiquitin-Specific Protease USP6 Regulates the Stability of the c-Jun Protein. *Mol Cell Biol,* 38.

LI, Q. V., DIXON, G., VERMA, N., ROSEN, B. P., GORDILLO, M., LUO, R., XU, C., WANG, Q., SOH, C. L., YANG, D., CRESPO, M., SHUKLA, A., XIANG, Q., DUNDAR, F., ZUMBO, P., WITKIN, M., KOCHE, R., BETEL, D., CHEN, S., MASSAGUE, J., GARIPPA, R., EVANS, T., BEER, M. A. & HUANGFU, D. 2019. Genome-scale screens identify JNK-JUN signaling as a barrier for pluripotency exit and endoderm differentiation. *Nat Genet,* 51**,** 999-1010.

LI, X. Y., THOMAS, S., SABO, P. J., EISEN, M. B., STAMATOYANNOPOULOS, J. A. & BIGGIN, M. D. 2011. The role of chromatin accessibility in directing the widespread, overlapping patterns of Drosophila transcription factor binding. *Genome Biol,* 12**,** R34.

LI, Y. & RAISMAN, G. 1995. Sprouts from cut corticospinal axons persist in the presence of astrocytic scarring in long-term lesions of the adult rat spinal cord. *Exp Neurol,* 134**,** 102-11.

LIEBERMAN, A. R. 1971. The axon reaction: a review of the principal features of perikaryal responses to axon injury. *Int Rev Neurobiol,* 14**,** 49-124.

LIN, Q., ZHOU, Z., LUO, W., FANG, M., LI, M. & LI, H. 2017. Screening of Proximal and Interacting Proteins in Rice Protoplasts by Proximity-Dependent Biotinylation. *Front Plant Sci,* 8**,** 749.

LINNEY, E. & UDVADIA, A. J. 2004. Construction and detection of fluorescent, germline transgenic zebrafish. *Methods Mol Biol,* 254**,** 271-88.

LIU, H., DENG, X., SHYU, Y. J., LI, J. J., TAPAROWSKY, E. J. & HU, C. D. 2006. Mutual regulation of c-Jun and ATF2 by transcriptional activation and subcellular localization. *EMBO J,* 25**,** 1058-69.

LIU, L., GUAN, H., LI, Y., YING, Z., WU, J., ZHU, X., SONG, L., LI, J. & LI, M. 2017. Astrocyte Elevated Gene 1 Interacts with Acetyltransferase p300 and c-Jun To Promote Tumor Aggressiveness. *Mol Cell Biol,* 37.

LIU, X., SALOKAS, K., TAMENE, F., JIU, Y., WELDATSADIK, R. G., OHMAN, T. & VARJOSALO, M. 2018. An AP-MS- and BioID-compatible MAC-tag enables comprehensive mapping of protein interactions and subcellular localizations. *Nat Commun,* 9**,** 1188.

LIU, X., SALOKAS, K., WELDATSADIK, R. G., GAWRIYSKI, L. & VARJOSALO, M. 2020. Combined proximity labeling and affinity purification-mass spectrometry workflow for mapping and visualizing protein interaction networks. *Nat Protoc,* 15**,** 3182-3211.

LIVELY, T. N., NGUYEN, T. N., GALASINSKI, S. K. & GOODRICH, J. A. 2004. The basic leucine zipper domain of c-Jun functions in transcriptional activation through interaction with the N terminus of human TATA-binding protein-associated factor-1 (human TAF(II)250). *J Biol Chem,* 279**,** 26257-65.

LOBINGIER, B. T., HÜTTENHAIN, R., EICHEL, K., MILLER, K. B., TING, A. Y., VON ZASTROW, M. & KROGAN, N. J. 2017. An approach to spatiotemporally resolve protein interaction networks in living cells. *Cell,* 169**,** 350-360. e12.

LOW, K., CULBERTSON, M., BRADKE, F., TESSIER-LAVIGNE, M. & TUSZYNSKI, M. H. 2008. Netrin-1 is a novel myelin-associated inhibitor to axon growth. *J Neurosci,* 28**,** 1099-108.

LU, P., WANG, Y., GRAHAM, L., MCHALE, K., GAO, M., WU, D., BROCK, J., BLESCH, A., ROSENZWEIG, E. S., HAVTON, L. A., ZHENG, B., CONNER, J. M., MARSALA, M. & TUSZYNSKI, M. H. 2012. Long-distance growth and connectivity of neural stem cells after severe spinal cord injury. *Cell,* 150**,** 1264-73.

LU, X., WINTRODE, P. L. & SUREWICZ, W. K. 2007. Beta-sheet core of human prion protein amyloid fibrils as determined by hydrogen/deuterium exchange. *Proc Natl Acad Sci U S A,* 104**,** 1510-5.

LUDWIN, S. K. 1990. Oligodendrocyte survival in Wallerian degeneration. *Acta Neuropathol,* 80**,** 184-91.

MA, J., PRZIBILLA, E., HU, J., BOGORAD, L. & PTASHNE, M. 1988. Yeast activators stimulate plant gene expression. *Nature,* 334**,** 631-3.

MAGGIRWAR, S. B., RAMIREZ, S., TONG, N., GELBARD, H. A. & DEWHURST, S. 2000. Functional interplay between nuclear factor-kappaB and c-Jun integrated by coactivator p300 determines the survival of nerve growth factor-dependent PC12 cells. *J Neurochem,* 74**,** 527-39.

MAIR, A., XU, S. L., BRANON, T. C., TING, A. Y. & BERGMANN, D. C. 2019. Proximity labeling of protein complexes and cell-type-specific organellar proteomes in Arabidopsis enabled by TurboID. *Elife,* 8.

MANGELSDORF, D. J. & EVANS, R. M. 1995. The RXR heterodimers and orphan receptors. *Cell,* 83**,** 841-50.

MANN, B., GELOS, M., SIEDOW, A., HANSKI, M. L., GRATCHEV, A., ILYAS, M., BODMER, W. F., MOYER, M. P., RIECKEN, E. O., BUHR, H. J. & HANSKI, C. 1999. Target genes of beta-catenin-T cell-factor/lymphoid-enhancer-factor signaling in human colorectal carcinomas. *Proc Natl Acad Sci U S A,* 96**,** 1603-8.

MANNA, P. R., EUBANK, D. W. & STOCCO, D. M. 2004. Assessment of the role of activator protein-1 on transcription of the mouse steroidogenic acute regulatory protein gene. *Mol Endocrinol,* 18**,** 558-73.

MARKUS, A., ZHONG, J. & SNIDER, W. D. 2002. Raf and akt mediate distinct aspects of sensory axon growth. *Neuron,* 35**,** 65-76.

MARQUES, C. A., KEIL, U., BONERT, A., STEINER, B., HAASS, C., MULLER, W. E. & ECKERT, A. 2003. Neurotoxic mechanisms caused by the Alzheimer's disease-linked Swedish amyloid precursor protein mutation: oxidative stress, caspases, and the JNK pathway. *J Biol Chem,* 278**,** 28294-302.

MASON, M. R., LIEBERMAN, A. R., GRENNINGLOH, G. & ANDERSON, P. N. 2002. Transcriptional upregulation of SCG10 and CAP-23 is correlated with regeneration of the axons of peripheral and central neurons in vivo. *Mol Cell Neurosci,* 20**,** 595-615.

MASON, M. R. J., VAN ERP, S., WOLZAK, K., BEHRENS, A., RAIVICH, G. & VERHAAGEN, J. 2022. The Jun-dependent axon regeneration gene program: Jun promotes regeneration over plasticity. *Hum Mol Genet,* 31**,** 1242-1262.

MATHAS, S., HINZ, M., ANAGNOSTOPOULOS, I., KRAPPMANN, D., LIETZ, A., JUNDT, F., BOMMERT, K., MECHTA-GRIGORIOU, F., STEIN, H., DORKEN, B. & SCHEIDEREIT, C. 2002. Aberrantly expressed c-Jun and JunB are a hallmark of Hodgkin lymphoma cells, stimulate proliferation and synergize with NF-kappa B. *EMBO J,* 21**,** 4104-13.

MATTAR, P., JOLICOEUR, C., DANG, T., SHAH, S., CLARK, B. S. & CAYOUETTE, M. 2021. A Casz1-NuRD complex regulates temporal identity transitions in neural progenitors. *Sci Rep,* 11**,** 3858.

MAZINA, M. Y., ZIGANSHIN, R. H., MAGNITOV, M. D., GOLOVNIN, A. K. & VOROBYEVA, N. E. 2020. Proximity-dependent biotin labelling reveals CP190 as an EcR/Usp molecular partner. *Sci Rep,* 10**,** 4793.

MEDEIROS, R., BAGLIETTO-VARGAS, D. & LAFERLA, F. M. 2011. The role of tau in Alzheimer's disease and related disorders. *CNS Neurosci Ther,* 17**,** 514-24.

MEHUS, A. A., ANDERSON, R. H. & ROUX, K. J. 2016. BioID Identification of Lamin-Associated Proteins. *Methods Enzymol,* 569**,** 3-22.

MEI, J. & NIU, C. 2015. Protective and reversal effects of conserved dopamine neurotrophic factor on PC12 cells following 6-hydroxydopamine administration. *Mol Med Rep,* 12**,** 297-302.

MENG, Q. & XIA, Y. 2011. c-Jun, at the crossroad of the signaling network. *Protein Cell,* 2**,** 889-98.

MENNERICK, S. & ZORUMSKI, C. F. 1994. Glial contributions to excitatory neurotransmission in cultured hippocampal cells. *Nature,* 368**,** 59-62.

MESNER, P. W., EPTING, C. L., HEGARTY, J. L. & GREEN, S. H. 1995. A timetable of events during programmed cell death induced by trophic factor withdrawal from neuronal PC12 cells. *J Neurosci,* 15**,** 7357-66.

MESULAM, M., SHAW, P., MASH, D. & WEINTRAUB, S. 2004. Cholinergic nucleus basalis tauopathy emerges early in the aging-MCI-AD continuum. *Ann Neurol,* 55**,** 815-28.

MICHAELEVSKI, I., SEGAL-RUDER, Y., ROZENBAUM, M., MEDZIHRADSZKY, K. F., SHALEM, O., COPPOLA, G., HORN-SABAN, S., BEN-YAAKOV, K., DAGAN, S. Y., RISHAL, I., GESCHWIND, D. H., PILPEL, Y., BURLINGAME, A. L. & FAINZILBER, M. 2010. Signaling to transcription networks in the neuronal retrograde injury response. *Sci Signal,* 3**,** ra53.

MILEDI, R. & SLATER, C. R. 1970. On the degeneration of rat neuromuscular junctions after nerve section. *J Physiol,* 207**,** 507-28.

MINER, J. N. & YAMAMOTO, K. R. 1992. The basic region of AP-1 specifies glucocorticoid receptor activity at a composite response element. *Genes Dev,* 6**,** 2491-501.

MITCHELL, B. L., YASUI, Y., LI, C. I., FITZPATRICK, A. L. & LAMPE, P. D. 2005. Impact of freeze-thaw cycles and storage time on plasma samples used in mass spectrometry based biomarker discovery projects. *Cancer informatics,* 1**,** 117693510500100110.

MONTALBAN, X., HAUSER, S. L., KAPPOS, L., ARNOLD, D. L., BAR-OR, A., COMI, G., DE SEZE, J., GIOVANNONI, G., HARTUNG, H. P., HEMMER, B., LUBLIN, F., RAMMOHAN, K. W., SELMAJ, K., TRABOULSEE, A., SAUTER, A., MASTERMAN, D., FONTOURA, P., BELACHEW, S., GARREN, H., MAIRON, N., CHIN, P., WOLINSKY, J. S. & INVESTIGATORS, O. C. 2017. Ocrelizumab versus Placebo in Primary Progressive Multiple Sclerosis. *N Engl J Med,* 376**,** 209-220.

MOREAU-FAUVARQUE, C., KUMANOGOH, A., CAMAND, E., JAILLARD, C., BARBIN, G., BOQUET, I., LOVE, C., JONES, E. Y., KIKUTANI, H., LUBETZKI, C., DUSART, I. & CHEDOTAL, A. 2003. The transmembrane semaphorin Sema4D/CD100, an inhibitor of axonal growth, is expressed on oligodendrocytes and upregulated after CNS lesion. *J Neurosci,* 23**,** 9229-39.

MORTENSEN, A. & SKIBSTED, L. H. 1997. Importance of Carotenoid Structure in Radical-Scavenging Reactions. *Journal of Agricultural and Food Chemistry,* 45**,** 2970-2977.

MUSATOV, S., ROBERTS, J., BROOKS, A. I., PENA, J., BETCHEN, S., PFAFF, D. W. & KAPLITT, M. G. 2004. Inhibition of neuronal phenotype by PTEN in PC12 cells. *Proc Natl Acad Sci U S A,* 101**,** 3627-31.

NATARAJAN, A., YARDIMCI, G. G., SHEFFIELD, N. C., CRAWFORD, G. E. & OHLER, U. 2012. Predicting cell-type-specific gene expression from regions of open chromatin. *Genome Res,* 22**,** 1711-22.

NATERI, A. S., SPENCER-DENE, B. & BEHRENS, A. 2005. Interaction of phosphorylated c-Jun with TCF4 regulates intestinal cancer development. *Nature,* 437**,** 281-5.

NAVEILHAN, P., ELSHAMY, W. M. & ERNFORS, P. 1997. Differential regulation of mRNAs for GDNF and its receptors Ret and GDNFR alpha after sciatic nerve lesion in the mouse. *Eur J Neurosci,* 9**,** 1450-60.

NDLOVU, M. N., VAN LINT, C., VAN WESEMAEL, K., CALLEBERT, P., CHALBOS, D., HAEGEMAN, G. & VANDEN BERGHE, W. 2009. Hyperactivated NF-kappaB and AP-1 transcription factors promote highly accessible chromatin and constitutive transcription across the interleukin-6 gene promoter in metastatic breast cancer cells. *Mol Cell Biol,* 29**,** 5488-504.

NEAGU, M., BOSTAN, M. & CONSTANTIN, C. 2019. Protein microarray technology: Assisting personalized medicine in oncology (Review). *World Academy of Sciences Journal*.

NEO, S. J., SU, X. & THOMSEN, J. S. 2009. Surface plasmon resonance study of cooperative interactions of estrogen receptor alpha and transcriptional factor Sp1 with composite DNA elements. *Anal Chem,* 81**,** 3344-9.

NEUBAUER, Z. & CALEF, E. 1970. Immunity phase-shift in defective lysogens: non-mutational hereditary change of early regulation of lambda prophage. *J Mol Biol,* 51**,** 1-13.

NISSL, F. 1892. Uber die veranderugen der ganglienzellen am facialiskern des kaninchen nach ausreiBung der nerven. *Allg Z Psychiat,* 48**,** 197-198.

NOVICK, P. & ZERIAL, M. 1997. The diversity of Rab proteins in vesicle transport. *Curr Opin Cell Biol,* 9**,** 496-504.

OGRYZKO, V. V., SCHILTZ, R. L., RUSSANOVA, V., HOWARD, B. H. & NAKATANI, Y. 1996. The transcriptional coactivators p300 and CBP are histone acetyltransferases. *Cell,* 87**,** 953-9.

ONG, S. E., BLAGOEV, B., KRATCHMAROVA, I., KRISTENSEN, D. B., STEEN, H., PANDEY, A. & MANN, M. 2002. Stable isotope labeling by amino acids in cell culture, SILAC, as a simple and accurate approach to expression proteomics. *Mol Cell Proteomics,* 1**,** 376-86.

ONO, Y., AOKI, S., OHNISHI, K., YASUDA, T., KAWANO, K. & TSUKADA, Y. 1998. Increased serum levels of advanced glycation end-products and diabetic complications. *Diabetes Res Clin Pract,* 41**,** 131-7.

PAEK, J., KALOCSAY, M., STAUS, D. P., WINGLER, L., PASCOLUTTI, R., PAULO, J. A., GYGI, S. P. & KRUSE, A. C. 2017. Multidimensional Tracking of GPCR Signaling via Peroxidase-Catalyzed Proximity Labeling. *Cell,* 169**,** 338-349 e11.

PANNE, D., MANIATIS, T. & HARRISON, S. C. 2007. An atomic model of the interferon-beta enhanceosome. *Cell,* 129**,** 1111-23.

PAPAVASSILIOU, A. G., TREIER, M. & BOHMANN, D. 1995. Intramolecular signal transduction in c-Jun. *EMBO J,* 14**,** 2014-9.

PARK, K. K., LIU, K., HU, Y., SMITH, P. D., WANG, C., CAI, B., XU, B., CONNOLLY, L., KRAMVIS, I., SAHIN, M. & HE, Z. 2008. Promoting axon regeneration in the adult CNS by modulation of the PTEN/mTOR pathway. *Science,* 322**,** 963-6.

PASTERKAMP, R. J., DE WINTER, F., GIGER, R. J. & VERHAAGEN, J. 1998. Role for semaphorin III and its receptor neuropilin-1 in neuronal regeneration and scar formation? *Prog Brain Res,* 117**,** 151-70.

PATEL, L. R., CURRAN, T. & KERPPOLA, T. K. 1994. Energy transfer analysis of Fos-Jun dimerization and DNA binding. *Proc Natl Acad Sci U S A,* 91**,** 7360-4.

PATTERSON, S. D., THOMAS, D. & BRADSHAW, R. A. 1996. Application of combined mass spectrometry and partial amino acid sequence to the identification of gel-separated proteins. *Electrophoresis,* 17**,** 877-91.

PEARSON, A. G., GRAY, C. W., PEARSON, J. F., GREENWOOD, J. M., DURING, M. J. & DRAGUNOW, M. 2003. ATF3 enhances c-Jun-mediated neurite sprouting. *Brain Res Mol Brain Res,* 120**,** 38-45.

PELICCI, G., LANFRANCONE, L., GRIGNANI, F., MCGLADE, J., CAVALLO, F., FORNI, G., NICOLETTI, I., GRIGNANI, F., PAWSON, T. & PELICCI, P. G. 1992. A novel transforming protein (SHC) with an SH2 domain is implicated in mitogenic signal transduction. *Cell,* 70**,** 93-104.

PESTRONK, A., DRACHMAN, D. B. & GRIFFIN, J. W. 1980. Effects of aging on nerve sprouting and regeneration. *Exp Neurol,* 70**,** 65-82.

PIQUE-REGI, R., DEGNER, J. F., PAI, A. A., GAFFNEY, D. J., GILAD, Y. & PRITCHARD, J. K. 2011. Accurate inference of transcription factor binding from DNA sequence and chromatin accessibility data. *Genome Res,* 21**,** 447-55.

PITA-THOMAS, W., GONCALVES, T. M., KUMAR, A., ZHAO, G. & CAVALLI, V. 2021. Genome-wide chromatin accessibility analyses provide a map for enhancing optic nerve regeneration. *Sci Rep,* 11**,** 14924.

POPOVICH, P. G., STOKES, B. T. & WHITACRE, C. C. 1996. Concept of autoimmunity following spinal cord injury: Possible roles for T lymphocytes in the traumatized central nervous system. *Journal of Neuroscience Research,* 45**,** 349-363.

POWERS, C. M., WRENCH, N., RYDE, I. T., SMITH, A. M., SEIDLER, F. J. & SLOTKIN, T. A. 2010. Silver impairs neurodevelopment: studies in PC12 cells. *Environ Health Perspect,* 118**,** 73-9.

PUIG, O., CASPARY, F., RIGAUT, G., RUTZ, B., BOUVERET, E., BRAGADO-NILSSON, E., WILM, M. & SERAPHIN, B. 2001. The tandem affinity purification (TAP) method: a general procedure of protein complex purification. *Methods,* 24**,** 218-29.

PULVERER, B. J., KYRIAKIS, J. M., AVRUCH, J., NIKOLAKAKI, E. & WOODGETT, J. R. 1991. Phosphorylation of c-jun mediated by MAP kinases. *Nature,* 353**,** 670-4.

QIN, W., CHO, K. F., CAVANAGH, P. E. & TING, A. Y. 2021. Deciphering molecular interactions by proximity labeling. *Nat Methods,* 18**,** 133-143.

RAMAN, D., SAI, J., HAWKINS, O. & RICHMOND, A. 2014. Adaptor protein2 (AP2) orchestrates CXCR2-mediated cell migration. *Traffic,* 15**,** 451-69.

RAMÓN Y CAJAL, S. 1928. Degeneration and regeneration of the nervous system.

RANSONE, L. J., KERR, L. D., SCHMITT, M. J., WAMSLEY, P. & VERMA, I. M. 1993. The bZIP domains of Fos and Jun mediate a physical association with the TATA box-binding protein. *Gene expression,* 3 1**,** 37-48.

RISAU, W. & WOLBURG, H. 1990. Development of the blood-brain barrier. *Trends Neurosci,* 13**,** 174-8.

ROONEY, J. W., SUN, Y. L., GLIMCHER, L. H. & HOEY, T. 1995. Novel NFAT sites that mediate activation of the interleukin-2 promoter in response to T-cell receptor stimulation. *Mol Cell Biol,* 15**,** 6299-310.

ROSENBERG, J. M. & UTZ, P. J. 2015. Protein microarrays: a new tool for the study of autoantibodies in immunodeficiency. *Front Immunol,* 6**,** 138.

ROSENBERG, M. M., YANG, F., GIOVANNI, M., MOHN, J. L., TEMBURNI, M. K. & JACOB, M. H. 2008. Adenomatous polyposis coli plays a key role, in vivo, in coordinating assembly of the neuronal nicotinic postsynaptic complex. *Mol Cell Neurosci,* 38**,** 138-52.

ROSENTHAL, S. M., MISRA, T., ABDOUNI, H., BRANON, T. C., TING, A. Y., SCOTT, I. C. & GINGRAS, A. C. 2021. A Toolbox for Efficient Proximity-Dependent Biotinylation in Zebrafish Embryos. *Mol Cell Proteomics,* 20**,** 100128.

ROUX, K. J., KIM, D. I., RAIDA, M. & BURKE, B. 2012. A promiscuous biotin ligase fusion protein identifies proximal and interacting proteins in mammalian cells. *Journal of cell biology,* 196**,** 801-810.

ROZEK, D. & PFEIFER, G. P. 1993. In vivo protein-DNA interactions at the c-jun promoter: preformed complexes mediate the UV response. *Mol Cell Biol,* 13**,** 5490-9.

RUFF, C. A., STAAK, N., PATODIA, S., KASWICH, M., ROCHA-FERREIRA, E., DA COSTA, C., BRECHT, S., MAKWANA, M., FONTANA, X., HRISTOVA, M., RUMAJOGEE, P., GALIANO, M., BOHATSCHEK, M., HERDEGEN, T., BEHRENS, A. & RAIVICH, G. 2012. Neuronal c-Jun is required for successful axonal regeneration, but the effects of phosphorylation of its N-terminus are moderate. *J Neurochem,* 121**,** 607-18.

SACHDEV, P., MENON, S., KASTNER, D. B., CHUANG, J. Z., YEH, T. Y., CONDE, C., CACERES, A., SUNG, C. H. & SAKMAR, T. P. 2007. G protein beta gamma subunit interaction with the dynein light-chain component Tctex-1 regulates neurite outgrowth. *EMBO J,* 26**,** 2621-32.

SAHENK, Z., SEHARASEYON, J. & MENDELL, J. R. 1994. CNTF potentiates peripheral nerve regeneration. *Brain Res,* 655**,** 246-50.

SCHLAEPFER, W. W. & BUNGE, R. P. 1973. Effects of calcium ion concentration on the degeneration of amputated axons in tissue culture. *J Cell Biol,* 59**,** 456-70.

SCHMID, E. M. & MCMAHON, H. T. 2007. Integrating molecular and network biology to decode endocytosis. *Nature,* 448**,** 883-888.

SCHNEIDER, T. L. & SCHEPARTZ, A. 2001. Hepatitis B virus protein pX enhances the monomer assembly pathway of bZIP.DNA complexes. *Biochemistry,* 40**,** 2835-43.

SCHONHOFF, C. M., BULSECO, D. A., BRANCHO, D. M., PARADA, L. F. & ROSS, A. H. 2001. The Ras-ERK pathway is required for the induction of neuronal nitric oxide synthase in differentiating PC12 cells. *J Neurochem,* 78**,** 631-9.

SCHWAB, M. E. 1990. Myelin-associated inhibitors of neurite growth and regeneration in the CNS. *Trends Neurosci,* 13**,** 452-6.

SCHWAB, M. E. & CARONI, P. 1988. Oligodendrocytes and CNS myelin are nonpermissive substrates for neurite growth and fibroblast spreading in vitro. *J Neurosci,* 8**,** 2381-93.

SHAMASH, S., REICHERT, F. & ROTSHENKER, S. 2002. The cytokine network of Wallerian degeneration: tumor necrosis factor-alpha, interleukin-1alpha, and interleukin-1beta. *J Neurosci,* 22**,** 3052-60.

SHEFFIELD, N. C., THURMAN, R. E., SONG, L., SAFI, A., STAMATOYANNOPOULOS, J. A., LENHARD, B., CRAWFORD, G. E. & FUREY, T. S. 2013. Patterns of regulatory activity across diverse human cell types predict tissue identity, transcription factor binding, and long-range interactions. *Genome Res,* 23**,** 777-88.

SIERRA-FONSECA, J. A., NAJERA, O., MARTINEZ-JURADO, J., WALKER, E. M., VARELA-RAMIREZ, A., KHAN, A. M., MIRANDA, M., LAMANGO, N. S. & ROYCHOWDHURY, S. 2014. Nerve growth factor induces neurite outgrowth of PC12 cells by promoting Gbetagamma-microtubule interaction. *BMC Neurosci,* 15**,** 132.

SKENE, J. H. & WILLARD, M. 1981. Changes in axonally transported proteins during axon regeneration in toad retinal ganglion cells. *J Cell Biol,* 89**,** 86-95.

SLOMNICKI, L. P., PIETRZAK, M., VASHISHTA, A., JONES, J., LYNCH, N., ELLIOT, S., POULOS, E., MALICOTE, D., MORRIS, B. E., HALLGREN, J. & HETMAN, M. 2016. Requirement of Neuronal Ribosome Synthesis for Growth and Maintenance of the Dendritic Tree. *J Biol Chem,* 291**,** 5721-5739.

SLOTKIN, T. A., MACKILLOP, E. A., RYDE, I. T., TATE, C. A. & SEIDLER, F. J. 2007. Screening for developmental neurotoxicity using PC12 cells: comparisons of organophosphates with a carbamate, an organochlorine, and divalent nickel. *Environ Health Perspect,* 115**,** 93-101.

SMEAL, T., BINETRUY, B., MERCOLA, D. A., BIRRER, M. & KARIN, M. 1991. Oncogenic and transcriptional cooperation with Ha-Ras requires phosphorylation of c-Jun on serines 63 and 73. *Nature,* 354**,** 494-6.

SMITH, L. M., WISE, S. C., HENDRICKS, D. T., SABICHI, A. L., BOS, T., REDDY, P., BROWN, P. H. & BIRRER, M. J. 1999. cJun overexpression in MCF-7 breast cancer cells produces a tumorigenic, invasive and hormone resistant phenotype. *Oncogene,* 18**,** 6063-70.

SMITH, P. D., SUN, F., PARK, K. K., CAI, B., WANG, C., KUWAKO, K., MARTINEZ-CARRASCO, I., CONNOLLY, L. & HE, Z. 2009. SOCS3 deletion promotes optic nerve regeneration in vivo. *Neuron,* 64**,** 617-23.

SNOW, D. M., LEMMON, V., CARRINO, D. A., CAPLAN, A. I. & SILVER, J. 1990. Sulfated proteoglycans in astroglial barriers inhibit neurite outgrowth in vitro. *Exp Neurol,* 109**,** 111-30.

SODERBLOM, C., LUO, X., BLUMENTHAL, E., BRAY, E., LYAPICHEV, K., RAMOS, J., KRISHNAN, V., LAI-HSU, C., PARK, K. K., TSOULFAS, P. & LEE, J. K. 2013. Perivascular fibroblasts form the fibrotic scar after contusive spinal cord injury. *J Neurosci,* 33**,** 13882-7.

SONG, L., ZHANG, Z., GRASFEDER, L. L., BOYLE, A. P., GIRESI, P. G., LEE, B. K., SHEFFIELD, N. C., GRAF, S., HUSS, M., KEEFE, D., LIU, Z., LONDON, D., MCDANIELL, R. M., SHIBATA, Y., SHOWERS, K. A., SIMON, J. M., VALES, T., WANG, T., WINTER, D., ZHANG, Z., CLARKE, N. D., BIRNEY, E., IYER, V. R., CRAWFORD, G. E., LIEB, J. D. & FUREY, T. S. 2011. Open chromatin defined by DNaseI and FAIRE identifies regulatory elements that shape cell-type identity. *Genome Res,* 21**,** 1757-67.

SPERRY, J. L., GUYETTE, F. X., BROWN, J. B., YAZER, M. H., TRIULZI, D. J., EARLY-YOUNG, B. J., ADAMS, P. W., DALEY, B. J., MILLER, R. S., HARBRECHT, B. G., CLARIDGE, J. A., PHELAN, H. A., WITHAM, W. R., PUTNAM, A. T., DUANE, T. M., ALARCON, L. H., CALLAWAY, C. W., ZUCKERBRAUN, B. S., NEAL, M. D., ROSENGART, M. R., FORSYTHE, R. M., BILLIAR, T. R., YEALY, D. M., PEITZMAN, A. B., ZENATI, M. S. & GROUP, P. A. S. 2018. Prehospital Plasma during Air Medical Transport in Trauma Patients at Risk for Hemorrhagic Shock. *N Engl J Med,* 379**,** 315-326.

SPERRY, R. W. 1963. Chemoaffinity in the Orderly Growth of Nerve Fiber Patterns and Connections. *Proc Natl Acad Sci U S A,* 50**,** 703-10.

SPIRA, M. E., BENBASSAT, D. & DORMANN, A. 1993. Resealing of the proximal and distal cut ends of transected axons: electrophysiological and ultrastructural analysis. *J Neurobiol,* 24**,** 300-16.

SPOLAR, R. S. & RECORD, M. T., JR. 1994. Coupling of local folding to site-specific binding of proteins to DNA. *Science,* 263**,** 777-84.

STEIN, B., ANGEL, P., VAN DAM, H., PONTA, H., HERRLICH, P., VAN DER EB, A. & RAHMSDORF, H. J. 1992. Ultraviolet-radiation induced c-jun gene transcription: two AP-1 like binding sites mediate the response. *Photochem Photobiol,* 55**,** 409-15.

STEPATH, M., ZULCH, B., MAGHNOUJ, A., SCHORK, K., TUREWICZ, M., EISENACHER, M., HAHN, S., SITEK, B. & BRACHT, T. 2020. Systematic Comparison of Label-Free, SILAC, and TMT Techniques to Study Early Adaption toward Inhibition of EGFR Signaling in the Colorectal Cancer Cell Line DiFi. *J Proteome Res,* 19**,** 926-937.

STOLL, G., GRIFFIN, J. W., LI, C. Y. & TRAPP, B. D. 1989. Wallerian degeneration in the peripheral nervous system: participation of both Schwann cells and macrophages in myelin degradation. *J Neurocytol,* 18**,** 671-83.

SU, Y., GUO, Y., GUO, J., ZENG, T., WANG, T. & LIU, W. 2023. Study of FOXO1-interacting proteins using TurboID-based proximity labeling technology. *BMC Genomics,* 24**,** 146.

SUN, F., PARK, K. K., BELIN, S., WANG, D., LU, T., CHEN, G., ZHANG, K., YEUNG, C., FENG, G., YANKNER, B. A. & HE, Z. 2011. Sustained axon regeneration induced by co-deletion of PTEN and SOCS3. *Nature,* 480**,** 372-5.

SUNDERLAND, S. 1947. Rate of regeneration in human peripheral nerves; analysis of the interval between injury and onset of recovery. *Arch Neurol Psychiatry,* 58**,** 251-95.

SURY, M. D., MCSHANE, E., HERNANDEZ-MIRANDA, L. R., BIRCHMEIER, C. & SELBACH, M. 2015. Quantitative proteomics reveals dynamic interaction of c-Jun N-terminal kinase (JNK) with RNA transport granule proteins splicing factor proline- and glutamine-rich (Sfpq) and non-POU domain-containing octamer-binding protein (Nono) during neuronal differentiation. *Mol Cell Proteomics,* 14**,** 50-65.

SUTHERLAND, J. A., COOK, A., BANNISTER, A. J. & KOUZARIDES, T. 1992. Conserved motifs in Fos and Jun define a new class of activation domain. *Genes Dev,* 6**,** 1810-9.

SWAFFIELD, J. C., MELCHER, K. & JOHNSTON, S. A. 1995. A highly conserved ATPase protein as a mediator between acidic activation domains and the TATA-binding protein. *Nature,* 374**,** 88-91.

SZPIR, M. 2006. New thinking on neurodevelopment. *Environ Health Perspect,* 114**,** A100-7.

TALOTTA, F., MEGA, T., BOSSIS, G., CASALINO, L., BASBOUS, J., JARIEL-ENCONTRE, I., PIECHACZYK, M. & VERDE, P. 2010. Heterodimerization with Fra-1 cooperates with the ERK pathway to stabilize c-Jun in response to the RAS oncoprotein. *Oncogene,* 29**,** 4732-40.

TAN, B., PENG, S., YATIM, S., GUNARATNE, J., HUNZIKER, W. & LUDWIG, A. 2020. An Optimized Protocol for Proximity Biotinylation in Confluent Epithelial Cell Cultures Using the Peroxidase APEX2. *STAR Protoc,* 1**,** 100074.

TANIUCHI, M., CLARK, H. B., SCHWEITZER, J. B. & JOHNSON, E. M., JR. 1988. Expression of nerve growth factor receptors by Schwann cells of axotomized peripheral nerves: ultrastructural location, suppression by axonal contact, and binding properties. *J Neurosci,* 8**,** 664-81.

TETZLAFF, W., BISBY, M. A. & KREUTZBERG, G. W. 1988. Changes in cytoskeletal proteins in the rat facial nucleus following axotomy. *J Neurosci,* 8**,** 3181-9.

TEURICH, S. & ANGEL, P. 1995. The glucocorticoid receptor synergizes with Jun homodimers to activate AP-1-regulated promoters lacking GR binding sites. *Chem Senses,* 20**,** 251-5.

THOMAS, C. K., STEIN, R. B., GORDON, T., LEE, R. G. & ELLEKER, M. G. 1987. Patterns of reinnervation and motor unit recruitment in human hand muscles after complete ulnar and median nerve section and resuture. *J Neurol Neurosurg Psychiatry,* 50**,** 259-68.

THOMPSON, A., SCHAFER, J., KUHN, K., KIENLE, S., SCHWARZ, J., SCHMIDT, G., NEUMANN, T., JOHNSTONE, R., MOHAMMED, A. K. & HAMON, C. 2003. Tandem mass tags: a novel quantification strategy for comparative analysis of complex protein mixtures by MS/MS. *Anal Chem,* 75**,** 1895-904.

TOJIMA, T., ITOFUSA, R. & KAMIGUCHI, H. 2010. Asymmetric clathrin-mediated endocytosis drives repulsive growth cone guidance. *Neuron,* 66**,** 370-7.

TREIER, M., STASZEWSKI, L. M. & BOHMANN, D. 1994. Ubiquitin-dependent c-Jun degradation in vivo is mediated by the delta domain. *Cell,* 78**,** 787-98.

TSUJINO, H., KONDO, E., FUKUOKA, T., DAI, Y., TOKUNAGA, A., MIKI, K., YONENOBU, K., OCHI, T. & NOGUCHI, K. 2000. Activating transcription factor 3 (ATF3) induction by axotomy in sensory and motoneurons: A novel neuronal marker of nerve injury. *Mol Cell Neurosci,* 15**,** 170-82.

TURNER, J. E. & GLAZE, K. A. 1977. The early stages of Wallerian degeneration in the severed optic nerve of the newt (Triturus viridescens). *Anat Rec,* 187**,** 291-310.

UDVADIA, A. J. 2008. 3.6 kb genomic sequence from Takifugu capable of promoting axon growth-associated gene expression in developing and regenerating zebrafish neurons. *Gene Expr Patterns,* 8**,** 382-388.

VAN DER PERREN, A., GELDERS, G., FENYI, A., BOUSSET, L., BRITO, F., PEELAERTS, W., VAN DEN HAUTE, C., GENTLEMAN, S., MELKI, R. & BAEKELANDT, V. 2020. The structural differences between patient-derived alpha-synuclein strains dictate characteristics of Parkinson's disease, multiple system atrophy and dementia with Lewy bodies. *Acta Neuropathol,* 139**,** 977-1000.

VASCONCELOS, I. C., CAMPOS, R. M., SCHWAEMMLE, H. K., MASSON, A. P., FERRARI, G. D., ALBERICI, L. C., FAÇA, V. M., GARCIA-CAIRASCO, N. & SEBOLLELA, A. 2021. A freeze-and-thaw-induced fragment of the microtubule-associated protein tau in rat brain extracts: implications for the biochemical assessment of neurotoxicity. *Bioscience Reports,* 41.

VÉLOT, L., LESSARD, F., BÉRUBÉ-SIMARD, F.-A., TAV, C., NEVEU, B., TEYSSIER, V., BOUDAOUD, I., DIONNE, U., LAVOIE, N., BILODEAU, S., POULIOT, F. & BISSON, N. 2021. Proximity-dependent Mapping of the Androgen Receptor Identifies Kruppel-like Factor 4 as a Functional Partner. *Molecular & Cellular Proteomics,* 20**,** 100064.

VENKATESH, I., SIMPSON, M. T., COLEY, D. M. & BLACKMORE, M. G. 2016. Epigenetic profiling reveals a developmental decrease in promoter accessibility during cortical maturation in vivo. *Neuroepigenetics,* 8**,** 19-26.

VINSON, C., ACHARYA, A. & TAPAROWSKY, E. J. 2006. Deciphering B-ZIP transcription factor interactions in vitro and in vivo. *Biochim Biophys Acta,* 1759**,** 4-12.

VINSON, C., MYAKISHEV, M., ACHARYA, A., MIR, A. A., MOLL, J. R. & BONOVICH, M. 2002. Classification of human B-ZIP proteins based on dimerization properties. *Mol Cell Biol,* 22**,** 6321-35.

VON MERING, C., KRAUSE, R., SNEL, B., CORNELL, M., OLIVER, S. G., FIELDS, S. & BORK, P. 2002. Comparative assessment of large-scale data sets of protein–protein interactions. *Nature,* 417**,** 399-403.

VRIES, R. G., PRUDENZIATI, M., ZWARTJES, C., VERLAAN, M., KALKHOVEN, E. & ZANTEMA, A. 2001. A specific lysine in c-Jun is required for transcriptional repression by E1A and is acetylated by p300. *EMBO J,* 20**,** 6095-103.

WAETZIG, V. & HERDEGEN, T. 2003. The concerted signaling of ERK1/2 and JNKs is essential for PC12 cell neuritogenesis and converges at the level of target proteins. *Mol Cell Neurosci,* 24**,** 238-49.

WALLER, A. V. 1850. Experiments on the section of the glossopharyngeal and hypoglossal nerves of the frog, and observations of the alterations produced thereby in the structure of their primitive fibres. *Philosophical Transactions of the Royal Society of London,* 140**,** 423-429.

WALTERS, R. D., DRULLINGER, L. F., KUGEL, J. F. & GOODRICH, J. A. 2013. NFATc2 recruits cJun homodimers to an NFAT site to synergistically activate interleukin-2 transcription. *Mol Immunol,* 56**,** 48-56.

WANG, C., BIAN, W., XIA, C., ZHANG, T., GUILLEMOT, F. & JING, N. 2006. Visualization of bHLH transcription factor interactions in living mammalian cell nuclei and developing chicken neural tube by FRET. *Cell Res,* 16**,** 585-98.

WANG, J. C. & GIAEVER, G. N. 1988. Action at a distance along a DNA. *Science,* 240**,** 300-4.

WANG, K., LU, W., CHEN, J., XIE, S., SHI, H., HSU, H., YU, W., XU, K., BIAN, C., FISCHER, W. B., SCHWARZ, W., FENG, L. & SUN, B. 2012a. PEDV ORF3 encodes an ion channel protein and regulates virus production. *FEBS Lett,* 586**,** 384-91.

WANG, Y., FONSLOW, B. R., WONG, C. C., NAKORCHEVSKY, A. & YATES, J. R., 3RD 2012b. Improving the comprehensiveness and sensitivity of sheathless capillary electrophoresis-tandem mass spectrometry for proteomic analysis. *Anal Chem,* 84**,** 8505-13.

WATKINS, T. A., WANG, B., HUNTWORK-RODRIGUEZ, S., YANG, J., JIANG, Z., EASTHAM-ANDERSON, J., MODRUSAN, Z., KAMINKER, J. S., TESSIER-LAVIGNE, M. & LEWCOCK, J. W. 2013. DLK initiates a transcriptional program that couples apoptotic and regenerative responses to axonal injury. *Proc Natl Acad Sci U S A,* 110**,** 4039-44.

WELLS, J. A., GLASSMAN, A. R., AYALA, A. R., JAMPOL, L. M., AIELLO, L. P., ANTOSZYK, A. N., ARNOLD-BUSH, B., BAKER, C. W., BRESSLER, N. M., BROWNING, D. J., ELMAN, M. J., FERRIS, F. L., FRIEDMAN, S. M., MELIA, M., PIERAMICI, D. J., SUN, J. K. & BECK, R. W. 2015. Aflibercept, bevacizumab, or ranibizumab for diabetic macular edema. *N Engl J Med,* 372**,** 1193-203.

WHITFIELD, J., NEAME, S. J., PAQUET, L., BERNARD, O. & HAM, J. 2001. Dominant-negative c-Jun promotes neuronal survival by reducing BIM expression and inhibiting mitochondrial cytochrome c release. *Neuron,* 29**,** 629-43.

WIATRAK, B., KUBIS-KUBIAK, A., PIWOWAR, A. & BARG, E. 2020. PC12 Cell Line: Cell Types, Coating of Culture Vessels, Differentiation and Other Culture Conditions. *Cells,* 9.

WIEDMER, L., DUCRAY, A. D., FRENZ, M., STOFFEL, M. H., WIDMER, H. R. & MEVISSEN, M. 2019. Silica nanoparticle-exposure during neuronal differentiation modulates dopaminergic and cholinergic phenotypes in SH-SY5Y cells. *J Nanobiotechnology,* 17**,** 46.

WOJCIK, R., DADA, O. O., SADILEK, M. & DOVICHI, N. J. 2010. Simplified capillary electrophoresis nanospray sheath-flow interface for high efficiency and sensitive peptide analysis. *Rapid Commun Mass Spectrom,* 24**,** 2554-60.

WOLFF, P., ABREU, P. A., ESPREAFICO, E. M., COSTA, M. C., LARSON, R. E. & HO, P. L. 1999. Characterization of myosin V from PC12 cells. *Biochem Biophys Res Commun,* 262**,** 98-102.

WOLOZIN, B., IWASAKI, K., VITO, P., GANJEI, J. K., LACANA, E., SUNDERLAND, T., ZHAO, B., KUSIAK, J. W., WASCO, W. & D'ADAMIO, L. 1996. Participation of presenilin 2 in apoptosis: enhanced basal activity conferred by an Alzheimer mutation. *Science,* 274**,** 1710-3.

WOODS, R., WESLEY, R. & KAPKE, P. 1988. Neutralization of porcine transmissible gastroenteritis virus by complement-dependent monoclonal antibodies. *American journal of veterinary research,* 49**,** 300-304.

WU, B. Y., FODOR, E. J., EDWARDS, R. H. & RUTTER, W. J. 1989. Nerve Growth Factor Induces the Proto-oncogene c-jun in PC12 Cells. *Journal of Biological Chemistry,* 264**,** 9000-9003.

WUJEK, J. R. & LASEK, R. J. 1983. Correlation of axonal regeneration and slow component B in two branches of a single axon. *J Neurosci,* 3**,** 243-51.

XIA, Z., DICKENS, M., RAINGEAUD, J., DAVIS, R. J. & GREENBERG, M. E. 1995. Opposing effects of ERK and JNK-p38 MAP kinases on apoptosis. *Science,* 270**,** 1326-31.

XU, X. G., ZHANG, H. L., ZHANG, Q., DONG, J., HUANG, Y. & TONG, D. W. 2015. Porcine epidemic diarrhea virus M protein blocks cell cycle progression at S-phase and its subcellular localization in the porcine intestinal epithelial cells. *Acta Virol,* 59**,** 265-75.

YAN, J., ENGE, M., WHITINGTON, T., DAVE, K., LIU, J., SUR, I., SCHMIERER, B., JOLMA, A., KIVIOJA, T., TAIPALE, M. & TAIPALE, J. 2013. Transcription factor binding in human cells occurs in dense clusters formed around cohesin anchor sites. *Cell,* 154**,** 801-13.

YANG, P., QIN, Y., BIAN, C., ZHAO, Y. & ZHANG, W. 2015. Intrathecal delivery of IL-6 reactivates the intrinsic growth capacity of pyramidal cells in the sensorimotor cortex after spinal cord injury. *PLoS One,* 10**,** e0127772.

YANG, P., WEN, H., OU, S., CUI, J. & FAN, D. 2012. IL-6 promotes regeneration and functional recovery after cortical spinal tract injury by reactivating intrinsic growth program of neurons and enhancing synapse formation. *Exp Neurol,* 236**,** 19-27.

YANG, W., LIU, P., LIU, Y., WANG, Q., TONG, Y. & JI, J. 2006. Proteomic analysis of rat pheochromocytoma PC12 cells. *Proteomics,* 6**,** 2982-90.

YOSHIDA, T. & YASUDA, K. 2002. Characterization of the chicken L-Maf, MafB and c-Maf in crystallin gene regulation and lens differentiation. *Genes Cells,* 7**,** 693-706.

YOUNG, J. Z. 1942. The functional repair of nervous tissue. *Physiol. Rev.* **,** 318-374.

YU, J. Z., DAVE, R. H., ALLEN, J. A., SARMA, T. & RASENICK, M. M. 2009. Cytosolic Galphas acts as an intracellular messenger to increase microtubule dynamics and promote neurite outgrowth. *J Biol Chem,* 284**,** 10462-72.

ZECHA, J., SATPATHY, S., KANASHOVA, T., AVANESSIAN, S. C., KANE, M. H., CLAUSER, K. R., MERTINS, P., CARR, S. A. & KUSTER, B. 2019. TMT Labeling for the Masses: A Robust and Cost-efficient, In-solution Labeling Approach. *Mol Cell Proteomics,* 18**,** 1468-1478.

ZENG, Z., XU, J. & ZHENG, W. 2017. Artemisinin protects PC12 cells against beta-amyloid-induced apoptosis through activation of the ERK1/2 signaling pathway. *Redox Biol,* 12**,** 625-633.

ZHAI, Q., WANG, J., KIM, A., LIU, Q., WATTS, R., HOOPFER, E., MITCHISON, T., LUO, L. & HE, Z. 2003. Involvement of the ubiquitin-proteasome system in the early stages of wallerian degeneration. *Neuron,* 39**,** 217-25.

ZHANG, A., QI, W., GOOD, T. A. & FERNANDEZ, E. J. 2009. Structural differences between Abeta(1-40) intermediate oligomers and fibrils elucidated by proteolytic fragmentation and hydrogen/deuterium exchange. *Biophys J,* 96**,** 1091-104.

ZHANG, A., QI, W., SINGH, S. K. & FERNANDEZ, E. J. 2011. A new approach to explore the impact of freeze-thaw cycling on protein structure: hydrogen/deuterium exchange mass spectrometry (HX-MS). *Pharm Res,* 28**,** 1179-93.

ZHANG, Q., SHI, K. & YOO, D. 2016. Suppression of type I interferon production by porcine epidemic diarrhea virus and degradation of CREB-binding protein by nsp1. *Virology,* 489**,** 252-68.

ZHANG, Q. C., PETREY, D., DENG, L., QIANG, L., SHI, Y., THU, C. A., BISIKIRSKA, B., LEFEBVRE, C., ACCILI, D., HUNTER, T., MANIATIS, T., CALIFANO, A. & HONIG, B. 2012a. Structure-based prediction of protein-protein interactions on a genome-wide scale. *Nature,* 490**,** 556-60.

ZHANG, W., BENMOHAMED, R., ARVANITES, A. C., MORIMOTO, R. I., FERRANTE, R. J., KIRSCH, D. R. & SILVERMAN, R. B. 2012b. Cyclohexane 1,3-diones and their inhibition of mutant SOD1-dependent protein aggregation and toxicity in PC12 cells. *Bioorg Med Chem,* 20**,** 1029-45.

ZHAO, L. L., ZHANG, T., HUANG, W. X., GUO, T. T. & GU, X. S. 2023. Transcriptional regulatory network during axonal regeneration of dorsal root ganglion neurons: laser-capture microdissection and deep sequencing. *Neural Regen Res,* 18**,** 2056-2066.

ZHONG, H., ZHANG, R., LI, G., HUANG, P., ZHANG, Y., ZHU, J., KUANG, J., HUTCHINS, A. P., QIN, D., ZHU, P., PEI, D. & LI, D. 2023. c-JUN is a barrier in hESC to cardiomyocyte transition. *Life Sci Alliance,* 6.

ZHOU, J., HAMDAN, H., YALAMANCHILI, H. K., PANG, K., POHODICH, A. E., LOPEZ, J., SHAO, Y., OSES-PRIETO, J. A., LI, L., KIM, W., DURHAM, M. A., BAJIKAR, S. S., PALMER, D. J., NG, P., THOMPSON, M. L., BEBIN, E. M., MULLER, A. J., KUECHLER, A., KAMPMEIER, A., HAACK, T. B., BURLINGAME, A. L., LIU, Z., RASBAND, M. N. & ZOGHBI, H. Y. 2022. Disruption of MeCP2-TCF20 complex underlies distinct neurodevelopmental disorders. *Proc Natl Acad Sci U S A,* 119.

ZHU, G., SUN, L., KEITHLEY, R. B. & DOVICHI, N. J. 2013. Capillary isoelectric focusing-tandem mass spectrometry and reversed-phase liquid chromatography-tandem mass spectrometry for quantitative proteomic analysis of differentiating PC12 cells by eight-plex isobaric tags for relative and absolute quantification. *Anal Chem,* 85**,** 7221-9.

ZIMMERMAN, U. J. & SCHLAEPFER, W. W. 1982. Characterization of a brain calcium-activated protease that degrades neurofilament proteins. *Biochemistry,* 21**,** 3977-82.

ZIV, N. E. & SPIRA, M. E. 1995. Axotomy induces a transient and localized elevation of the free intracellular calcium concentration to the millimolar range. *J Neurophysiol,* 74**,** 2625-37.

Appendix: DNA sequence for *ef1α*-linker-APEX2

5’
TATGAGCTCCATATGCCGCGGTCCGGAATCGATGCTAGCCGTCGAGCAGGGGGATCATCTAATCAAGC
ACAAATAAGGGGCGTGTAACACAAAAGCCAGCGACCCTTTCCAATGCAAATCAAACTTGCAATTCTTTG
CCGTTTTTATCATTTAAGTGTCGGCTTAAGGTCCACTATCAGATGTAAACAGCCTTATCTAACAAAGGTA
TCATTACATTCTGAAATTCTCAGGCATGCAAGCTAGCTTATGACGCACTAGGGAGTGCCACCCTTCCTTT
CGCCCTAACTTCGTGATAACTCGCGCGTTTCACTCAACAGCTGCATCCGCCCTAGTGCTACTGGGAGTT
GTAGTATACAAGACGCTTACAGGCTGAATGTTCTGTCAAGACCCCGCCTCTAGCACTTTGGGAATTCTG
GACTTGATGATGTCATGGTTAATCCCCGCCCAGTAGAGGCGGCTATATAAAGGGTGGTTAAGGCCCGG
TTCGCTCTCTTCCTCACCGGGTCTGCGGCGAGTTCTAGCTGAGCTAGCTGATCAGAATTCGTCGACTCT
AGACCATGGACGCGTGGTGGATCTGGTGGATCTGGTGGATCTGGATCCGGAAAGTCTTACCCAACTGT
GAGTGCTGATTACCAGGACGCCGTTGAGAAGGCGAAGAAGAAGCTCAGAGGCTTCATCGCTGAGAAG
AGATGCGCTCCTCTAATGCTCCGTTTGGCATTCCACTCTGCTGGAACCTTTGACAAGGGCACGAAGACC
GGTGGACCCTTCGGAACCATCAAGCACCCTGCCGAACTGGCTCACAGCGCTAACAACGGTCTTGACAT
CGCTGTTAGGCTTTTGGAGCCACTCAAGGCGGAGTTCCCTATTTTGAGCTACGCCGATTTCTACCAGTT
GGCTGGCGTTGTTGCCGTTGAGGTCACGGGTGGACCTAAGGTTCCATTCCACCCTGGAAGAGAGGAC
AAGCCTGAGCCACCACCAGAGGGTCGCTTGCCCGATCCCACTAAGGGTTCTGACCATTTGAGAGATGT
GTTTGGCAAAGCTATGGGGCTTACTGACCAAGATATCGTTGCTCTATCTGGGGGTCACACTATTGGAGC
TGCACACAAGGAGCGTTCTGGATTTGAGGGTCCCTGGACCTCTAATCCTCTTATTTTCGACAACTCATA
CTTCACGGAGTTGTTGAGTGGTGAGAAGGAAGGTCTCCTTCAGCTACCTTCTGACAAGGCTCTTTTGTC
TGACCCTGTATTCCGCCCTCTCGTTGACAAATATGCAGCGGACGAAGATGCCTTCTTTGCTGATTACGC
TGAGGCTCACCAAAAGCTTTCCGAGCTTGGGTTTGCTGATGCCTAAGGATCCAGATCTCTGCAGCTCGA
GACTAGTTA
3’